DEFENCE S&T TECHNICAL BULLETIN

VOL. 16 NUM. 1 YEAR 2023 ISSN 1985-6571

CONTENTS

Ministry of Defence Malaysia

SCIENCE & TECHNOLOGY RESEARCH INSTITUTE FOR DEFENCE (STRIDE)

AIMS AND SCOPE

The Defence S&T Technical Bulletin is the official journal of the Science & Technology Research Institute for Defence (STRIDE). The journal, which is indexed in, among others, Scopus, Index Corpenicus, ProQuest and EBSCO, contains manuscripts on research findings in various fields of defence science & technology. The primary purpose of this journal is to act as a channel for the publication of defence-based research work undertaken by researchers both within and outside the country.

WRITING FOR THE DEFENCE S&T TECHNICAL BULLETIN

Contributions to the journal should be based on original research in areas related to defence science & technology. All contributions should be in English.

PUBLICATION

The editors' decision with regard to publication of any item is final. A manuscript is accepted on the understanding that it is an original piece of work that has not been accepted for publication elsewhere.

PRESENTATION OF MANUSCRIPTS

The format of the manuscript is as follows:

a) Page size A4
b) MS Word format
c) Single space
d) Justified
e) In Times New Roman, 11-point font
f) Should not exceed 20 pages, including references
g) Texts in charts and tables should be in 10-point font.

Please e-mail the manuscript to:

1) Gs. Dr. Dinesh Sathyamoorthy (dinesh.sathyamoorthy@stride.gov.my)
2) Dr. Mahdi bin Che Isa (mahdi.cheisa@stride.gov.my)

The next edition of the journal (Vol. 16, Num. 2) is expected to be published in November 2023. The due date for submissions is 2 August 2023. **It is strongly iterated that authors are solely responsible for taking the necessary steps to ensure that the submitted manuscripts do not contain confidential or sensitive material.**

The template of the manuscript is as follows:

TITLE OF MANUSCRIPT

Name(s) of author(s)

Affiliation(s)

Email:

ABSTRACT

Contents of abstract.

Keywords: *Keyword 1; keyword 2; keyword 3; keyword 4; keyword 5.*

1. TOPIC 1

Paragraph 1.

Paragraph 2.

1.1 Sub Topic 1

Paragraph 1.

Paragraph 2.

2. TOPIC 2

Paragraph 1.

Paragraph 2.

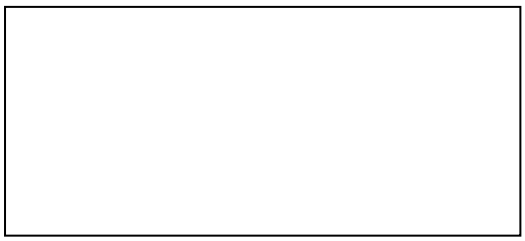

Figure 1: Title of figure.

Table 1: Title of table.

Content	Content	Content
Content	Content	Content
Content	Content	Content
Content	Content	Content

Equation 1 (1)
Equation 2 (2)

REFERENCES

Long lists of notes of bibliographical references are generally not required. The method of citing references in the text is 'name date' style, e.g. 'Hanis (1993) claimed that...', or '…including the lack of interoperability (Bohara *et al.*, 2003)'. End references should be in alphabetical order. The following reference style is to be adhered to:

Books

Serra, J. (1982). *Image Analysis and Mathematical Morphology*. Academic Press, London.

Book Chapters

Goodchild, M.F. & Quattrochi, D.A. (1997). Scale, multiscaling, remote sensing and GIS. *In* Quattrochi, D.A. & Goodchild, M.F. (Eds.), *Scale in Remote Sensing and GIS*. Lewis Publishers, Boca Raton, Florida, pp. 1-11.

Journals / Serials

Jang, B.K. & Chin, R.T. (1990). Analysis of thinning algorithms using mathematical morphology. *IEEE T. Pattern Anal.*, **12**: 541-550.

Online Sources

GTOPO30 (1996). *GTOPO30: Global 30 Arc Second Elevation Data Set*. Available online at: http://edcwww.cr.usgs.gov/landdaac/gtopo30/gtopo30.html (Last access date: 1 June 2009).

Unpublished Materials (e.g. theses, reports and documents)

Wood, J. (1996). *The Geomorphological Characterization of Digital Elevation Models*. PhD Thesis, Department of Geography, University of Leicester, Leicester.

PERFORMANCE MEASUREMENT OF TACTICAL RADIO STATION DEPLOYMENT USING VERY HIGH FREQUENCY (VHF) IN SUBURBAN AREA ENVIRONMENT

Aliff Zakuan Rasidi[1], Darmawaty Mohd Ali[2*], Norsuzila Ya'acob[2], Azita Laily Yusof[2] & Divine Senanu Ametefe[2]

[1]Signals Directorate, Malaysian Army Headquarters, Malaysia
[2]Wireless Communication Technology Group, School of Electrical Engineering, College of Engineering, Universiti Teknologi MARA (UiTM), Malaysia

[*]Email: darma504@uitm.edu.my

ABSTRACT

A reliable and effective communications system is the main factor in military deployment to maintain command and control in a battlefield environment. Therefore, a good communications planner needs to plan and justify each radio station's location, so that these stations can provide high-speed and secure voice and data transmission. One of the main problems in military deployment is operators having difficulty identifying the optimum locations for the transmitter station and receiver stations. Based on several research works, most of the reference models that have been designed mainly focused on broadcast and commercial communications systems, which are unsuitable for military deployment. This paper studies the appropriate locations to install low-power static stations for the deployment of very high frequency (VHF) military tactical radios in suburban areas. Experiments were conducted using theoretical approaches and measurements. The results of this experiment can help determine the locations of the transmitter station and the receiver stations for analog and digital transmissions to provide the best quality of service. The experimental results and findings can also proffer guidance for military deployment in suburban areas.

Keywords: *Very high frequency (VHF); suburban; military tactical radio; propagation; analog and digital performance.*

1. INTRODUCTION

Communications is the key to success in military warfare and is essential before any military combat or operation is deployed. This is because communications is a medium between commanders and soldiers to interact and deliver information on the mission. A tactical radio is a military communications equipment that works well in any environment with less interference, high security and high performance, as well as possessing the capability to operate in a static or mobile setting (Mahajan, 2018).

Very high frequency (VHF) is a specific range of radio frequencies used in many applications, such as television and radio broadcasting, radar monitoring systems, and broadband mobile communication systems. These applications are deployed in diverse environments, which include coarse terrains such as tropical and forest areas. These areas are often exposed to inconsistent signal transmission problems, which makes planning for stable and reliable communication highly challenging (Shehadeh *et al.*, 2020).

Most of Malaysia's army operations are in jungles and suburban areas, necessitating VHF tactical radio use. A VHF tactical radio promotes high bandwidth to speed up the information delivery between receiver and transmitter stations. The main challenge of VHF communications is the propagation of the VHF signal, which quickly deteriorates because of atmospheric reflection,

diffraction, refraction, absorption and material obstruction (Mello *et al.*, 2018). In order to mitigate the aforementioned problems, various methods have been proposed by researchers. These methods typically involve radio wave modelling of attenuation, propagation loss and path loss using analytical and empirical approaches. Though the study of the signal propagation effect is important, prior works did not give much attention to finding the optimal location for antenna placement in order to provide good quality of service (QoS) during the transmission of the signal.

For this reason, this study aims to determine the optimal locations of the transmitter station and receiver stations. The findings of this study can help operation planners to determine the suitable communications coverage to maintain efficient dissemination of information. Furthermore, the findings of this work can help in facilitating the propagation of VHF military communications in suburban areas of Malaysia.

2. LITERATURE REVIEW

The models in this study were selected based on empirical models and a field site test, which resembled VHF military tactical radios with operating frequency of 30 - 88 MHz (Yusof *et al.*, 2021), low antenna height, and low power transmission. As a foundation, VHF communications depends on line of sight (LoS), where the location of the transmitter and receiver are visible to each other without any obstruction between them.

2.1 Empirical Models

2.1.1 Free-Space Path Loss (FSPL) Model

LoS occurs when electromagnetic radiation or acoustic wave propagation travels in a straight line. In a practical environment, waves that travel from the transmitter station to the receiver station are affected by factors such as reflection, diffraction, refraction, shadowing and absorption caused by the atmosphere and obstacles (Barrios-Ulloa *et al.*, 2022). LoS communications using the FSPL model has no losses. The following equation is used to explain the amount of received power, where P_t is the transmitted power, λ is the wavelength of frequency used, and d is the distance between the transmitter and the receiver station in metres:

$$P_r(dBm) = P_t(dBm) - 21.98 + 20log_{10}\lambda - 20log_{10}d \quad (1)$$

2.1.2 Two-Ray Model

This model is dominant when a particular reflection from the slope is used to predict large-scale signal strength over a few tens of kilometres. This model is applicable when different antenna heights are used, and the signal between the direct-sight signal and reflection signal at the receiving point is summed up. An experiment was conducted in Beijing, which resulted in a low signal reflected from the building (Zochmann *et al.*, 2017). This method can be used in VHF communications because the reflection from the transmitter's radiation power still exists even after the breakpoint distance. The significance of this model is that the receiver station can regenerate and sum up the received signal from the transmitted signal's reflection, diffraction and scattering. As illustrated in Figure 1, using the following equation, the power received can be computed from the two-ray model, where P_t is the transmitted power, d is the distance between the radio stations, G is the gain of the radio signal, h_t is the transmitter's antenna height, and h_r is the receiver's antenna height (Botella-Campos *et al.*, 2020). Some limitations in this model arise during the simulation, that is the transmitter and receiver should be placed at the same height from each other. This model gives efficient result and performance at a long distance in contrast with the free space, which delivers the best in short distance.

$$E_{TOT}(d,t) = \frac{E_{od_0}}{d'} cos\left(\omega_c\left(t - \frac{d'}{c}\right)\right) + (-1)\frac{E_{od_0}}{d''}\ cos\left(\omega_c\left(t - \frac{d''}{c}\right)\right)$$

$$P_r(dBm) = P_t(dBm) - 40log_{10}(d) + 10log_{10}(Gh_t^2h_r^2) \quad (2)$$

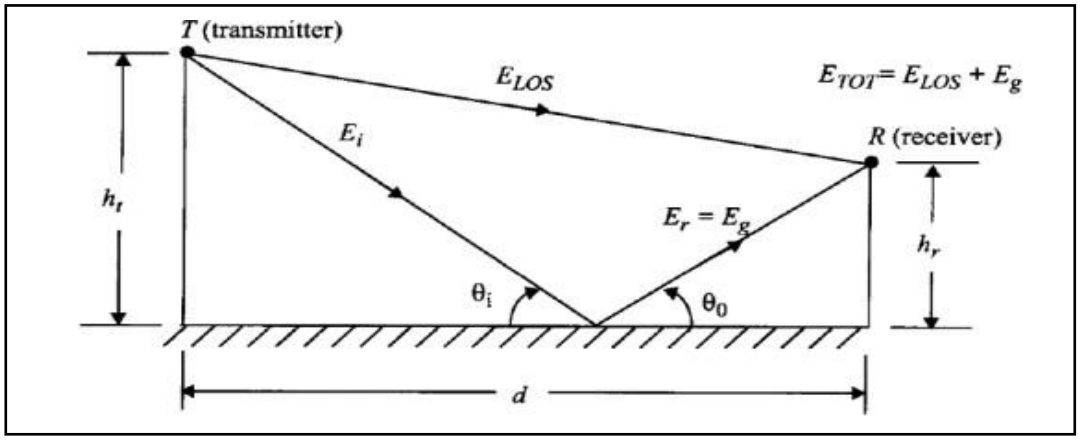

Figure 1: Two-ray model.

2.1.3 Jansky and Bailey (J&B) Model

This model was tested in Thailand's tropical forest (Weissberger *et al*., 1982). The testing environment is quite similar to Malaysia's region in terms of climate because of its location in Southeast Asia. This model specifies the distance between the transmitting and receiving antennas of within the range of 8 m to 1.6 km for frequency range of 25 - 400 MHz and antenna height of 2 - 7 m. This method predicts attenuation using the distance between the transmitting and receiving antennas. This model can also be tested with low antenna height and lower band of VHF. The following equation shows the calculation to determine the losses using the Jansky and Bailey (J&B) model:

$$L_b(dB) = 36.57 + 20logf(MHz) - 20\log\frac{Ae^{1609ad}}{d} + \frac{B}{d^2} \quad (3)$$

where $A = 0$, $a = 0$, and $B = 0.00424$

2.2 Field Test

Field test experiments can also be referenced to interpret VHF radio performance. The Thales Group conducted an experiment on VHF military radio performance in Switzerland, which focused on propagation delay and received power (Naour, *et al.*, 2014). The experiment measured the performances based on two frequency bands at different locations. The results showed that the receiver station located in mountainous areas experienced high propagation delay at high-frequency band as compared with low-frequency band. In terms of the received power, when the transmission was obstructed by any obstacle, the receiver station captured low signal strength.

The propagation delay when using VHF tactical radios was measured by researchers in Japan (Pugh *et al.*, 2006, 2007). The experiment was conducted in three different environments using a mounted vehicular antenna in fixed and mobile terminals. The frequencies used were 37.8, 57.0, and 77.5 MHz with an omnidirectional military whip antenna at base height of 2 m. The results showed a significant delay in a more cluttered environments, indicating a sizeable multipath situation. The results also showed that signal strength varied with location.

The Institute for Defence Analyses (IDA) measured the performance of the Soldier Radio Waveform (Marwick, 2015). The group also analysed the performance of throughput against frequency throughout the experiment. The results showed that throughput increased linearly with bandwidth, but the results also depended on modulation, attenuation and interference. The following equation is used to determine the amount of throughput, where C is the channel capacity (throughput), B is the bandwidth (MHz), and SNR is the signal-to-noise ratio:

$$C = Blog_2(1 + SNR) \tag{4}$$

From the various highlighted studies, it can be concluded that no specific empirical models can be utilised for the use of VHF tactical radios in suburban areas.

3. METHODOLOGY

Figure 2 shows the flow chart of the experimental work conducted in this study. The initial step involving the selection of the suburban area was based on the suburban environment, consisting of a mixed-used residential area and some vegetation areas located on the outskirts of the city centre. The field test location was at an army camp in Kuala Lumpur, as shown in Figure 3. The transmitter station was positioned at height of 143 m from the sea level. The receiver stations were at heights of 50 - 70 m from the sea level. The transmitter station communicated to the five receiver stations, with the distances from the receiver stations to the transmitter station shown in Table 1. Voice signal was transmitted first during the measurement, followed by file transfer.

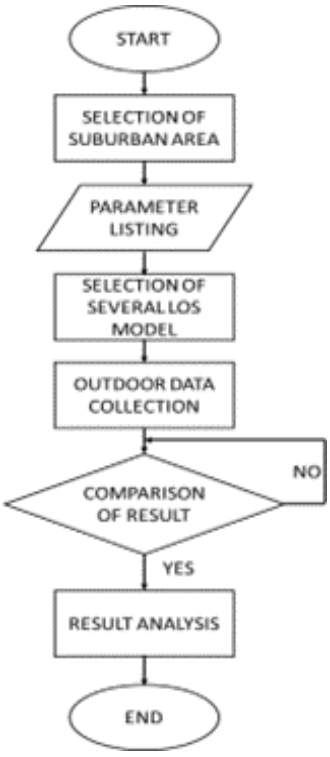

Figure 2: Flow chart of experiment.

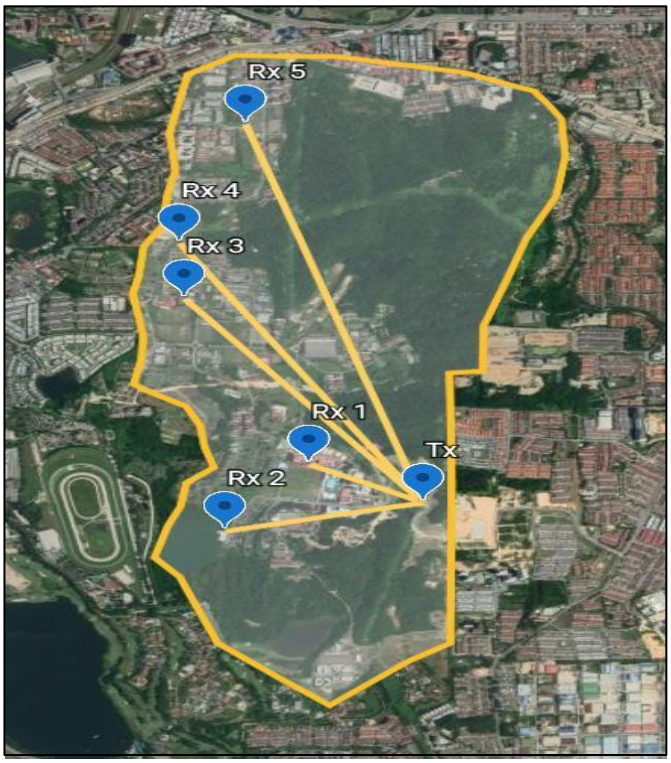

Figure 3: Locations of transmitter station and receiver stations.

Table 1: Distances between transmitter and receiver stations.

Station	Altitude (m)	Distance (km)
Tx	143	-
Rx 1	65	0.5
Rx 2	52	1
Rx 3	48	1.6
Rx 4	53	2.6
Rx 5	68	3

The parameters for the measurements are tabulated in Table 2. The calculation of theoretical values was based on three selected models, as shown in Table 3. Since there are no specific models designed for VHF tactical radios, the models in Table 3 were selected because the operating frequency was 30 - 88 MHz, which is similar to a VHF tactical radio's frequency range.

Table 2: Parameters for measurements.

Power	10 W
Transmitter's Antenna Height	12 m
Receiver's Antenna Height	2 m
Frequency (MHz)	38.7, 57.4, and 77.7
Digital Voice	VOCODER 2400 b/s MELP 2400 b/s
Data Transfer	Text: 8 kb/s Audio: 2,000 kb/s Image: 4,000 kb/s
Throughput	4,800 bps
Receiver Sensitivity	–113 dBm
SNR	22 dB

Table 3: Models selected for validation.

Model	Equation
Free-Space Path Loss (FSPL)	$P_r(dBm) = P_t\,(dBm) - 21.98 + 20log_{10}(\lambda) - 20\,log_{10}(d))$
Two-Ray Model	$P_r(dBm) = P_t(dBm) - 40log_{10}\,(d) + 10log_{10}\,(Gh_t^2h_r^2)$
Jansky and Bailey (J&B) Model	$L_b(dB) = 36.57 + 20logf(MHz) - 20\log\frac{Ae^{1609ad}}{d} + \frac{B}{d^2}$

The radio path for each receiver station, to determine whether it was in a LoS area from the transmitter station, was determined using the RF LoS SCADACORE application, which is a tool for obtaining point-to-point LoS information (SCADACORE, 2022). The radio paths for the receiver stations are illustrated in Figure 4, showing that only Rx 5 was in a non-LoS area from the transmitter station.

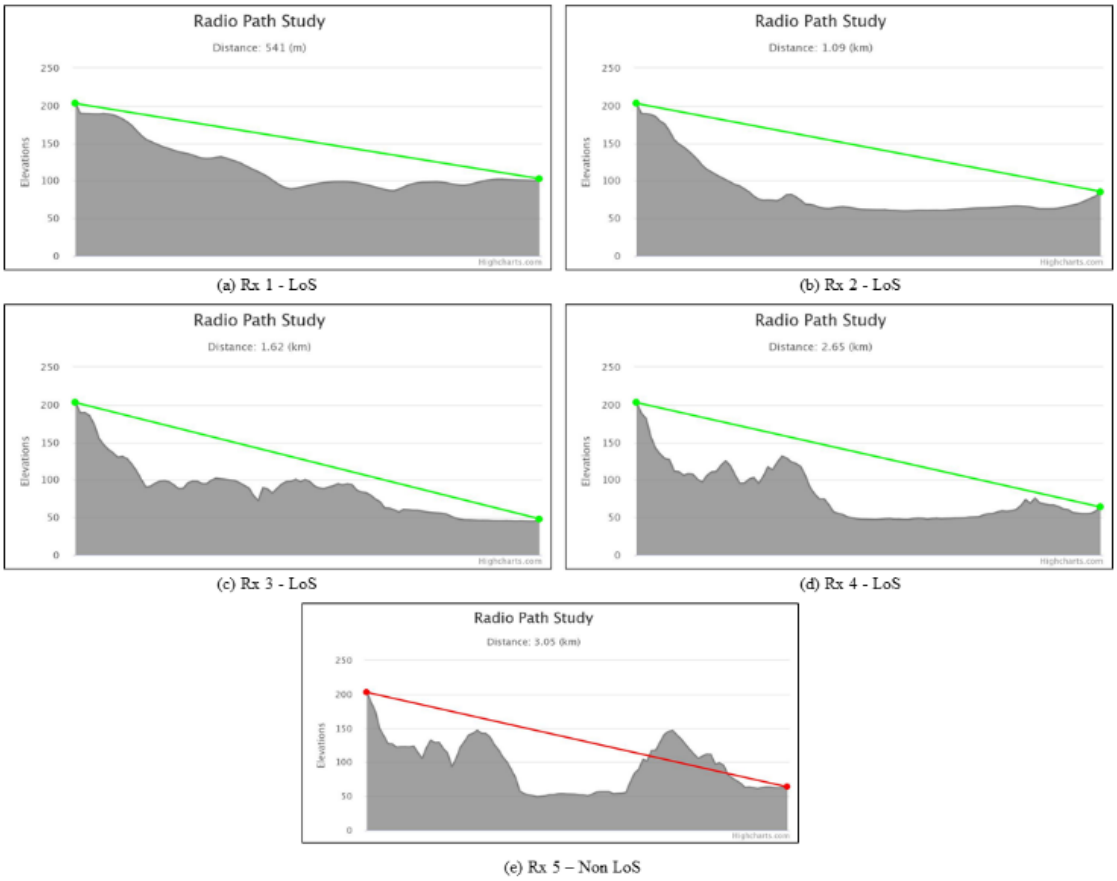

Figure 4: Radio paths for the receiver stations.

The next phase involved measurements for validating the theoretical results. The equipment used for the measurements were VHF tactical radios, a data terminal, and a spectrum analyser. The VHF tactical radios operated within the frequency range of 30 to 87.9 MHz with analog and digital transmission modes. Voice and file transfers were the variables to be tested in the measurements. The test was conducted in three conditions. First, the analog and digital voice signals were transmitted three times. Each transmission took 5 to 10 min to complete. The digital voice transmission used two types of encoders: VOCODER 2400 and Mixed-Excitation Linear Predictive 2400 (MELP 2400). After the signals were received, throughput and delay were measured using the iPerf software. The data rate for audio and file transfer transmissions was 56 kb/s. The protocol used for the transmission was the Transmission Control Protocol (TCP). This protocol is connection-oriented, where the server and client must establish the connection before any data transfer. The data being transferred for the measurements were audio, text and image files with sizes of 250, 1, and 500 kb respectively. The delay measurement was critical to ensure that the file being transferred was received successfully by the receiver within a short time.

4. RESULTS AND DISCUSSION

The data collected from the measurements were compared with the calculated theoretical values from the three selected models shown in Table 3. The analysis was based on the parameters of received strength, throughput, and delay experienced at all five receiver stations.

4.1 Received Power

The FSPL model can be used as the benchmark to determine the suitable locations for the transmitter station and receiver stations to deploy VHF tactical radios in a suburban environment. The measurement results shown in Table 4 were based on the average values of the received signal strengths after being measured three times. The measured values of the received signal strength, ranging from -20.41 to -36.92 dBm for the five receiver stations, were quite similar to the FSPL model's theoretical values. The main reason is that the signal transmission using the FSPL model have the best performance when the distance between the transmitter and receiver is short. The longest distance between the transmitter and receiver stations setup for the measurement is only 3.6 km. On the other hand, the two-ray model is appropriate when the distance between the transmitter and receiver stations is farthest. Furthermore, the J&B empirical model was found to be applicable where both antennas are immersed in a tropical forest (Weissberger *et al*., 1982), which does not resemble the area of measurement.

The values obtained from the measurements and theoretical computations were more than -113 dBm of the sensitivity threshold stated in the technical specification of the equipment (Sapura Thales Electronics, 2019). The results of the received signal strength showed that the voice signal transmission can be performed with good reception, even though Rx 5 was in a non-LoS area. This proved that the measurement results were above the sensitivity level.

Table 4: Received signal strengths.

Receiver	Theoretical			Measurement (dBm)
	FSPL (dBm)	Two-Ray (dBm)	J&B (dBm)	
Rx 1	-21.33	-30.36	-78.80	-20.41
Rx 2	-27.35	-42.40	-82.40	-26.03
Rx 3	-31.43	-50.56	-87.80	-25.46
Rx 4	-35.65	-59.00	-91.60	-21.67
Rx 5	-36.89	-61.48	-95.30	-36.92

Measurements were also conducted to determine the best encoder for transmission, as well as to compare the analog and digital voice transmissions. Figure 5 shows that the MELP 2400 encoder provided better voice quality than those of the other two encoders based on the received signal strength. This is as the MELP 2400 encoder had an adaptive enhancement filter, where the filter is capable of matching synthetic and natural bandpasses to render high quality output speech (Melp, 2022).

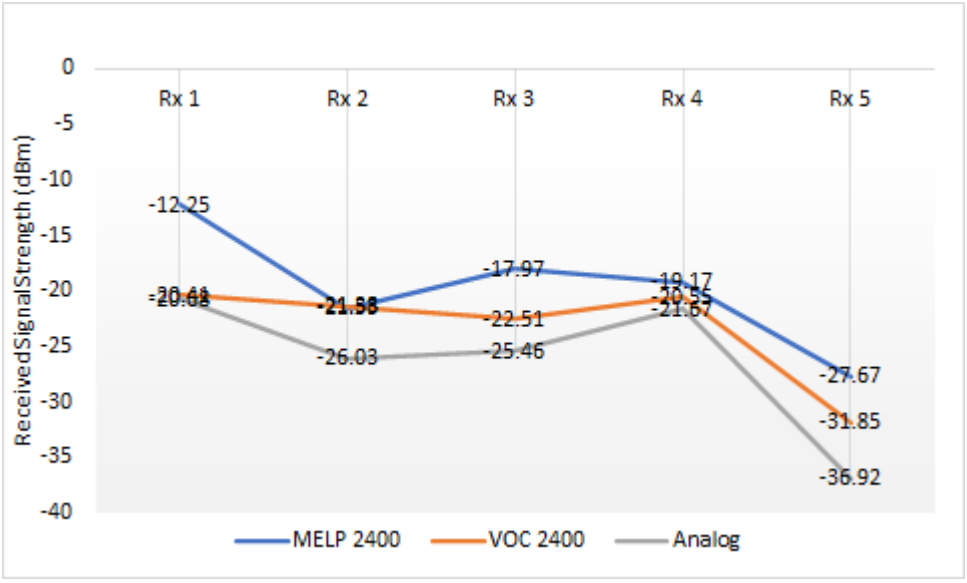

Figure 5: Received signal strength for analog and digital encoders.

4.2 Throughput

The throughput of the system was measured using the iPerf software. The data rate of 56 kb/s was used for determining the throughput for each receiver station. Based on the throughput results shown in Table 5, the measured throughput values were lower than the theoretical values, mainly due to interference and attenuation in the suburban environment. As Rx 5 was in a non-LoS area from the transmitter station, the results from the measurements showed that the reception for Rx 5 could not be accomplished.

Table 5: Throughput for the receiver stations.

Receiver	Theoretical value (kb/s)	Measurement (kb/s)
Rx 1	4.8	3.94
Rx 2	4.8	4.66
Rx 3	4.8	2.92
Rx 4	4.8	2.23
Rx 5	4.8	-

4.3 Transmission Delay

In this experiment, the data was transferred using the forward error correction (FEC) method to control the error in the transmission. The transmission delay of the system was based on the type and size of the data transferred. This experiment measured the delay in the transmission of audio, text, and image files with sizes of 250, 1, and 500 kb respectively. The measured values of the delay parameter were compared with values calculated using Equation 5. Based on the analysis, the system experienced at least 15 min of transmission time delay when transferring data over 2,000 kb/s, even though the distance between the transmitter and receiver was only 1.6 km. One factor contributing to the high delay was the system's use of frequency-hopping spread spectrum (FHSS). This is because FHSS transmission must continuously change the centre frequency during the file transfer. This process affected the delay, where the system needed some time to change the centre frequency before the file was transferred entirely.

In point-to-point communications, it is important for the LoS to be free from any obstruction such as terrain, vegetation and buildings as any interference or obstruction can result in a loss of signal. It is important to keep an elliptical region between the transmit and receive antennas free from any obstruction for proper functioning of the system. The Fresnel zone is a long ellipsoid that stretches between the two antennas. If a significant portion of the Fresnel zone is obstructed, the receive-signal-strength at the receiving antenna can be greatly attenuated. A rule of thumb is that at least 60% of the first Fresnel zone should be clear of any obstructions to ensure optimum transmission performance. However, the receiver stations' locations were surrounded by dense area and experienced multipath fading of the transmitted signal, which contributed to the increase in delay. In addition, as shown in Figure 6, the locations of Rx 3 and Rx 4 had less than 60% of the Fresnel zone's clearance area, thereby causing their delay to be higher than those of Rx 1 and Rx 2. The theoretical and measured delay values are shown in Figures 7 for the text, audio and image file transmissions. The following equation shows the delay calculation, where D_t is the transmission delay in seconds, N is the number of bits, and R is the transmission rate:

$$D_t = N / R \tag{5}$$

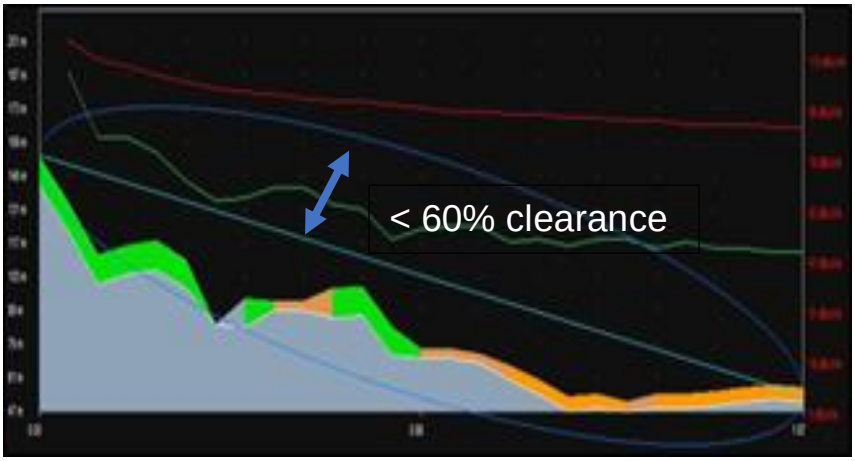

(a)

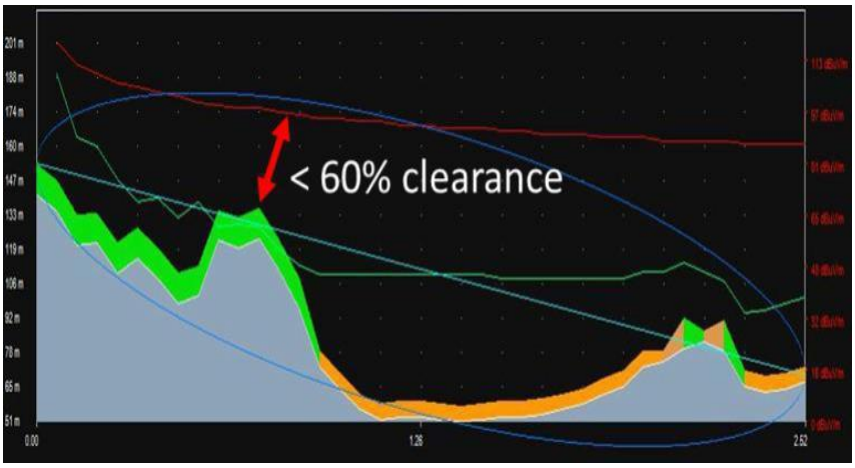

(b)

Figure 6: Conditions of Fresnel zone for (a) Rx 3 and (b) Rx 4.

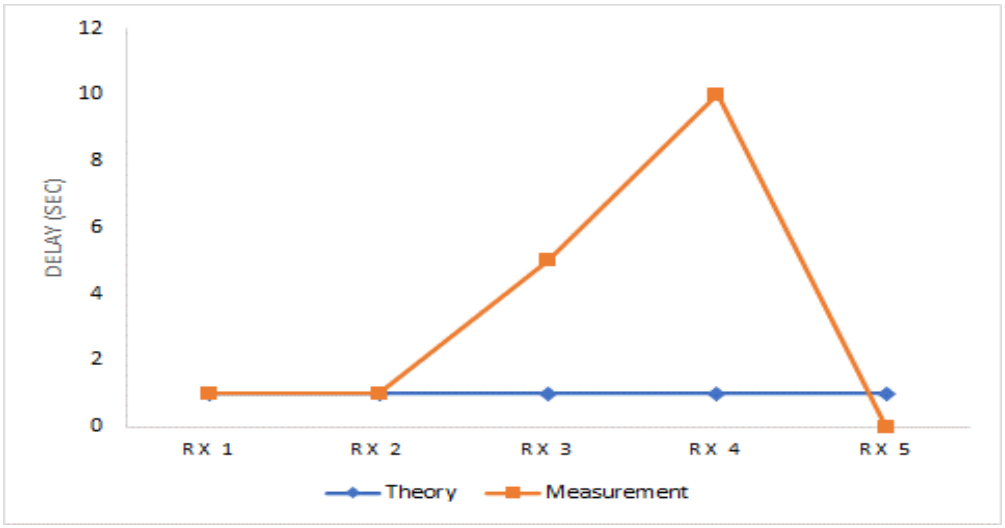

(a)

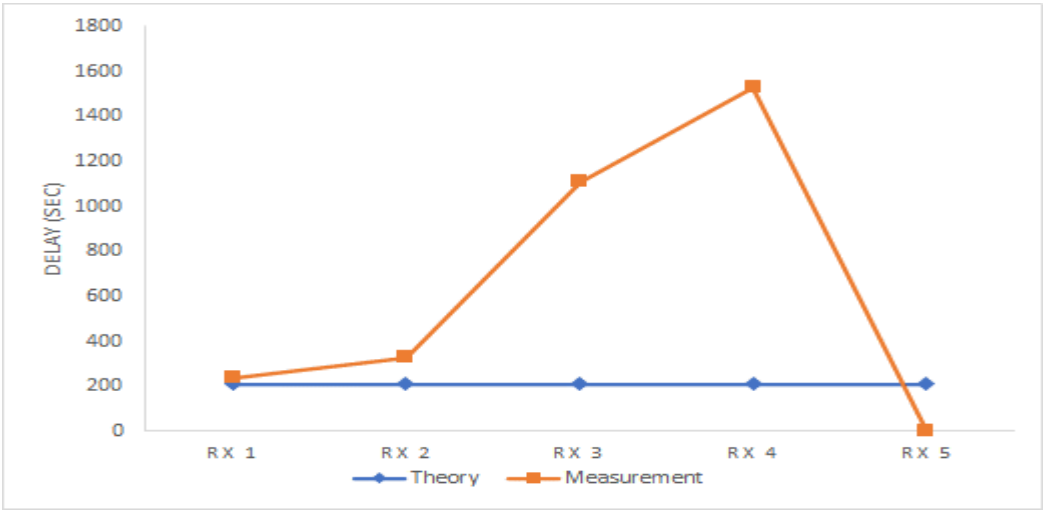

(b)

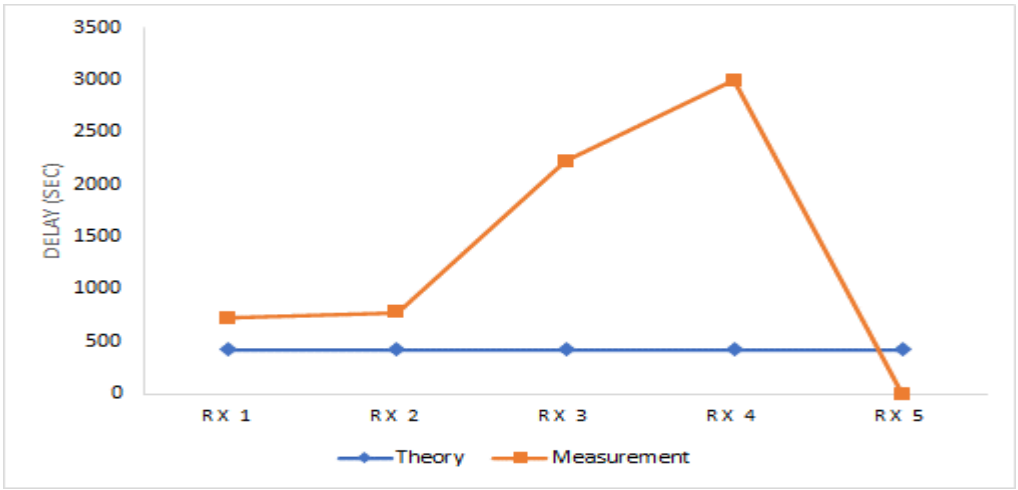

(c)

Figure 7: Delay for (a) text, (b) audio and (c) image file transmissions

5. CONCLUSION

This research work studied the performance of VHF tactical radios in suburban areas. The performance was based on signal strength, analog and digital voice quality, throughput, as well as delay. The posited system could provide voice service even though the location of Rx 5 was in a non-LoS area from the transmitter. Although the outdoor transmission was influenced by interference and attenuation, which affected transmission quality, the measurement results were still acceptable and comparable with the values from the theoretical models. Finally, based on the results and observation, the FSPL model can be used to deploy VHF tactical radios in suburban areas. For future works, it is suggested that the measurement of VHF tactical radio transmission be conducted for a mobile receiver because the consistency of the transmission could also affect the QoS.

REFERENCES

Barrios-Ulloa, A., Ariza-Colpas, P.P., Sánchez-Moreno, H., Quintero-Linero, A.P., De la Hoz-Franco, E. (2022). Modeling radio wave propagation for wireless sensor networks in vegetated environments: A systematic literature review. *Sensors*, **22**: 1–28.

Botella-Campos, M., Jiménez, J. M., Sendra, S. and Lloret, J. (2020). Near-ground wireless coverage design in rural environment. 2020 *Int. Conf. on Adv. Sens., Actr., Metering Sensing,* (*ALLSENSORS 2020)*, 21–25 November 2020, Valencia, Spain.

Marwick, M.S. (2015). *Analysis of Soldier Radio Waveform Performance in Operational Test.* Institute for Defense Analyses. Alexandria, Virginia.

Mahajan, R. (2018). Tactical wireless network and commercial wireless. *Journal Emerg. Tech. Innovative Res.*, **5**: 593–596.

Melp (2022). *Mixed Excitation Linear Predictive (MELP)*. Available online at: https://melp.org/. (Last access date: 6 December 2022).

Mello, L.A.d.S. and Tjelta, T. (2018). *Handbook of Radiowave Propagation Information for Designing Terrestrial Point-To-Points Links.* International Telecommunication Union (ITU), Geneva, Switzerland.

Naour, A.L., Pipon, F., Nahoum, B., Merel, D. & Obrist, B. (2014). Performance of the FASTNET narrowband VHF frequency hopping tactical radio in challenging multipath environments. *2014 IEEE Milit. Commun. Conf. (MILCOM 2014)*, 6–8 October 2014, Baltimore, Maryland, US.

Pugh, J.A., Bultitude, R.J.C. & Vigneron, P.J. (2006). Path loss measurements with low antennas for segmented wideband communications at VHF. *2006 IEEE Milit. Commun. Conf. (MILCOM 2006)*, 23–25 October 2016, Washington DC., US

Pugh, J.A., Bultitude, R.J.C. & Vigneron, P.J. (2007). Propagation measurements and modelling for multiband communications on tactical VHF channels. *2007 IEEE Milit. Commun. Conf. (MILCOM 2007)*, 29–31 October 2007, Orlando, Florida, US

SCADACORE (2022). *RF Line of Sight*. Available online at: https://www.scadacore.com/tools/rf-path/rf- line-of-sight (Last access date: 5 December 2022).

Shehadeh, H. A, Idris, M., Ahmedy, I., Hassen, H. R. (2020). Optimal placement of near ground VHF/UHF radio communication network as a multi objective problem. *Wirel. Pers. Commun.*, **110**: 1169–1197.

Sapura Thales Electronics (2019). *PR4G F@stnet TRC9210*. Sapura Thales Electronics. Available online at: https://www.ste.com.my/products/vhf-trc9210. (Last access date: 3 January 2021).

Weissberger, M.A. (1982). *An Initial Critical Summary of Models for Predicting the Attenuation of Radio Waves by Trees*. U.S. Department of Defense, Virginia, United States.

Yusof, A.L, Halim, H., Ya'acob, N. & Mohd Hanapiah, N.H. (2021). Performance analysis of propagation in VHF military tactical communication system. *Baghdad Sci. J.*, **18**: 1378–1386.

Zochmann, E., Guan, K. & Rupp, M. (2017). Two-ray models in mmWave communications. 2017 *IEEE 18th Int. Worksh. Sig. Proc. Adv. Wireless Commun. (SPAWC 2017)*, 3–6 July 2017, Sapporo, Japan.

EVALUATION OF MULTI-GNSS PERFORMANCE VIA GNSS SIMULATION

Dinesh Sathyamoorthy*, Hafizah Mohd Yusoff, Ahmad Firdaus Ahmad Kazmar, Mohd Zuryn Mohd Daud & Maizurina Kifli

Science & Technology Research Institute for Defence (STRIDE), Ministry of Defence, Malaysia

*Email: dinesh.sathyamoorthy@stride.gov.my

ABSTRACT

This paper is aimed at evaluating the performance of a Garmin GPSMAP 66sr multi-GNSS receiver via GNSS simulation. The study focuses on two important parameters in evaluating GNSS performance, namely performance under varying GNSS signal power levels and radio frequency interference (RFI). This study is conducted for the GPS L1 coarse acquisition (C/A) and Galileo E1 open service (OS) signals, for two conditions: 1) GPS only with six satellites (assuming an obstruction scenario with limited view of satellites); 2) GPS with six satellites and Galileo with six satellites. It is observed that at lower GNSS signal power levels and higher interference signal power levels, the higher number of GNSS signals observed for the GPS + Galileo mode allows it to have lower probable errors as compared to the GPS only mode. This highlights the advantage of multi-GNSS in degraded environments, such as dense urban and forest areas.

Keywords: *Global Navigation Satellite System (GNSS) simulation; GNSS signal power level; radio frequency interference (RFI); probable error; GNSS satellite geometry.*

1. INTRODUCTION

Global Navigation Satellite System (GNSS) refers to constellations of satellites providing signals from space that transmit positioning and timing data to GNSS receivers. It includes the four major global systems, which are Global Positioning System (GPS), Galileo, BeiDou and GLONASS, as well as regional systems such as Quasi-Zenith Satellite System (QZSS) and Navigation Indian Constellation (NAVIC). The advantage to having access to multiple satellites or multi-GNSS is for heightened accuracy, redundancy and availability. If the line of sight to satellite is obstructed, having access to multiple satellites ensures uninterrupted service provision (Knedlik, 2016; Kaplan & Hegarty, 2017; Jin *et al*., 2022).

This paper is aimed at evaluating the performance of a Garmin GPSMAP 66sr multi-GNSS receiver. It is capable to observe GPS, GLONASS, Galileo and QZSS, as well as perform dual-frequency observations for GPS, Galileo and QZSS (Garmin, 2021). The study will focus on two important parameters in evaluating GNSS performance, namely performance under varying GNSS signal power levels and radio frequency interference (RFI).

This study is conducted using GNSS simulation, which allows for the tests to be conducted with various repeatable conditions, as defined by the users. As the tests are conducted in controlled laboratory environments, they are not be inhibited by unintended signal interferences and obstructions (Pozzobon *et al*., 2013; Arul Elango & Sudha, 2016; Bi & Yuan *et al*., 2021; Emerick, 2022). In our previous studies, GNSS simulation was used to evaluate the vulnerabilities of GPS to varying power levels (Dinesh *et al*., 2012a, Dinesh, 2021), RFI (Dinesh *et al*., 2012b, 2017a, 2020), multipath (Dinesh *et al*., 2013, 2014), GPS satellite clock error (Dinesh *et al*., 2015a, 2019), varying speeds (Dinesh *et al*., 2015b, 2022), power consumption (Dinesh *et al*., 2016) and GPS antenna orientation (Dinesh *et al*., 2017b).

2. METHODOLOGY

The apparatus used in this study are an Aeroflex GPSG-1000 GNSS simulator (Aeroflex, 2010) and a notebook running GPS Diagnostics v1.05 (CNET, 2008) The study is conducted in STRIDE's semi-anechoic chamber (A. Faridz, 2010) to avoid external interferences signals and multipath errors. The following assumptions are made for the tests conducted:

i) No ionospheric or troposheric delays
ii) Zero unintended GPS satellite clock or ephemeris error
iii) No obstructions or multipath
iv) No interference signals.

The tests are conducted for coordinated universal time (UTC) times of 0000, 0300, 0600 and 0900, with the location set at Kajang, Selangor, Malaysia (N 2° 58', E 101° 48'). The almanac data for the periods is downloaded from the US Coast Guard's web site (USCG, 2022) and imported into the GNSS simulator.

Based on the functionalities of the GNSS simulator employed, this study is conducted for the GPS L1 coarse acquisition (C/A) and Galileo E1 open service (OS) signals. The GPS L1 C/A signal is an unencrypted civilian GPS signal that is widely used by various GPS receivers. The signal has a fundamental frequency of 1,575.42 MHz and a code structure that modulates the signal over a 2 MHz bandwidth (USACE, 2011; Kaplan & Hegarty, 2017; DOD, 2020). The Galileo E1 OS signal also has a fundamental frequency of 1,575.42 MHz, with a code structure that modulates the signal over a 4 MHz bandwidth (Kaplan & Hegarty, 2017; Povero, 2019; ESA, 2021).

The evaluated GNSS receiver is able to observe up to 12 satellites for the L1 / E1 signals (Wanninger *et al*., 2022). The tests are conducted for two conditions: 1) GPS only with six satellites (assuming an obstruction scenario with limited view of satellites); 2) GPS with six satellites and Galileo with six satellites.

3. VARYING GNSS SIGNAL POWER LEVELS

The setup employed to study the performance of the GNSS receiver under varying GNSS signal power levels is as shown in Figure 1. Simulated GPS signals are generated using the GNSS simulator and transmitted via the coupler. For each test, transmission is started at GNSS signal power level of -130 dBm and reduced to -180 dBm at decrements of 3 dBm and intervals of 1 min. At each power level, the GNSS receiver's values of horizontal probable error (HPE), vertical probable error (VPE) and estimate probable error (EPE) are recorded.

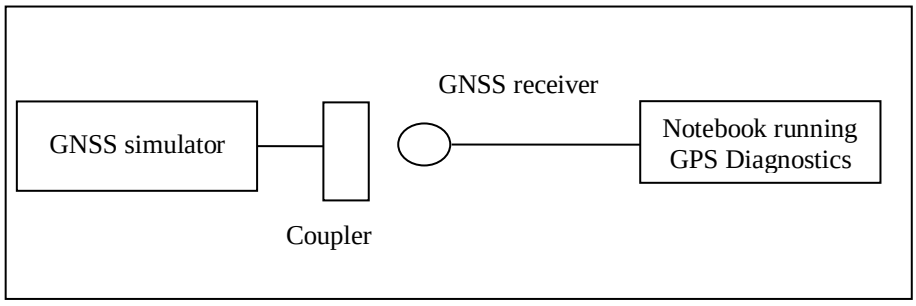

Figure 1: Test setup employed for evaluation of the effect of varying GNSS signal power levels.

As shown in Figures 2-3 and Table 1, with decreasing GNSS signal power level, probable error values increase due to decreasing carrier-to-noise density (C/N_0) levels for GNSS satellites tracked by the receiver, which is the ratio of received GNSS signal power level to noise density. Lower C/N_0 levels result in increased data bit error rate when extracting navigation data from GNSS signals, and hence, increased carrier and code tracking loop jitter. This, in turn, results in more noisy range measurements and thus, less precise positioning (Petovello, 2009; USACE, 2011; Kaplan & Hegarty, 2017; DOD, 2020).

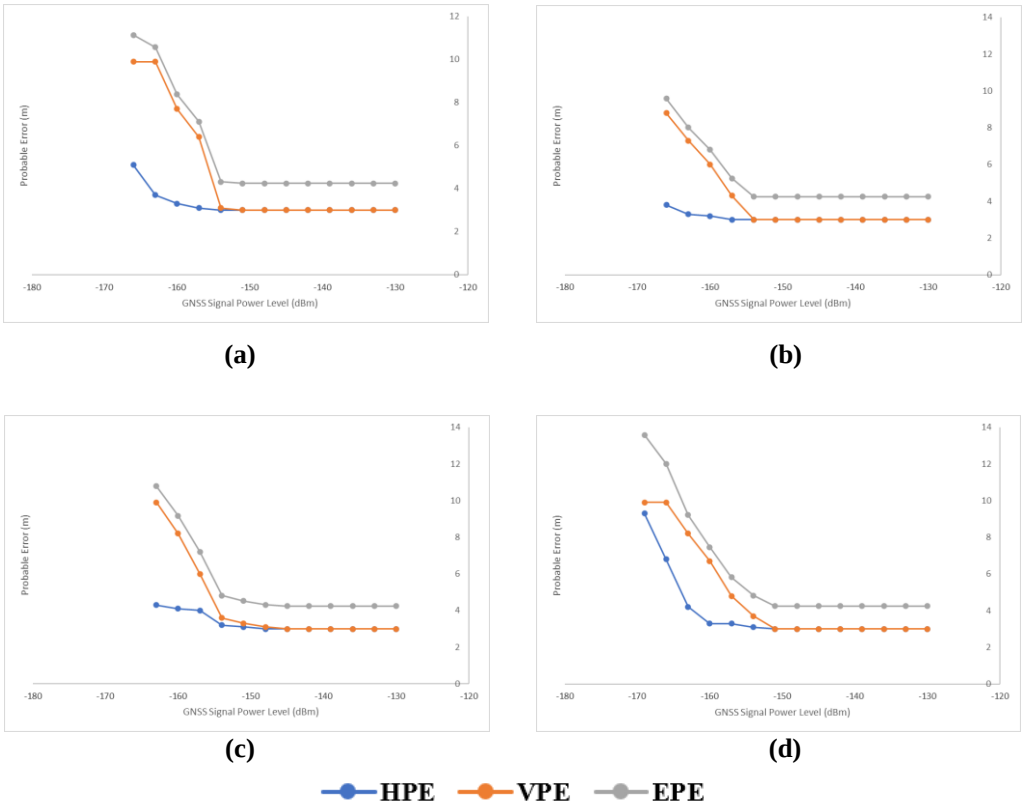

Figure 2: Recorded probable error values for the GPS only mode at UTC times of: (a) 0000 (b) 0300 (c) 0600 (d) 0900.

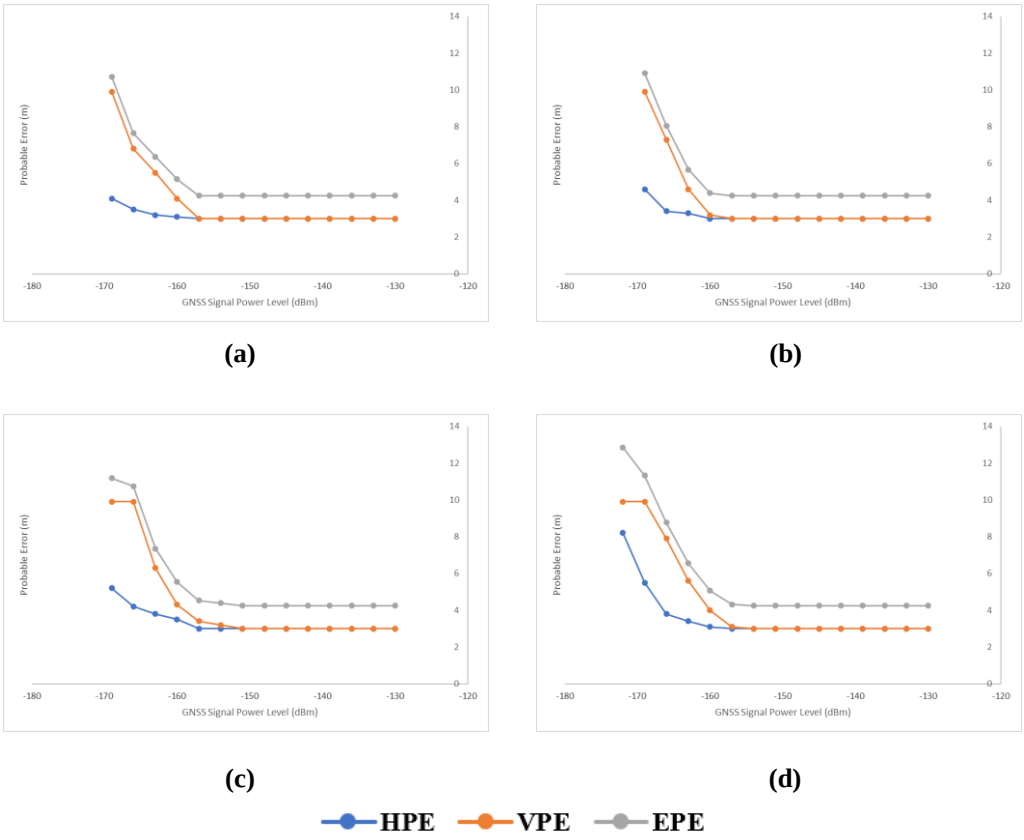

Figure 3: Recorded probable error values for the GPS + Galileo mode at UTC times of: (a) 0000 (b) 0300 (c) 0600 (d) 0900.

Table 1: GNSS signal power levels at which first degradation of accuracy is noticed and location fix is lost.

UTC Time	GNSS Signal Power Level (dBm)			
	GPS Only		GPS + Galileo	
	First degradation of accuracy	Location fix lost	First degradation of accuracy	Location fix lost
0000	-154	-169	-160	-172
0300	-157	-169	-160	-172
0600	-148	-166	-154	-172
0900	-154	-172	-157	-175

4. RADIO FREQUENCY INTERFERENCE (RFI)

The setup for the evaluation of the effect of RFI on the GNSS receiver is as shown in Figure 4. GNSS signal power level of -130 dBm is used for the tests. Interference signals are generated using an IFR 2023B signal generator (IFR, 1999) and transmitted via a Hyperlog 60180 directional antenna (Aaronia, 2009). An Advantest U3751 spectrum analyser (Advantest, 2009) is used to ensure that there are no external interference signals during the tests.

The interference signal used is a frequency modulated (FM) signal with information frequency of 5 kHz, with bandwidths of 2 and 4 MHz used. Interference signal transmission is started at power level of -140 dBm. The power level is increased by increments of 3 dBm at 1 min, and the corresponding values of HPE, VPE and EPE are recorded.

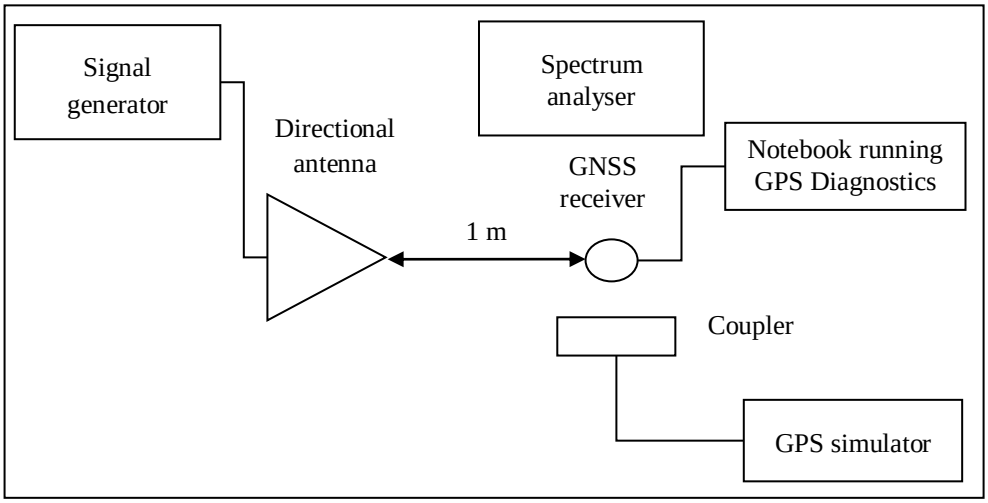

Figure 4: Test setup employed for evaluation of the effect of RFI.

As observed in Figures 5-8 and Table 2-3, with increasing interference signal power level, probable error values increase due to decreasing C/N_0 levels for GNSS satellites tracked by the receiver. For the GPS only mode, the interference signal with bandwidth of 2 MHz is found to cause larger probable error values as compared to the interference signal with bandwidth of 4 MHz. This is as for the interference signal with bandwidth of 4 MHz, the signal's strength is dispersed over a wider bandwidth.

For the GPS + Galileo mode, the differences between the probable errors caused by the interference signals with bandwidths of 2 and 4 MHz are smaller as compared to the GPS only mode. This is as the interference signal with bandwidth of 4 MHz has larger effect on the Galileo E1 OS signal that also has bandwidth of 4 MHz. An interesting scope of future study would be the effect of interference signals with various bandwidths for standalone Galileo E1 OS signal.

It is observed that the interference signal power levels required to affect the GNSS signals are significantly high as compared to the corresponding GNSS signal power levels. The noise-like GPS C/A and Galileo OS code structures, which modulate the L1 and E1 signals over 2 and 4 MHz bandwidths respectively, allow for the signals to be received at low levels of interferences. The GPS precision (P(Y)) and Galileo public regulated service (PRS) codes (restricted codes) have more robust structures, modulating the L1 and E1 signals over 20 and 24 MHz bandwidths respectively, and thus have better resistance to interference. The absence of other error parameters, including ionospheric and tropospheric delays, satellite clock, ephemeris and multipath errors, and unintentional signal interferences and obstructions, resulted in the required minimum jamming power levels in this study to be significantly higher as compared to field evaluations conducted in Dinesh *et al*. (2010) and Ahmad Norhisyam *et al*. (2013).

The tests conducted in this study employed GNSS signal power level of-130 dBm. Usage of lower GNSS signal power levels would result in reduced C/N_0 levels and hence, higher rates of increase of probable error values. In addition, the minimum interference signal power levels required to jam the GNSS receivers would also be lower.

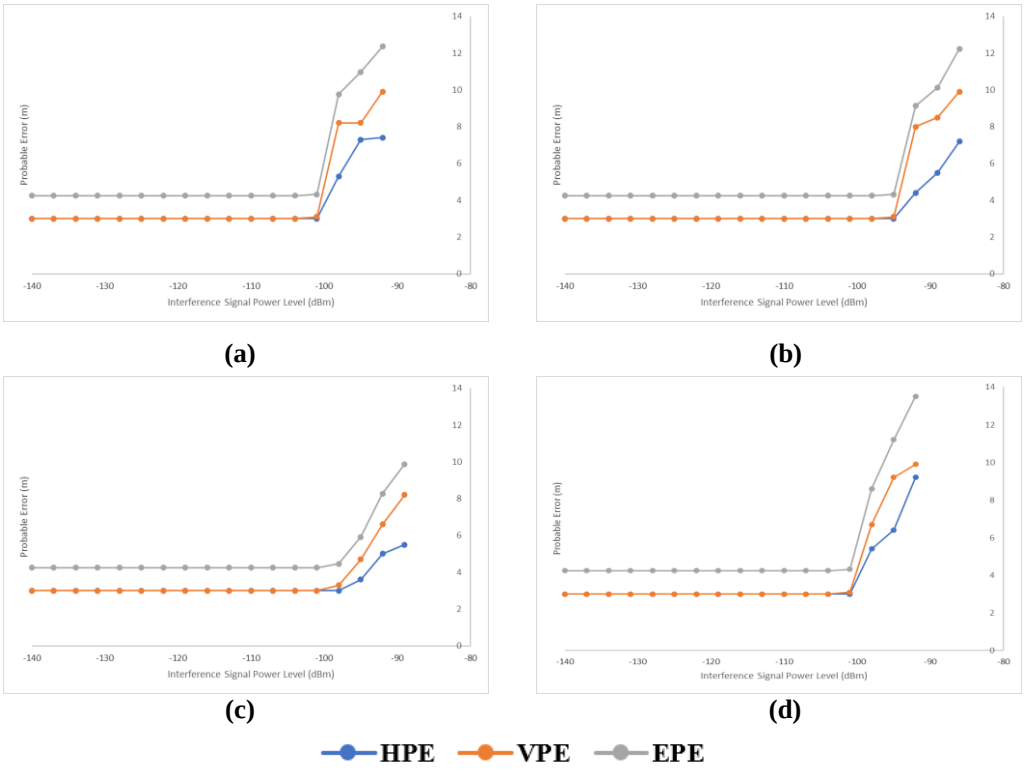

Figure 5: Recorded probable error values for the GPS only mode for interference signal bandwidth of 2 MHz at UTC times of: (a) 0000 (b) 0300 (c) 0600 (d) 0900.

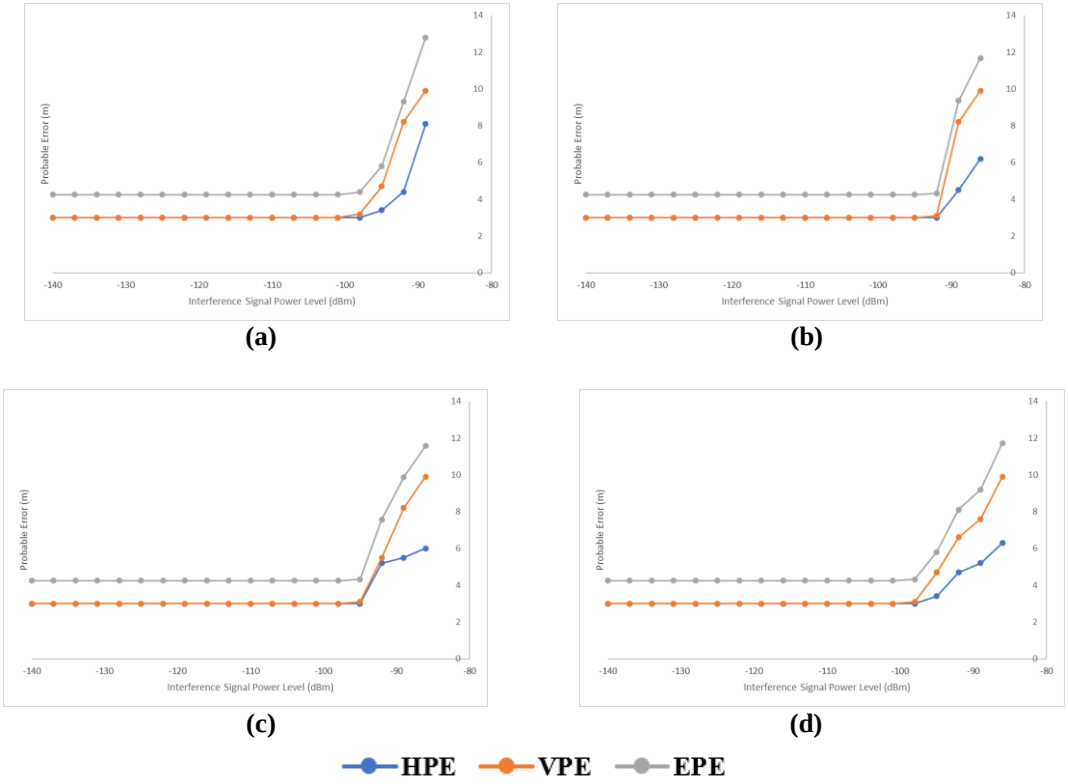

Figure 6: Recorded probable error values for the GPS + Galileo mode for interference signal bandwidth of 2 MHz at UTC times of: (a) 0000 (b) 0300 (c) 0600 (d) 0900.

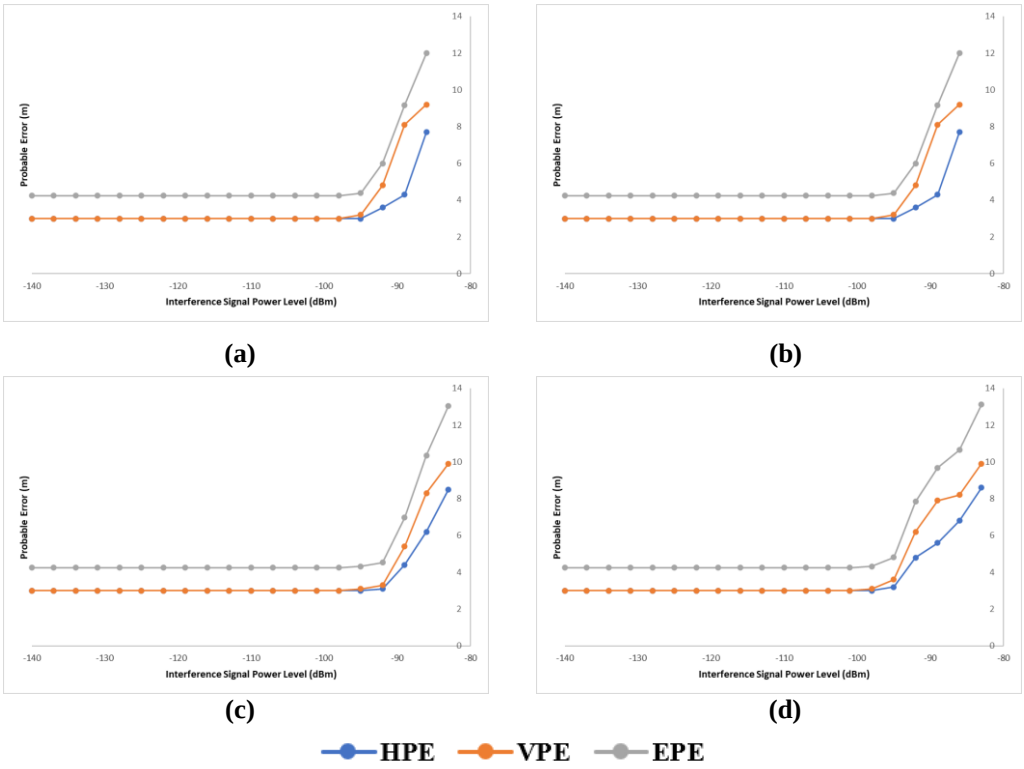

Figure 7: Recorded probable error values for the GPS only mode for interference signal bandwidth of 4 MHz at UTC times of: (a) 0000 (b) 0300 (c) 0600 (d) 0900.

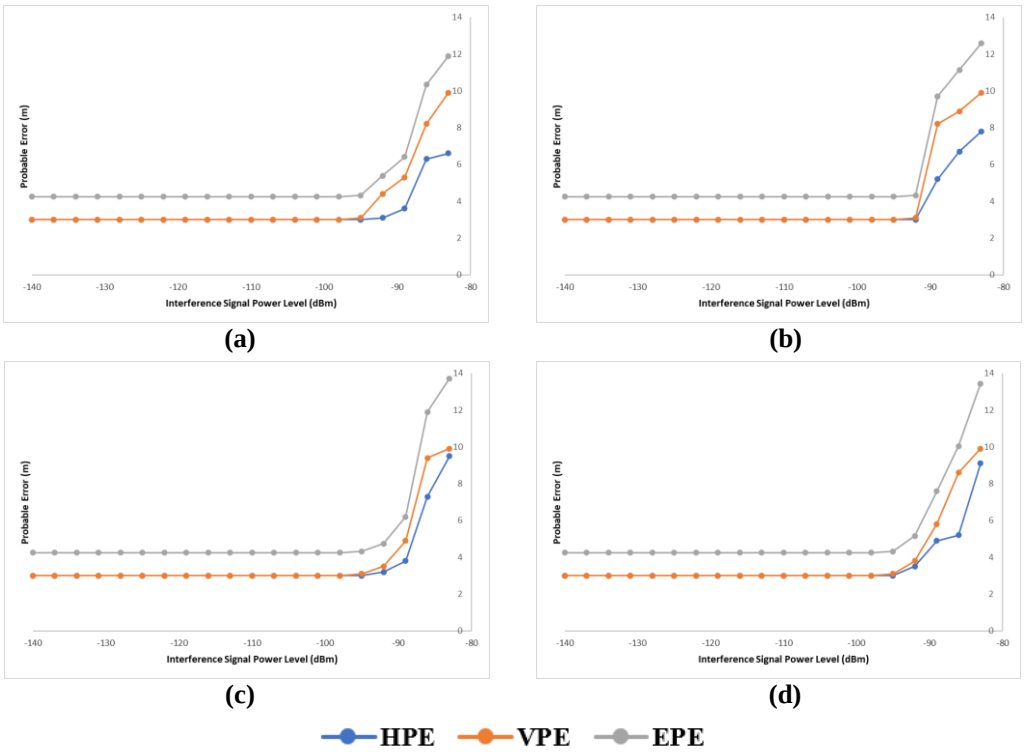

Figure 8: Recorded probable error values for the GPS + Galileo mode for interference signal bandwidth of 4 MHz at UTC times of: (a) 0000 (b) 0300 (c) 0600 (d) 0900.

Table 2: Interference signal power levels (bandwidth of 2 MHz) at which first degradation of accuracy is noticed and location fix is lost.

UTC Time	Interference Signal Power Level (dBm)			
	GPS Only		GPS + Galileo	
	First degradation of accuracy	Location fix lost	First degradation of accuracy	Location fix lost
0000	-101	-89	-98	-86
0300	-95	-83	-92	-83
0600	-98	-86	-95	-83
0900	-101	-89	-98	-83

Table 3: Interference signal power levels (bandwidth of 4 MHz) at which first degradation of accuracy is noticed and location fix is lost.

UTC Time	Interference Signal Power Level (dBm)			
	GPS Only		GPS + Galileo	
	First degradation of accuracy	Location fix lost	First degradation of accuracy	Location fix lost
0000	-95	-83	-95	-80
0300	-92	-80	-92	-80
0600	-95	-80	-95	-80
0900	-98	-80	-95	-80

5. DISCUSSION

It is observed that at higher GNSS signal power levels and lower interference signal power levels, the GPS only and GPS + Galileo modes have similar probable errors. However, at lower power levels and higher interference signal power levels, the higher number of GNSS satellites observed for the GPS + Galileo mode allows it to have lower probable errors as compared to the GPS only mode. This highlights the advantage of multi-GNSS in degraded environments, such as in dense urban and forest areas.

Varying probable error patterns are observed for each of the readings. This is due to the GNSS satellite constellation being dynamic, causing varying satellite geometry over time, resulting in GNSS accuracy being location / time dependent (USACE, 2011; Kaplan & Hegarty, 2017; DOD, 2020).

In general, values of VPE are higher as compared to HPE for GNSS readings, as overhead satellites have higher C/N_0 levels as compared to satellites above the horizon, resulting in GNSS height solution being less precise than the horizontal solution (USACE, 2011; Kaplan & Hegarty, 2017; DOD, 2020). However, for the evaluated GNSS receiver, at higher GNSS signal power levels and lower interference signal power levels, the values of VPE and HPE are similar, as the receiver's high receiver sensitivity allows for similar C/N_0 levels for overhead satellites and satellites above the horizon. At lower GNSS signal power levels and higher interference signal power levels, the values of VPE become larger than HPE, due to significant reduction of C/N_0 levels for satellites above the horizon as compared to overhead satellites.

A limitation faced in this study is that the GNSS simulator employed only allows for the transmission of the GPS and Galileo signals. While it can transmit GPS L1 / Galileo E1 and GPS L5 / Galileo E5 signals, this cannot be done simultaneously. However, the settings of the GNSS receiver's chip seem to ensure that readings can only be taken when the GPS L1 signal is available. Hence, this study could only be conducted for modes of GPS L1 only and GPS L1 + Galileo E1. In this regard, the scope for future work includes:

1) Evaluation of the GNSS receiver's dual-frequency performance using field evaluation. However, such field evaluations are subject to various error parameters, such as ionospheric and tropospheric delays, GNSS satellite clock and ephemeris errors, GNSS satellite positioning and geometry, RFI, as well as obstructions and multipath, which are uncontrollable by users (Pozzobon *et al*., 2013; Arul Elango & Sudha, 2016; Bi & Yuan *et al*., 2021; Emerick, 2022).
2) Procurement of a GNSS simulator that transmits multi-frequency GNSS signals to allow for evaluation of the performance of the GNSS receiver's dual-frequency performance using GNSS simulation.
3) Evaluation of the performance of a wider range of multi-frequency multi-GNSS receivers.

6. CONCLUSION

The findings of this study have highlighted the advantage of multi-GNSS in degraded environments. At lower GNSS signal power levels and higher interference signal power levels, the higher number of GNSS signals observed for the GPS + Galileo mode allows it to have lower probable errors as compared to the GPS only mode. Future studies will evaluate the dual-frequency performance of the evaluated GNSS receiver, as well as evaluation of a wider range multi-frequency multi-GNSS receivers.

REFERENCES

A. Faridz, A.G., M. Razali, M.Y. & W. Salwa, W.H. (2010). STRIDE's 3 meters EMC semi-anechoic chamber: Design considerations and compliance to standards. *2010 IEEE Asia-Pacific Conf. Appl. Electromagnetics (APACE 2010)*, 9-11 November 2010, Port Dickson, Negeri Sembilan, Malaysia.

Aaronia (2009). *Precompliance Test Antenna Series HyperLOG® 60xxx: Span 680 MHz to 18 GHz*. Aaronia AG, Strickscheid, Germany.

Advantest (2009). *U3741/3751 Spectrum Analyzers*. Advantest Corporation, Chiyoda-ku, Tokyo, Japan.

Aeroflex (2010). *Avionics GPSG-1000 GPS / Galileo Portable Positional Simulator*. Aeroflex Inc., Plainview, New York.

Ahmad Norhisyam, I., Dinesh, S. & Azman, M.S. (2013). Effect of radio frequency interference (RFI) on the performance of Global Positioning System (GPS) static observations. *9th IEEE Colloq. Signal Process. Appl. (CSPA 2013)*, 8-10 March 2013, Kuala Lumpur.

Arul Elango, G. & Sudha, G.F. (2016). Design of complete software GPS signal simulator with low complexity and precise multipath channel model. *J. Electr. Syst., Inform. Tech.*, **3**: 161-180.

Bi. Y. & Yuan, J. (2021). A portable GPS signal simulator design based on ZYNQ. *2nd Int. Symp. Comp. Eng. Intell. Comm. (ISCEIC 2021)*, 6-8 August 2021, Nanjing, China.

CNET (2008). *GPSDiag 1.0*. Available online at: https://download.cnet.com/GPSDiag/3000-2130_4-10055902.html (Last access date: 9 June 2022).

Dinesh, S., Wan Mustafa, W.H., Mohd Faudzi, M., Kamarulzaman, M., Hasniza, H., Nor Irza Shakhira, B., Siti Robiah, A., Shalini, S., Jamilah, J., Aliah, I., Lim, B.T., Zainal Fitry, M.A., Mohd Rizal, A.K., Azlina, B. & Mohd Hasrol, H.M.Y. (2010). Evaluation of the effect of radio frequency interference (RFI) on Global Positioning System (GPS) accuracy. *Defence S&T Tech. Bull.*, **3**: 100-118.

Dinesh, S., Mohd Faudzi., M., Rafidah, M., Nor Irza Shakhira, B., Siti Robiah, A., Shalini, S., Aliah, I., Lim, B.T., Zainal Fitry, M.A., Mohd. Rizal, A.K., & Mohd Hasrol, H.M.Y. (2012a). Evaluation of the effect of varying Global Positioning System (GPS) signal power levels on GPS accuracy. *Defence S&T Tech. Bull.*, **5**: 57-71.

Dinesh, S, Mohd Faudzi, M. & Zainal Fitry, M.A. (2012b). Evaluation of the effect of radio frequency interference (RFI) on Global Positioning System (GPS) accuracy via GPS simulation. *Defence. Sci. J.*, **62**: 338-347.

Dinesh, S., Shalini, S., Zainal Fitry, M.A. & Siti Zainun, A. (2013). Evaluation of the repeatability of Global Positioning System (GPS) performance with respect to GPS satellite orbital passes. *Defence S&T Tech. Bull.*, **6**: 130-140.

Dinesh, S., Shalini, S., Zainal Fitry, M.A., Siti Zainun, A., Siti Robiah, A., Mohd Idris, I. & Mohd Hasrol Hisam, M.Y. (2014). Evaluation of the effect of commonly used materials on multipath propagation of Global Positioning System (GPS) signals via GPS simulation. *Adv. Mil. Tech.*, **9**: 81-95.

Dinesh, S., Shalini, S., Zainal Fitry, M.A., Asmariah, J. & Siti Zainun, A. (2015a). Evaluation of the effect of Global Positioning System (GPS) satellite clock error via GPS simulation. *Defence S&T Tech. Bull.*, **8**: 51-62.

Dinesh, S., Shalini, S., Zainal Fitry, M.A., Asmariah, J. & Siti Zainun, A. (2015b). Evaluation of the accuracy of Global Positioning System (GPS) speed measurement via GPS simulation. *Defence S&T Tech. Bull.*, **8**: 121-128.

Dinesh, S., Shalini, S., Zainal Fitry, M.A., Asmariah, J. & Siti Zainun, A. (2016). Evaluation of trade-off between Global Positioning System (GPS) accuracy and power saving from reduction of number of GPS receiver channels. Appl. Geomatics, **8**: 67-75.

Dinesh, S., Zainal Fitry, M.A. & Shahrudin, A.H. (2017a). Evaluation of Global Positioning System (GPS) adjacent band compatibility via GPS simulation. *Defence S&T Tech. Bull.*, **10**: 229 – 235.

Dinesh, S., Shalini, S., Zainal Fitry, M.A., Mohamad Firdaus, A., Asmariah, J. & Siti Zainun, A. (2017b). Evaluation of the effect of Global Positioning System (GPS) antenna orientation on GPS performance. *Defence S&T Tech. Bull.*, **10**: 33-39.

Dinesh, S., Zainal Fitry, M.A & Esa, S. (2019). Evaluation of the effectiveness of receiver autonomous integrity monitoring (RAIM) in Global Positioning System (GPS) receivers. *Defence S&T Tech. Bull.*, **12**: 295-300.

Dinesh, S., Zainal Fitry, M.A, Esa, S.,Shahrudin, E.S., Ahmad Firdaus, A.K & Zaherudin, Z. (2020). Evaluation of the vulnerabilities of unmanned aerial vehicles (UAVs) to Global Positioning System (GPS) jamming and spoofing. *Defence S&T Tech. Bull.*, **13**: 333-343.

Dinesh, S. (2021). Evaluation of accuracy of Global Positioning System (GPS) receivers. *Defence S&T Tech. Bull.*, **14**: 211-216.

Dinesh, S., Hafizah, M.Y., Ahmad Firdaus, A.K. Mohd Zuryn, M.D. & Maizurina, K. (2022). Evaluation of performance of Global Positioning System (GPS) speed meters. *Defence S&T Tech. Bull.*, **15**: 222-227.

DOD (Department of Defence) (2020). *Global Positioning System Standard Positioning Service Performance Standard, Command, Control, Communications, and Intelligence, 5th Ed*. Department of Defence (DOD), Washington D.C.

Emerick, M. (2022). *EUSPA to hold GNSS Signal Simulator Manufacturers Forum in December*. Available online at: https://www.gpsworld.com/euspa-to-hold-gnss-signal-simulator-manufacturers-forum-in-december (Last access date: 23 November 2022).

ESA (European Space Agency) (2021). *European GNSS (Galileo) Open Service Signal-in-Space Interface Control Document*. European Space Agency (ESA), Paris, France.

Garmin (2021). *GPSMAP 66 Owner's Manual*. Garmin International Inc., Olathe, Kansas.

IFR (1999). *2023A/B, 2025 Signal Generators*. IFR Americas Inc., Wichita, Kansas.

Jin, S., Qisheng, W. & Dardanelli, G. (2022). *A Review on Multi-GNSS for Earth Observation and Emerging Applications*. *Remote Sens.*, **14**: 3930.

Kaplan, E.D. & Hegarty, C.J. (2017). *Understanding GPS: Principles and Applications*. Artech House, Norwood, Massachusetts.

Knedlik, S. (2016). *Introduction to Satellite Navigation, Inertial Navigation, and GNSS/INS Integration*. Springer, Berlin, Germany.

Petovello, M. (2009). Carrier-to-noise density and AI for INS / GPS integration. *Inside GNSS*, **4**: 20-29.

Povero, G. (2019). *GNSS Signals Introduction*. Links Foundation, Torino, Italy.

Pozzobon, O., Sarto, C., Chiara, A.D., Pozzobon, A., Gamba, G., Crisci, M. & Ioannides, R. (2013). Developing a GNSS position and timing authentication testbed: GNSS vulnerability and mitigation techniques. *Inside GNSS*, **8**: 45-53.

USACE (US Army Corps of Engineers) (2011). *Engineer Manual EM 1110-1-1003: NAVSTAR Global Positioning System Surveying*. US Army Corps of Engineers (USACE), Washington D.C.

USCG (US Coast Guard) (2022). *GPS NANUs, Almanacs, & Ops Advisories*. Available online at: https://www.navcen.uscg.gov/gps-nanus-almanacs-opsadvisories-sof (Last access date: 8 June 2022).

EVALUATION OF NEUROEVOLUTIONARY APPROACH TO NAVIGATE AUTONOMOUS SURFACE VEHICLES IN RESTRICTED WATERS

Nur Izzati Mohd Jalal[1], Ahmad Faisal Mohamad Ayob[1*], Shahrizan Jamaludin[1] & Nur Afande Ali Hussain[2]

[1]Maritime Technology and Naval Architecture Programme, Universiti Malaysia Terengganu (UMT), Malaysia
[2]Maritime Technology Division, Science & Technology Research Institute for Defence (STRIDE), Ministry of Defence, Malaysia

*Email: ahmad.faisal@umt.edu.my

ABSTRACT

Unmanned autonomous surface vehicles (ASVs) carry out tasks beyond human limitations, such as offshore surveillance, offshore target detection, search & rescue (SAR), bathymetry and coastal monitoring. An ASV equipped with sensors and decision-making support may operate for long duration and distances without human intervention. Although ASVs can perform autonomous navigation safely and accurately in open waters, there is a gap in the study of ASVs for river transportation and berthing. This paper uses a neuroevolution algorithm to train ASV navigation in restricted waters. Two scenarios are investigated using preliminary training data; autonomous manoeuvring in an inland waterway and autonomous berthing with the assistance of path trajectory. This work employs a geofencing method to assist ASV navigation owing to the limited detection range of distance sensors. Although the ASVs are trained for restricted waters, the results show that the proposed algorithm can adapt to different waterway environments. It is demonstrated that the neuroevolutionary technique is robust and efficient for controlling ASVs in restricted waters.

Keywords: *Neuroevolution; autonomous surface vehicle (ASV); autonomous manoeuvring and berthing; geofencing; restricted waters.*

1. INTRODUCTION

An unmanned autonomous surface vehicle (ASV) is a marine craft that operates without a pilot on board. The onboard system is completely responsible for handling safe navigation. The advantage of ASVs is to carry out tasks that are beyond human limitations, such as offshore surveillance, offshore target detections, search & rescue (SAR) (Villa *et al*., 2020), bathymetry and coastal monitoring (Nikishin *et al*., 2020). In the military sector, ASVs are used to conduct warfare and minesweeping missions since these tasks are risky to the navy's personnel (Heins *et al*., 2017). The contributions of advanced intelligent control, information technology, communications, as well as satellite positioning and navigation systems have empowered ASVs to operate effectively and robustly (Mou *et al*., 2020). Several projects such as Maritime Unmanned Navigation through Intelligence in Networks (MUNIN) (Burmeister *et al*., 2014), Advanced Autonomous Waterborne Applications Initiative (AAWA) (Rolls-Royce, 2016), ReVolt (DNV, 2014), and Yara Birkeland (Kongsberg Maritime, 2017) aim to investigate the practicality of ASVs in open seas. Such projects have proven that the operation of ASVs can bring benefits by producing zero-emission.

Researchers and technologists have conducted various kinds of research to construct a deep learning model to achieve the level of autonomy required for a surface vehicle to navigate autonomously. An ASV should typically navigate without humans actively engaging the controls. In addition, the ASV needs to avoid collisions, besides being able to navigate and berth autonomously to achieve the required

level of autonomy (Liu *et al.*, 2016; Miyauchi *et al.*, 2022). Several works on autonomous navigation were reported in the literature by Saeed *et al.* (2005), Escario *et al.* (2009), Lacki (2018) and Ayob *et al.* (2020). The reported results showed promising outcomes in demonstrating that ASVs can learn autonomous navigation via artificial intelligence. Studies on autonomous collision avoidance were conducted by Campbell & Naeem, (2012), Naeem *et al.* (2016), Kozynchenko & Kozynchenko (2018) and Cho *et al.* (2018), while studies on autonomous berthing for ASVs were caried out by Tran & Im (2012), Vu *et al*. (2016), Im & Nguyen (2018) and Liao *et al.* (2019). The literature shows that ASVs managed to avoid collision during navigation with contributions of deep learning neural networks.

This study aims to evaluate the performance of a neuroevolution algorithm to handle ASVs in different unknown restricted waters. It demonstrates that an artificial neural network (ANN) model can perform autonomous manoeuvring and berthing without re-training in the different water tracks. In addition, the performance of the ANN with different numbers of neurons and hidden layers is presented. This paper adjusts the sizes of neurons (two to nine neurons) and hidden layers (one and two hidden layers) to examine the learning performance of the ANN model.

This study also applies the geofencing method to assist path trajectory for ASVs, by incorporating geofences for manoeuvring and berthing tests. Geofencing refers to virtual boundaries for a specific geographical area that can be dynamically generated around a point location. Nowadays, geofences are widely used for the sectors such as logistics (Oliveira *et al*., 2015; Rao *et al.*, 2019), transportation (Liazos *et al.*, 2022), military (Nabi & Sujatha, 2021) and agriculture (Ilyas & Ahmad, 2020). For vehicles that operate autonomously, the geofencing method can provide boundary alerts when the vehicles exceed the boundaries (Krishnan *et al.*, 2019).

2. METHODOLOGY

In this study, an ANN model was trained using genetic algorithm (GA) to optimise the weights and biases within its architecture. The pseudo-code of the algorithm is shown in Algorithm 1. The work was initialised with the first population *P(n)* consisting of 40 agents, with each agent representing a neural net. The fitness function is evaluated within each agent to solve the autonomous manoeuvring task to steer to starboard and port according to the design of the water track. The agents that collide with objects, such as walls and boats, will be terminated in the GA process. The other agents that are not terminated will go through the selection, crossover and mutation process as shown in lines 5-7. The algorithm then sorts the population according to their fitness values. The process of identifying the next population is shown in lines 9 and 10, in which the best children were selected based on their rank to become the parent for the next generation.

Algorithm 1: Pseudo-code of GA for agents' evolution (Ayob *et al.*, 2020).

1 *n = 1;*
2 Initialize *P(n = 1);*
3 **while** termination condition is not met () **do**
4 evaluateFitness *(P(n));*
5 *P(n)* = selectIndividual *(P(n));*
6 *P(n)* = crossover*(P(n));*
7 *P(n)* = mutation *(P(n));*
8 sortFitness *(P(n));*
9 $P_c(n)$ = selectParent *(P(n));*
10 *P(n)* = $P_c(n)$ // Children population become parent for next generation;
11 *n = n + 1;*
12 **end**

In this case study, the architecture of the ANN (Figure 1) is fixed with 10 input neurons (nine distance sensors and one velocity) and two neurons in the output layer (rudder angle and percentage of thrust). In this work, the comparison of architectures of ANN with single- and two-hidden layers is presented. The number of neurons for the single hidden layer is set from 2 to 9. For the structure of the ANN with two hidden layers, the study is initiated with the first hidden layer having 2 fixed neurons, and the second hidden layer is set up from 2 to 9 neurons. The feedforward method is used as the learning process to determine the weights and biases to produce the output values as presented in the mathematical model, as shown in Equation 1. The activation input neuron (α) is multiplied by weight (w) with the presence of bias (b). An activation function (σ) is incorporated to non-linear output values to prevent the neural network from being a linear regression model. In this work, the *tanh* activation function (Equation 2) is used in the ANN to produce positive and negative values.

$$\sigma(w_1\alpha_1 + w_2\alpha_2 + w_3\alpha_3 + \ldots\ldots + w_n\alpha_n + b \tag{1}$$

where;

σ = Activation function
w = Weight
α = Activation
b = Biases

$$tanh\,(x) = \frac{2}{(1+ e^{-2x})-1} \tag{2}$$

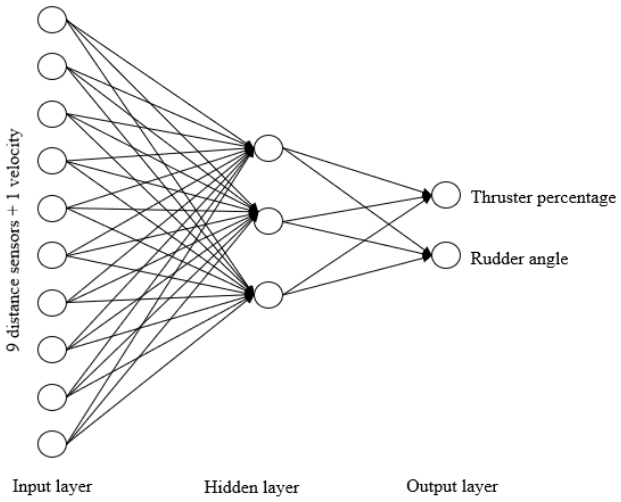

Figure 1: Architecture of the ANN.

Figure 2 shows the ASVs used in this study, with their physical parameters given in Table 1. Section 2.1 explains the training of the USVs, while the testing of the ASVs to perform autonomous manoeuvring in different water tracks and autonomous berthing in a port are explained in Sections 2.2 and 2.3 respectively.

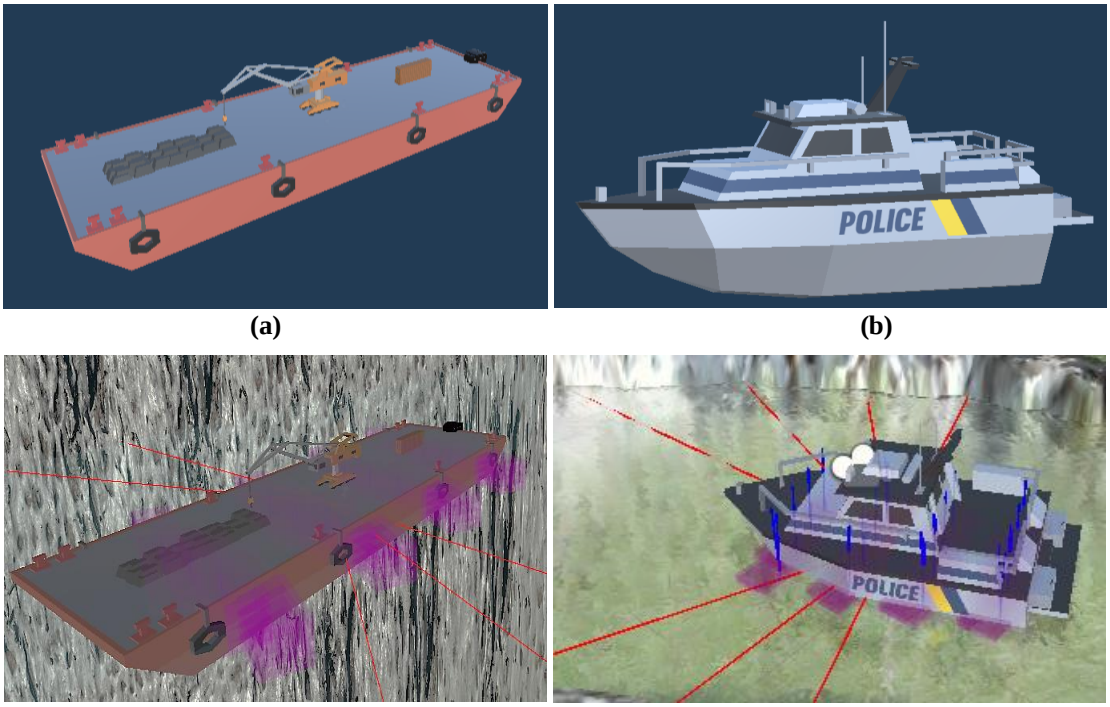

(a) **(b)**

(c) **(d)**

Figure 2: The ASVs used in this study: (a) Autonomous barge; (b) Autonomous boat; (c) Autonomous barge with sensors arrays indicated by lines; (d) Autonomous boat with sensors arrays indicated by lines.

Table 1: Physical parameters of the ASVs used in this study.

Parameters	Boat	Barge
Length	4.40m	60 m
Breadth	2.48m	25 m
Depth	0.30m	5 m
Draft	0.20m	1 m
Displacement	1.09 m^3	270 m^3

The governing equation that models the physics of the USVs are shown in Equations 3 and 4. The physical motions of the USVs are defined by buoyancy (Wongsuwan & Huntula, 2019) and resistance model. This is to ensure that the approximation of the physics is closer to real-life operations.

$$F_B = \rho V g \tag{3}$$

where;

F_B = Buoyant force
ρ = Water density
V = Water volume
g = Earth gravity

$$F_D = \frac{C\rho A v^2}{2} \tag{4}$$

where;

F_D = Drag force

C = Drag coefficient
ρ = Water density
A = Area of ASV
v^2 = ASV's velocity

2.1 Training for the ASV

The neural network training utilised GA (neuroevolution) to create an autonomous boat that navigates on a water track, as shown in Figure 3. The acquired model from the training session is applied to the autonomous barge to perform the manoeuvring test in a river track, which is discussed in Section 2.2. The autonomous boat is equipped with nine distance sensors to assist it in decision-making to steer to starboard or port while it manoeuvres in a water track consisting of three straight trajectories, four 90º sharp corners, five 45º curved corners and three small boats aligned in the straight trajectory.

The training session starts with a population containing 40 units of agents evolved to produce the best agent that carries the best performing output values that maximise the distance in the track without collision. Then, the agent inherits the ANN's output to the next generation until the 100th generation. The acquired ANN model will be applied in the ASVs to perform testing, which is further discussed in Sections 2.2 and 2.3.

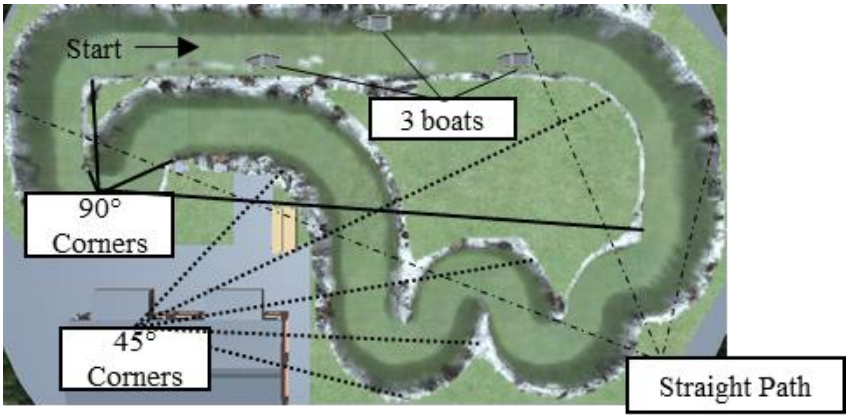

Figure 3: Training track for the USVs.

2.2 Testing for Autonomous Manoeuvring

In the testing session for autonomous manoeuvring, the autonomous barge is used to navigate in a water track, as shown in Figure 4. The water track is adopted based on a natural river track in Pahang, namely Sungai Pahang, which is the longest river in Peninsular Malaysia. Sungai Pahang is chosen for this experiment because it is a centre of sand mining, where barges carry sand from the river to the land. These barges operate at 5 knots, with significant time spent on handling. Therefore, an autonomous barge may be beneficial to reduce the operational time and cost.

In this work, a 65 km stretch of Sungai Pahang is modelled, with 1 km width for the river body and 2.2 km width for the river mouth. The autonomous barge presented in this work has nine distance sensors with a detection range of 50 m. With the limitation of range sensor detection, the geofencing method is proposed to assist the autonomous barge in completing the manoeuvring across the river. In this work, the geofences shown in Figure 4 are aligned on both the right and left sides of the autonomous barge, with the distance of fences being 35 m to assist the autonomous barge to manoeuvre.

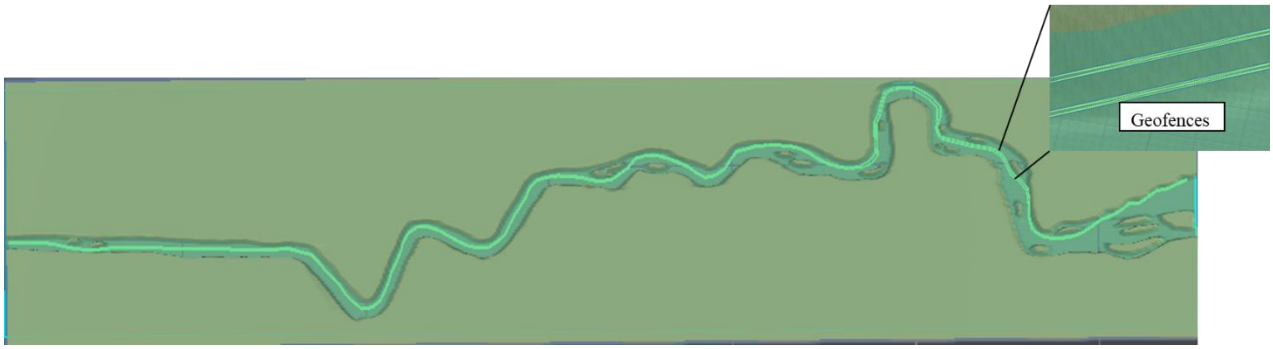

Figure 4: A testing track (Sungai Pahang) with geofences for an autonomous barge.

2.3 Testing for Autonomous Berthing

This section elaborates on the experiment for autonomous berthing in a simulated port, as shown in Figure 5. For the berthing process, the autonomous boat manoeuvres from the open sea to conduct course-changing procedure to enter the assigned wharf. When the autonomous boat approaches the wharf, it reduces its velocity before it stops the engine (no velocity). Similar to the trained model, the autonomous boat relies on nine distance sensors to move forward, with each distance sensor able to detect obstacles and buildings within 50 m. Since the simulated port is vast, the geofencing method is applied to resolve the limitation of sensor detection to assist the boat in manoeuvring and performing berthing. The geofences are aligned for the starboard and port sides for 120 m to guide the boat's trajectory.

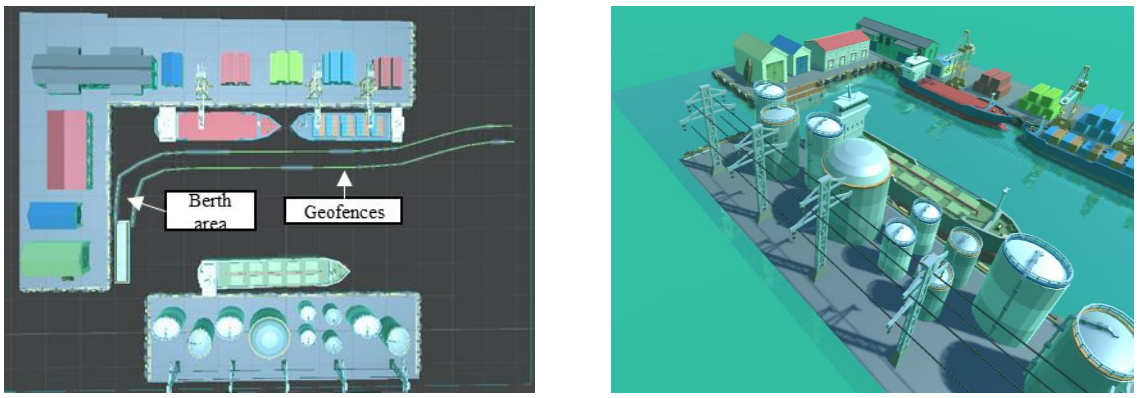

(a) **(b)**

Figure 5: The berthing track for conducting autonomous berthing: (a) Top view of the berth track with geofences. (b) Side view of the environment of the port.

2.4 Examine the learning behaviour for ANN models.

This section presents the experiment to examine the performance of ANN models with different numbers of neurons in hidden layers. This work compared the learning of ANN with single- and two-hidden layers to carry out the manoeuvring task in the water track in Figure 3. This study examines the size of neurons from two to nine neurons. The ANN's architectures with two hidden layers will examine when the first hidden layer has fixed size (two neurons) and the second hidden neurons are set up from two to nine neurons. Then, the work examines the ANN's learning when the ANN has two hidden layers, where the first hidden layer is set to two to nine neurons, while the second hidden layer has fixed size (two neurons). Figure 6 shows the architecture of the ANN models for single- and two- hidden layers that are used to study the learning behaviour of ANNs.

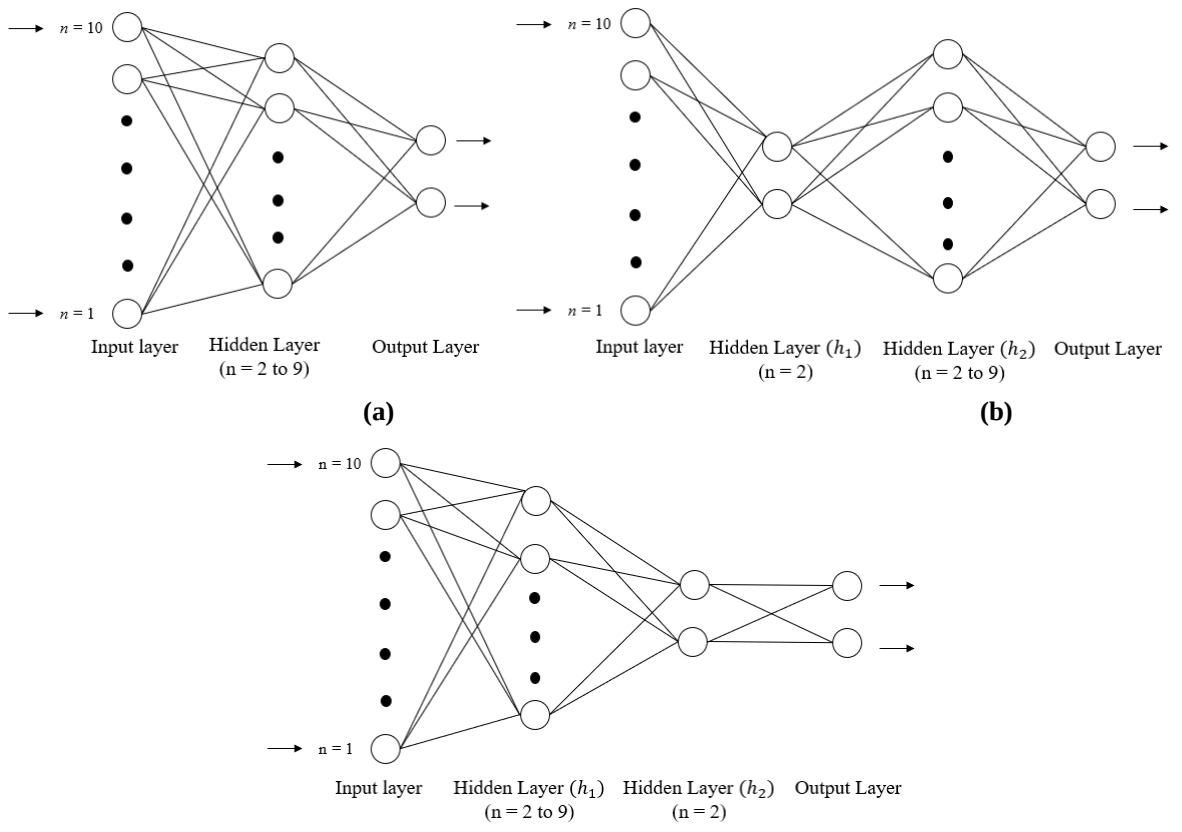

Figure 6: The architectures of the ANN models used to examine the learning performance for ANN: (a) Single hidden layer. (b) Two hidden layers with first hidden layer having fixed size neurons. (c) Two hidden layers with second hidden layer having fixed size neurons.

3. RESULTS AND DISCUSSION

This section is separated into four sub-sections, in which Section 3.1 elaborates on the training of ASVs, while Sections 3.2 and 3.3 discuss the testing results for autonomous manoeuvring and berthing. Section 3.4 compares the learning performances of the ANN's single and double hidden layers.

3.1 Training of the ASVs

Figure 7 shows the up and down spikes of the thrust percentage and rudder angle due to the ANN model's responses along the autonomous boat's training track. Positive values show the ASV turning to the right, while negative values show the ASV turning to the left. Figure 7(a) shows that the rudder angle tends to steer the rudder to starboard and port more than 20° when it passes the last boat at the straight trajectory (t = 22 and 24 s) and manoeuvres at 45° corners. It shows that the autonomous boat is capable for safe manoeuvring while course-changing. The characteristic of the ANN model for rudder angle shows that it is biased to steer to starboard due to the waterway setup.

Figure 7(b) presents the thrust percentage produced with an average value of 99%. It shows that the percentage of thrust reduces below 99% when the autonomous boat avoids the small boats and manoeuvres in the corners. The velocity values influenced the thrust percentage across the operation since velocity is one of the input neurons of the ANN model. The velocity reduction indicates that the ASV can make decisions to ensure safe manoeuvring.

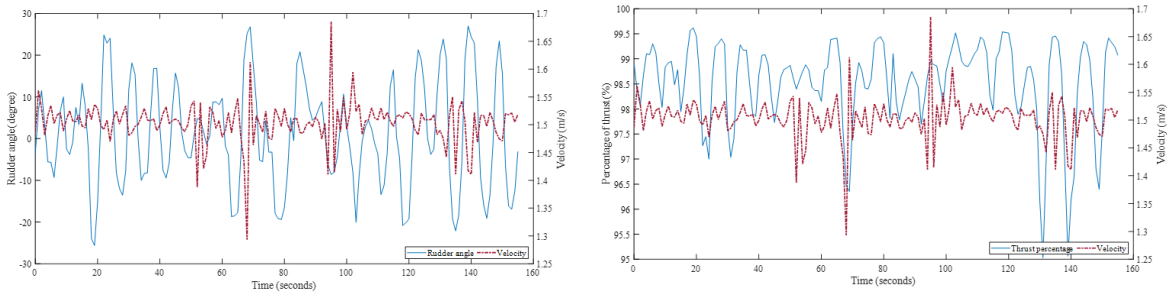

(a) **(b)**

Figure 7: Training performance for autonomous manoeuvring: (a) Rudder angle (b) Percentage of thrust.

3.2 Testing for Autonomous Manoeuvring

The resulting training model from the previous section is incorporated into the autonomous barge to test the manoeuvring capability in the river with curvy corners. In this simulation, the autonomous barge took 916 min (approximately 15 hours) to complete the manoeuvring. Figure 8(a) shows that the rudder aggressively turned to large angles at the 100th 200th, and 700th min. Such significant values of rudder angle are due to the ANN model's response and the wide position of geofences. Figure 8(b) presents the percentage of thrust produced by autonomous barge across manoeuvring with an average percentage of 99%, indicating that the autonomous barge is operating in a stable cruise throughout the path.

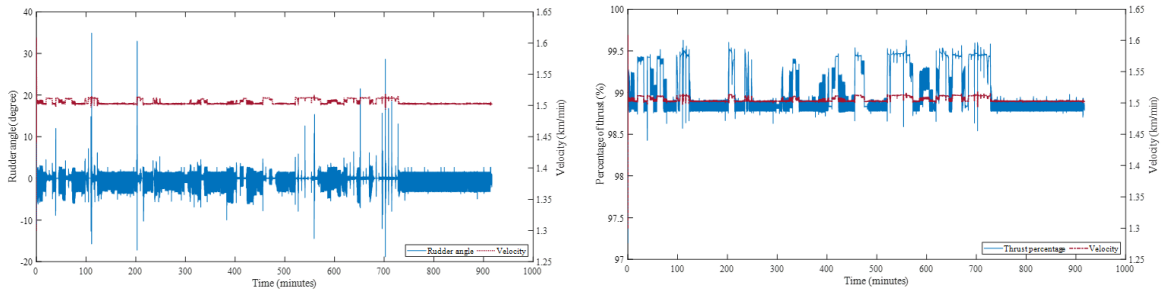

(a) **(b)**

Figure 8: Results for autonomous manoeuvring of the autonomous barge in Sungai Pahang: (a) Rudder angle (b) Thrust percentage.

3.3 Autonomous Surface Vehicle Test in a Simulated Port

This part incorporates the resulting ANN model acquired from the training session to test its capability to perform in a different water track. Based on Figure 9, the autonomous boat completed the operation within t = 90 s for a distance of 120 m. At t = 75 s, the boat changes direction to enter the assigned berth area. Then, the boat is ready to berth by decelerating its velocity from 1.5 m/s and slowly stopping its engine (0 m/s). The velocity reduction is caused by the percentage of thrust reduced from 99% to 89%, as shown in Figure 9(b). In addition, Figure 9(a) shows that the rudder angle turned to 14º when the boat made a course change to the berth area, indicating that the vessel is capable to manoeuvre autonomously and safely. The rudder angle oscillates to the starboard and port while the boat manoeuvres in a straight trajectory, indicating that the ANN model responded to the geofence to ensure a safe cruise.

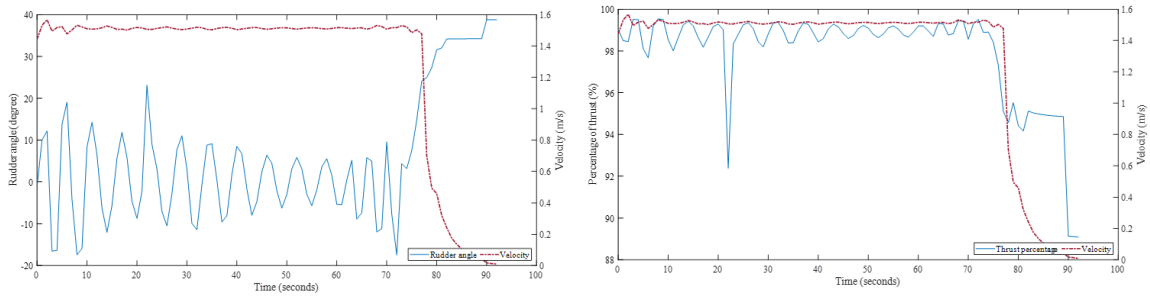

(a) **(b)**

Figure 9: Performance of autonomous berthing for the autonomous boat: (a) Rudder angle (b) Percentage of thrust.

3.4 Comparison of Learning Performance for Single and Double Hidden Layers of ANN

This section discusses the analysis of the performance of the ANN model with different numbers of nodes in the hidden layer. The experiment is conducted with three different setups of the ANN architectures. The experiment began with simulating an ASV with a single hidden layer, with the simulation repeated with different numbers of hidden neurons (HN). Figure 10 presents the results of a single hidden layer of ANN with different sizes of hidden neurons.

Next, the simulation is carried out by setting up the structure of ANN with two hidden layers. In the first case, the first hidden layer has fixed sizes of hidden neurons (two neurons), while the second hidden layer incorporates variables size of hidden neurons (Figure 11). For the second case, size of hidden neurons is variable in the first hidden layer, while the size of hidden neurons in the second hidden layer is fixed (two neurons) (Figure 12).

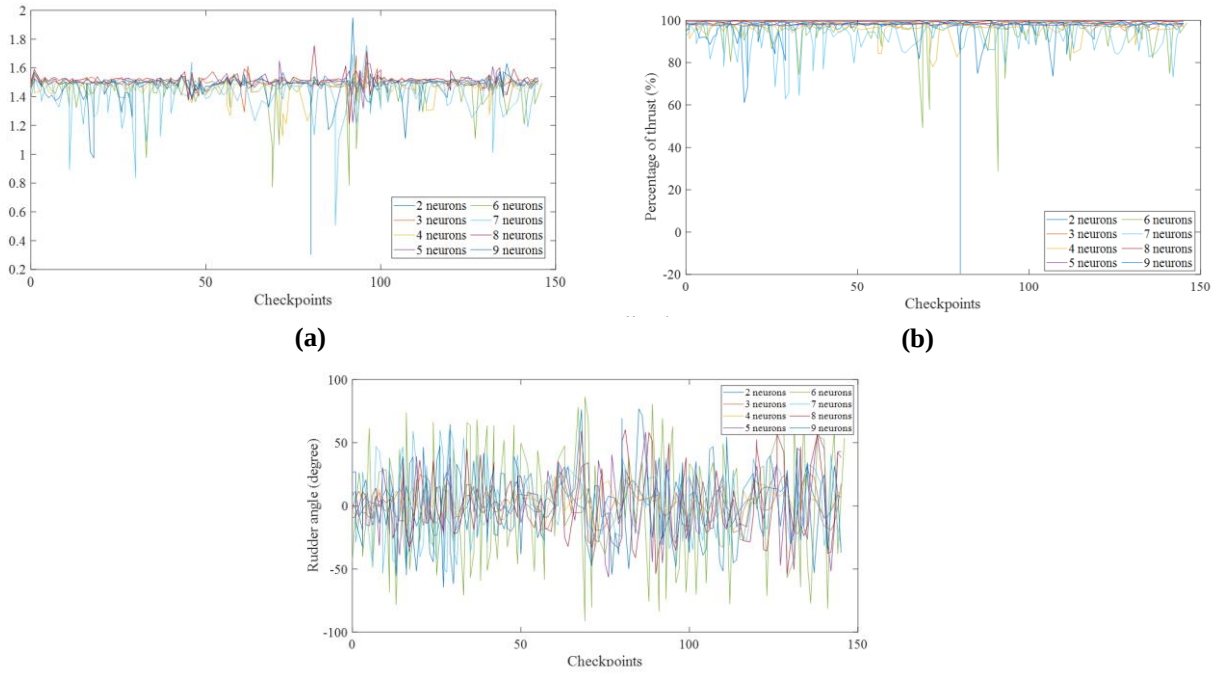

(a) **(b)**

(c)

Figure 10: Comparison of performance of the ANN for different numbers of neurons in a single hidden layer: (a) Velocity (b) Percentage of thrust (c) Rudder angle.

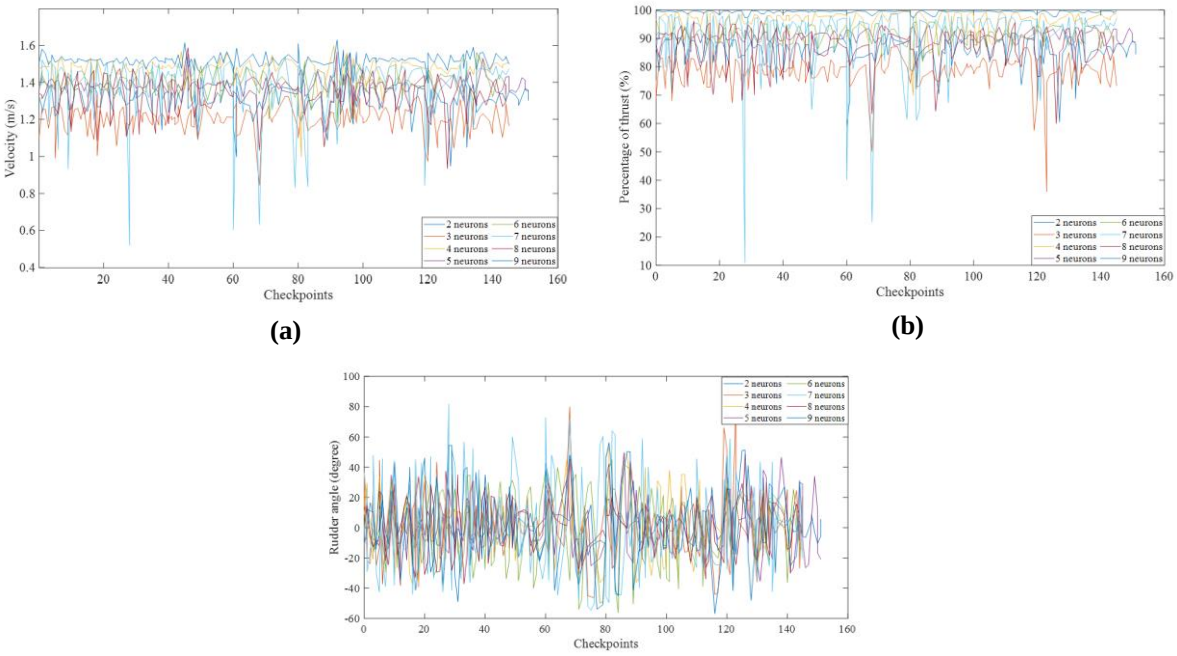

(a) **(b)** **(c)**

Figure 11: Comparison of performance of an ANN with two hidden layers with different numbers of neurons in the second hidden layer: (a) Velocity (b) Percentage of thrust (c) Rudder angle.

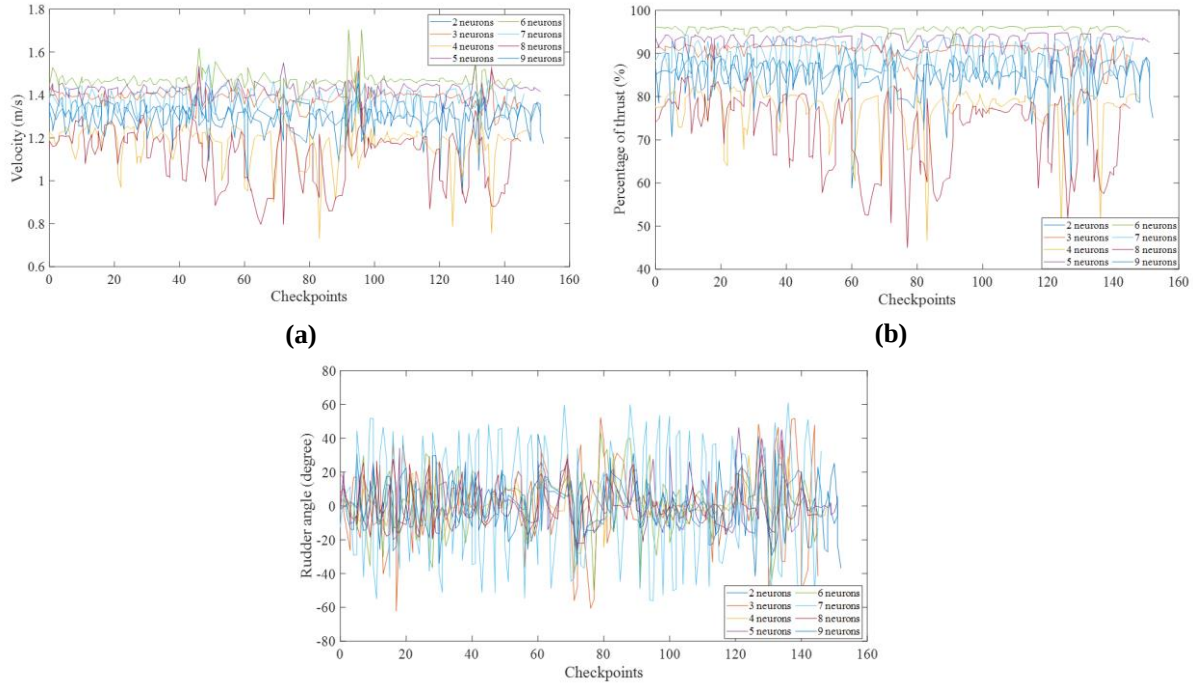

(a) **(b)** **(c)**

Figure 12: Comparison of performance of the ANN with two hidden layers with different numbers of neurons in the first hidden layer: (a) Velocity (b) Percentage of thrust (c) Rudder angle.

Figures 13 to 15 present the standard deviations (SD) for the ANN's performance when the ASV is steering in one of the straight trajectories and curvy corners (45°). The objective of examining the performance of the different neuron numbers is to determine which number shows the best performance for safe manoeuvring. Figures 14 and 15 show that the SD for six neurons in one hidden layer produced significant values for thrust percentage and rudder angle, indicating that the ANN model produced an unstable manoeuvring characteristic.

The ANN's learning with the architecture incorporating two hidden layers shows good performance in steering the rudder angle for safe manoeuvring. Figures 13 and 14 show that the velocity and thrust percentage produced high SD values when the ANN consists of seven neurons in the first hidden layer, while the second hidden layer is fixed with two neurons. Meanwhile, good performance is observed for thrust percentage and velocity for the ANN with seven neurons in the second hidden layer, while the first hidden layer has fixed two neurons. Based on the results shown for the SD values, the structure of ANN with seven neurons in the second hidden layer for two hidden layers is more stable than seven neurons in the first hidden layer.

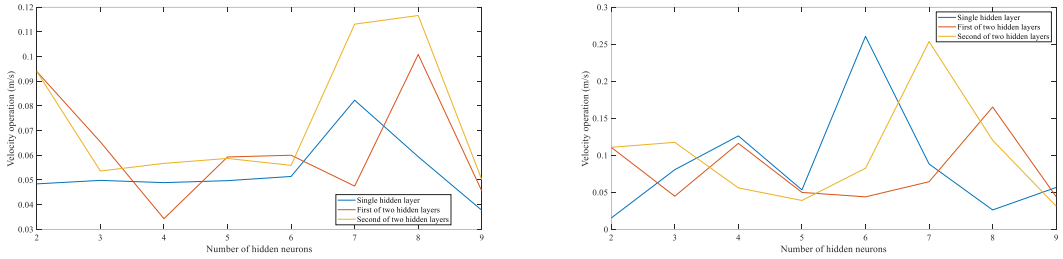

(a) **(b)**

Figure 13: Comparison of SD of velocity during ASV manoeuvring: (a) At a straight path (b) At 45° corner.

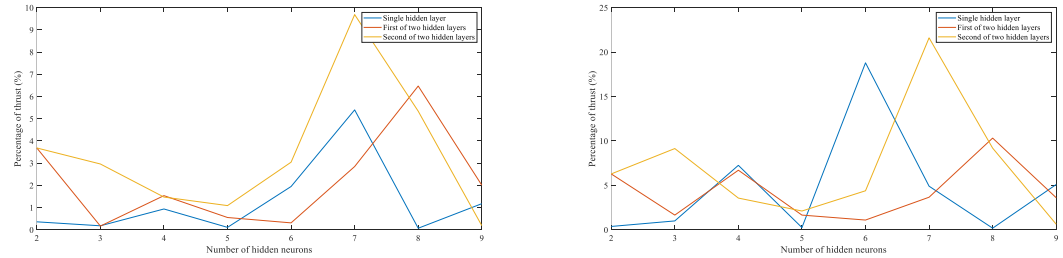

(a) **(b)**

Figure 14: Comparison of SD of the percentage of thrust during ASV manoeuvring: (a) At a straight path (b) At 45° corner.

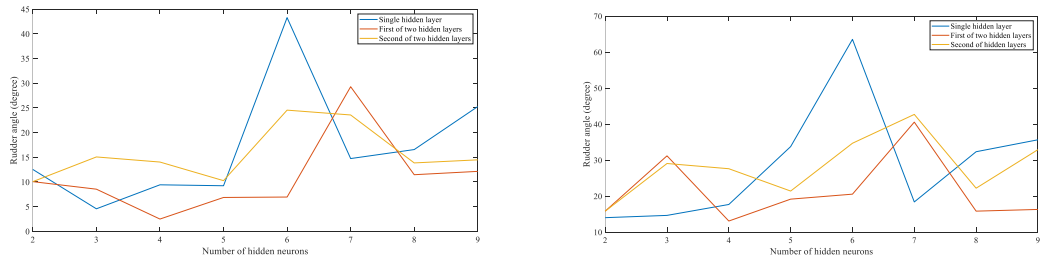

(a) **(b)**

Figure 15: Comparison of SD of rudder angle during ASV manoeuvring: (a) At a straight path (b) At 45° corner.

4. CONCLUSION

This work has presented the analysis of a neuroevolutionary model to train two types of ASVs to navigate in restricted waters. The results of the ANN model for rudder angle indicate that the ANN's sensitivity responded to the objects in the surroundings, such as walls and small boats, for collision avoidance. The characteristics of the waterway setup reflect that the ANN model is biased to turn the rudder angle to the starboard. The production of thrust percentage indicates that the ANN model can keep stable manoeuvring, although the ASV manoeuvres in challenging corners and avoids objects.

Based on the analysis of the performance of ANN with various numbers of neurons and hidden layers, it is shown that six and seven neurons for single- and two-hidden layers produced unstable manoeuvring characteristics. The ANN's learning with various numbers in the second hidden layer, while the first hidden layer had fixed size, performed well. When the ANNs learned with two hidden layers, the rudder angle showed good manoeuvring.

ACKNOWLEDGEMENT

The work presented in this research article is funded by Universiti Malaysia Terengganu (Research Intensified Grant Scheme, RIGS, Grant Number: 55192/12) under the theme of Technology & Engineering (Infrastructure and Transportation).

REFERENCES

Ayob, A., Jalal, N., Hassri, M., Rahman, S. & Jamaludin, S. (2020). Neuroevolutionary autonomous surface vehicle simulation in restricted waters. *Int. J.Mar. Nav. Safety of Sea Trans.*, **14**: 866-873.

Burmeister, H. C., Bruhn, W. C., Rodseth, O. J. & Porathe, T. (2014). Can unmanned ships improve navigational safety? *Trans. Res. Arena*, (pp. 1-10). Paris

Campbell, S. & Naeem, W. (2012). A rule-based heuristic method for COLREGS-compliant collision avoidance for an unmanned surface vehicle. *Int. Fed. Auto. Control*, 19-21 September 2012, Arenzano, Italy.

Cho, Y., Han, J. & Kim, J. (2018). Intent inference of ship manoeuvring for automatic ship collision avoidance. *Int. Fed. Auto. Control*, **51**: 384-388.

DNV (2014). *The ReVolt - A New Inspirational Ship Concept*. Available online at: https://www.dnv.com/technology-innovation/revolt/ (Last access date: 17 May 2022)

Escario, J., Jimenez, J.F. & Giron Sierra, J. (2009). Autonomous ship manoeuvring planning based on the ant colony optimisation algorithm. *Proc.8th IFAC Int. Conf. Manoeuvring and Control Mar. Craft*, 16-18 September 2009, Guarujá (SP), Brazil.

Heins, P.H., Jones, B.L. & Taunton, D.J. (2017). Design and validation of an unmanned surface vehicle simulation model. *Appl. Math. Modelling*, **48**: 749-774.

Ilyas, Q.M. & Ahmad, M. (2020). Smart farming: An enhanced of pursuit of sustainable remote livestock tracking and geofencing using IoT and GPRS. *Wire. Commun. Mob. Comp.*, **Vol. 2020**: 1-12.

Im, N.K. & Nguyen, V.S. (2018). Artificial neural network controller for automatic ship berthing using head-up coordinate system. *Int. J. Nav. Arch. Ocean*, **10:** 235-249.

Kongsberg Maritime (2017). *Autonomous ship project, key facts about YARA Birkeland*. Available online at: https://www.kongsberg.com/maritime/support/themes/autonomous-ship-project-key-facts-about-yara-birkeland/ (Last access date: 17 May 2022).

Kozynchenko, A.I. & Kozynchenko, S.A. (2018). Applying the dynamic predictive guidance to ship collision avoidance: Crossing case study simulation. *Ocean Eng.*, **164**: 640-649.

Krishnan, M.M., Saveetha, D., Jovith, A.A. & Rajasekar, P. (2019). Fisherman navigation and safety system. *Int. J. Inno. Tech. Exp. Eng.*, **8**: 5762-5766.

Lacki, M. (2018). Indirect encoding in neuroevolutionary ship handling. *Int. J.Mar. Nav. Safety of Sea Trans.,* **12**: 71-76.

Liao, Y., Jia, Z., Zhang, W., Jia, Q. & Li, Y. (2019). Layered berthing method and experiment of unmanned surface vehicle based on multiple constraints analysis. *Appl. Ocean Res.,* **86:** 47-60.

Liazos, A., Iliopoulou, C., Kepaptsoglou, K. & Bakogiannis, E. (2022). Geofence planning for electric scooters. *Trans. Res. P. D,* **102**: 1-17.

Liu, Z., Zhang, Y., Yu, X. & Yuan, C. (2016). Unmanned surface vehicles: An overview of developments and challenges. *Annu. Rev. Contr.,* **41**: 71-93

Miyauchi, Y., Sawada, R., Akimoto, Y., Umeda, N. & Maki, A. (2022). Optimisation on planning trajectory and control of autonomous berthing and unberthing for the realistic port geometry. *Ocean Eng.*, **245**: 1-15.

Mou, J., He, Y., Zhang, B., Li, S. & Xiong, Y. (2020). Path following of a water-jetted USV based on manoeuvrability tests. *J. Mar. Sci. Technol.,* **8**: 1-18.

Nabi, A. & Sujatha, D. B. (2021). Autonomous army robot with geofencing technology. *Int. J. Adv. Res. Comput. Commun. Eng.,* **10**: 855-862.

Naeem, W., Henrique, S. & Hu, L. (2016). A reactive COLREGs - Compliant navigation strategy for autonomous maritime navigation. *Int. Fed. Auto. Control,* **49**: 207-213.

Nikishin, V., Durmanov, M. & Skorik, I. (2020). Autonomous unmanned surface vehicle for water surface monitoring. *Int. J. Mar. Nav. Safety of Sea Trans.,* **14**: 853-858.

Oliveira, R.R., Cardoso, I.M., Barbosa, J.L., Costa, C.A. & Prado, P.M. (2015). An Intellight model for logistics management based on geofencing algortithms and RFID technology. *Exp. Systems Appl.,* **42**: 6082-6097.

Rao, S., Pydee, S.P., Tripathi, S.K. & Halakundi, S. (2019). Automobile speed control using geo-fencing. *J. Emerging Tech. Innovation Res.*, **6**: 233-235

Rolls-Royce (2016). *Autonomous ships The next step*. Available online at: https://www.rolls-royce.com/~/media/Files/R/Rolls-Royce/documents/%20customers/marine/ship-intel/rr-ship-intel-aawa-8pg.pdf (Last access date: 17 May 2022).

Saeed, A., Attia, E., Helmy, A. & Awad, T. (2005). Design of a neuro-autopilot manoeuvring controller for underactuated ships. *Alexandria Eng. J.,* **44**: 493-500.

Tran, V.L. & Im, N. (2012). A study on ship automatic berthing with assistance of auxiliary devices. *Int. J. Nav. Arch. Ocean,* **4**: 199-210.

Villa, J., Aaltonen, J., Virta, S. & Koskinen, K. T. (2020). A cooperative autonomous offshore system for target detection using multi-sensor technology. *Remote Sens.,* **12**: 1-24.

Vu, M.T., Choi, H.S., Oh, J.Y. & Jeong, S.K. (2016). A study on automatic berthing control of an unmanned surface vehicle. *J. Adv. Res. Ocean Eng.,* **4:** 192-201.

Wongsuwan, W. & Huntula, J. (2019). The students' basic conceptions by buoyant force. *J. Phy. Conf. Ser.*, **1380**: 012139

EXPERIMENTAL INVESTIGATION AND FINITE ELEMENT METHOD SIMULATION OF TIME DOMAIN PULSED EDDY CURRENT TECHNIQUE ON NON-FERROMAGNETIC CONDUCTIVITY PLATES

Nurul A'in Ahmad Latif [1,2*], Ilham Mukriz Zainal Abidin[2], Nordin Jamaludin[1] & Mohd Zaki Nuawi[1]

[1]Department of Mechanical and Materials Engineering, Faculty of Engineering and Built Environment Universiti Kebangsaan Malaysia (UKM), Malaysia
[2]Leading Edge NDT Technology (LENDT) Group, Industrial Technology Division, Malaysian Nuclear Agency, Malaysia

[*]Email: nurul_ain@nuclearmalaysia.gov.my

ABSTRACT

Pulsed eddy current (PEC) is an advanced non-destructive testing (NDT) technique based on the electromagnetic principle. The excitation consists of a broad frequency spectrum for detection of defects in various depths of specimens. This paper details out the experimental and simulation investigations in determining the correlation between PEC signals and conductivity of different non-ferromagnetic materials. The finite element method (FEM) simulation work provided understanding on the underlying phenomena by visualising the eddy current density and magnetic field distribution in specimens with varying conductivity values. The FEM results show that conductivity affects the induced current density within the specimens. Specimens with high conductivities generate high current density within the specimen, which increases the net magnetic field acquired from the specimen. In addition, the results obtained from the conductivity experiments demonstrated good agreement with that of the FEM simulation. Both approaches generate increment in the amplitude of the net magnetic field acquired from specimens with different conductivity values.

Keywords: *Pulsed eddy current (PEC); finite element method (FEM) simulation; magnetic field; conductivity testing; time domain analysis.*

1. INTRODUCTION

Eddy current testing (ET) is a non-contact electromagnetic-based non-destructive testing (NDT) method that is widely used in various industries to ensure the safety, integrity and reliability of electrically-conductive structures and components (Shim *et al*., 2016; Zhang *et al*., 2018; Chandran *et al*., 2019; Ma *et al*., 2020). This method can detect defects that occur either on both surfaces or subsurface of the specimen based on the disruption of the eddy current flow (Sophian *et al*., 2017). ET operates based on single frequency sinusoidal excitation, with the defects detected based on the impedance changes (Latif *et al.* 2018)

This conventional method is quite sensitive to various parameters that influence the accuracy of signal detection and evaluation. Even though multi-frequency ET has been introduced, drawbacks have been reported, such as penetration limitations due to the skin effect, which causes the eddy current density to decrease exponentially with depth (Sophian *et al*., 2017). In addition, the eddy current strength is influenced by volumetric losses of the specimen (Dwivedi *et al*., 2018). Non-defective specimens generate the highest eddy current intensity because the current flows uninterrupted. However, in defective specimens, eddy current intensity is lower as defects disrupt eddy current flow throughout the specimen (Abdallah *et al*., 2018).

Contrary to conventional ET, which utilises sinusoidal waves, pulsed eddy current (PEC) uses a square waveform to drive an excitation coil, which significantly improves its penetration. During the inspection, the excitation coil carrying the square waveform induces transient eddy currents and resultant magnetic fields in the specimen (Xie *et al*., 2020; Sha *et al*., 2021). The square waveform consists of a series of frequency contents where its excitation allows for deeper eddy current penetration, resulting in higher robustness of anti-interference and decreasing power consumption during operations. In addition, the wideband pulse consists of frequency ranges of components leading to the potential for gathering information about defects that occur in both ferromagnetic and non-ferromagnetic materials. Furthermore, this technique does not require a specific saturation magnetisation device for ferromagnetic material inspection (Johnston *et al*., 2018; Piao *et al*., 2019; Yu *et al*. 2021; Han *et al*., 2022).

While conventional eddy current displays signals in an impedance plan diagram, the PEC signals are represented in a time domain (Wen et al. 2019; Yang et al. 2017). Similar to other ET techniques, PEC does not require surface preparation before the inspection, which reduces time consumption and cost. One advantage of PEC over ET is the use a magnetic sensor to replace the function of the pick-up coil. The magnetic sensor offers a high range of magnetic field detection over wideband frequencies (Rocha *et al*., 2015; Angani *et al*., 2016; Ye *et al*., 2016; Li *et al*., 2017). In PEC, Hall effect device is the most widely used magnetic sensor due to its wide dynamic range and relatively low cost (Fan *et al*. 2021).

The application of finite element method (FEM) to solve problems has been practiced by many researchers, with the objective of gaining a better understanding of the PEC phenomena when used in NDT inspection. Therefore, the successful modelling of PEC has advanced its applications in various fields (Sophian *et al*., 2017). In order to have a better understanding of PEC results for quantitative evaluation, simulation works are conducted to establish the correlation between PEC signals and materials having different conductivity values. Such investigations would be very helpful in understanding and interpreting PEC responses through transient profiles based on the magnetic field acquired and eddy current distribution within the specimen.

This study conducted an experimental evaluation and a series of FEM numerical modelling simulations to investigate the relationship between the acquired magnetic field and induced current density profiles on conductivity characteristics for non-ferromagnetic materials. The FEM results can be used to understand the underlying phenomenon of PEC, which can then be explained via the visualisation of the induced current density generated in the specimen.

2. METHODOLOGY

2.1 PEC Conductivity Experimental Evaluation

Figure 1 shows the PEC system developed for the test. A basic PEC system comprising of a function generator, power amplifier, power supply and PEC coil was used to experiment on multiple conductivity plates. A 5 V output from a power supply was used to operate the magnetic sensor. The function generator provided the rectangular input current to drive the excitation coil and the 5 ms pulse width used for current excitation. For signal processing, all of the signals detected by the PEC coil were transferred, displayed and processed using a computer installed with a data acquisition card.

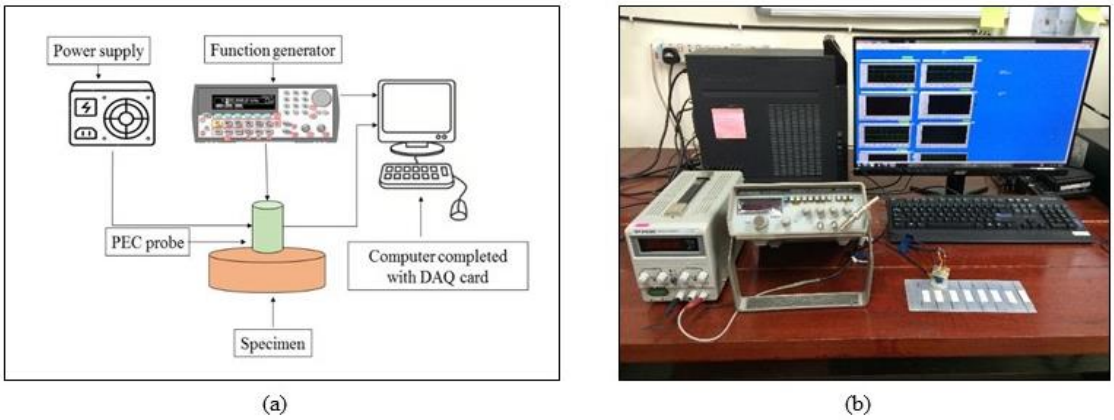

Figure 1: (a) Schematic diagram of the PEC system. (b) The PEC system developed for the experimental work.

Figure 2 shows the schematic diagram of the PEC coil fabricated for the experiment, with dimensions of 18 mm outer diameter, 12 mm inner diameter and 30 mm height, made up of 300 turns of copper wire. In order to replace the function of the pick-up coil and for magnetic field detection, a magnetic sensor (Hall) was installed at the centre of the ferrite core.

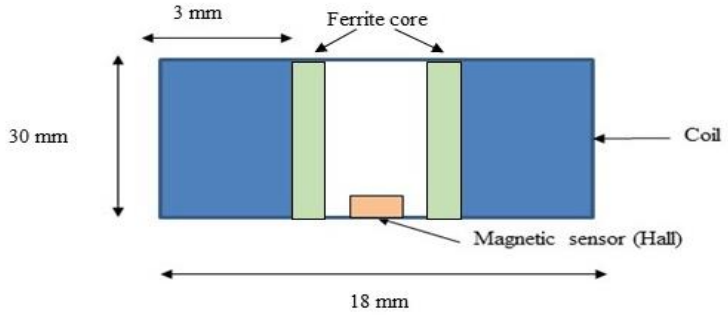

Figure 2: Schematic diagram of PEC coil.

The specimens evaluated were tungsten, Al-7075-T6, Al-6061-T3, Al-1100-F and copper with their conductivities listed in Table 1. Al-7075-T6, Al-6061-T3, Al-1100-F are aluminium alloys produced through specific designation and temper systems. Each specimen produces varying magnetic field strengths due to different conductivities. The specimens were cut into square plates with dimensions of 50 mm x 50 mm and 5 mm thick. For the experiment, a PEC coil is positioned above the plate with a 2 mm lift-off distance, as shown in Figure 3.

Table 1: Conductivity and resistivity values of specimens simulated in simulation and experimental work.

Specimen	Conductivity (S/m)	Resistivity (Ω/m)
Tungsten	1.856×10^{7}	5.388×10^{-8}
Al-7075-T6	1.890×10^{7}	5.291×10^{-8}
Al-6061-T3	2.459×10^{7}	4.066×10^{-8}
Al-1100-F	3.445×10^{7}	2.903×10^{-8}
Copper	5.800×10^{7}	1.724×10^{-8}

The magnetic field of the PEC within the vicinity of a conductive sample can be determined using the following equation:

$$B_z = B_z^e - B_{zm} \quad (1)$$

where B_z denotes the magnetic field at the z-axis of the specimen, B_z^e is the field produced by the coil, and B_{zm} is the field change caused by the specimen.

The magnitude of change in the acquired magnetic field, B_z is relatively minimal. Thus, in order to observe the magnetic field changes acquired from each plate, the differential net magnetic field was calculated by taking the difference between the magnetic field acquired, B_z, and the reference signal of each specimen. The ΔB_z of each plate can be mathematically defined using the following equation:

$$\Delta B_z = B_{zref} - B_z \quad (2)$$

where B_{zref} is the reference magnetic field acquired while the PEC coil is held in the air.

2.2 FEM Modelling and Setup

Two series of FEM works were conducted in this research. The first numerical modelling simulations were undertaken to build the relationship between the acquired magnetic field transient profiles and the induced eddy currents density within the specimens with different conductivity values. The second numerical model involved conductivity testing simulation to compare the acquired results with that of the experimental works. Both FEM works were modelled according to the experimental setup, encompassing the coil's parameters, specimen dimensions and orientation. A plate with various conductivities is expected to exhibit different net magnetic field profiles. In order to ensure that the magnetic field generated by the specimen is not influenced by unwanted signals such as electrical conductivity, the FEM works were modelled within a magnetic insulator boundary. A 5 ms excitation pulse width with 100 Hz operation frequency was used as a pulse waveform. All the simulations were modelled and performed using COMSOL®. Figure 3 shows the 3D model of the simulation layout of the PEC coil and the plate specimen.

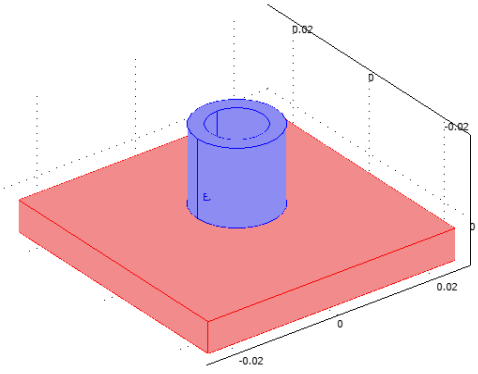

Figure 3: 3D model of PEC coil and specimens with different conductivity values.

3. RESULTS AND DISCUSSION

Figure 4 shows the normalised transient magnetic field, B_z acquired by the PEC coil from the experiment. It can be seen from the results that air has the highest B_z as compared to the rest of the specimens. Meanwhile, the second highest B_z is acquired from tungsten, followed by Al-7075-T6, Al-6061-T3, Al-1100-F and copper. These net magnetic fields were obtained by taking the difference between the magnetic fields of the coil, B_z^e and specimen, B_{zm}. B_{zm} of air is acquired while the coil is holding in the air. Air has the lowest B_{zm} because the Hall sensor measures the magnetic field that exists in the ambience without any field change from the specimen. This in turn causes air to have the highest B_z as mathematically calculated according to Eq. 1.

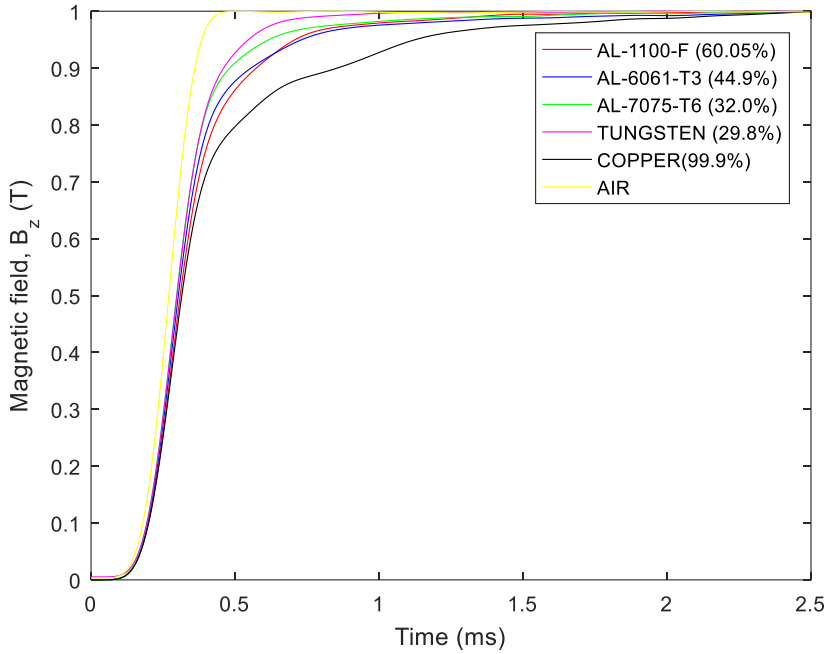

Figure 4: Normalised transient magnetic field, B_z acquired from the specimen with different conductivity values.

Figure 5 shows the net magnetic field, ΔB_z for each specimen with various conductivities. Copper exhibits the highest ΔB_z, followed by Al-1100-F, Al-6061-T3, Al-7075-T6 and tungsten. Consequently, it can be observed that as the conductivity increases, the amplitude of the respective profiles increases. As copper has smaller resistance, more currents are allowed to pass within it. The specimen with higher conductivity will allow for more current flow, increasing the magnetic field. Each specimen's conductivity influences the eddy current's path, phase and distribution. In addition, the strength of the magnetic field depends on the strength of the induced current density within the specimens (Brauer & Ziolkowski, 2019).

Figure 6 shows the ΔB_z acquired from the simulation works. The resultant net magnetic field is obtained based on the interaction between the primary current from the PEC coil and the secondary magnetic field generated by the induced eddy current inside the specimen. The results show good agreement with the experimental works, whereby copper, with the highest conductivity values, exhibits the highest magnetic field, followed by Al-1100-F, Al-6061-T3, Al-7075-T6 and tungsten. Based on the results, it can be surmised that as the conductivity value increases, the amplitude of the magnetic field produced by the specimen also increases.

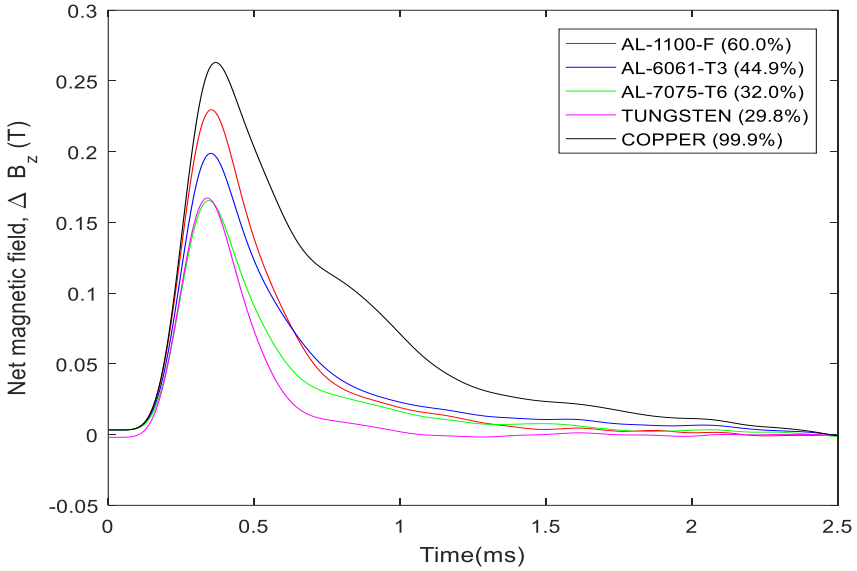

Figure 5: Net magnetic field, ΔB_z acquired from the experimental works for specimens with different conductivities.

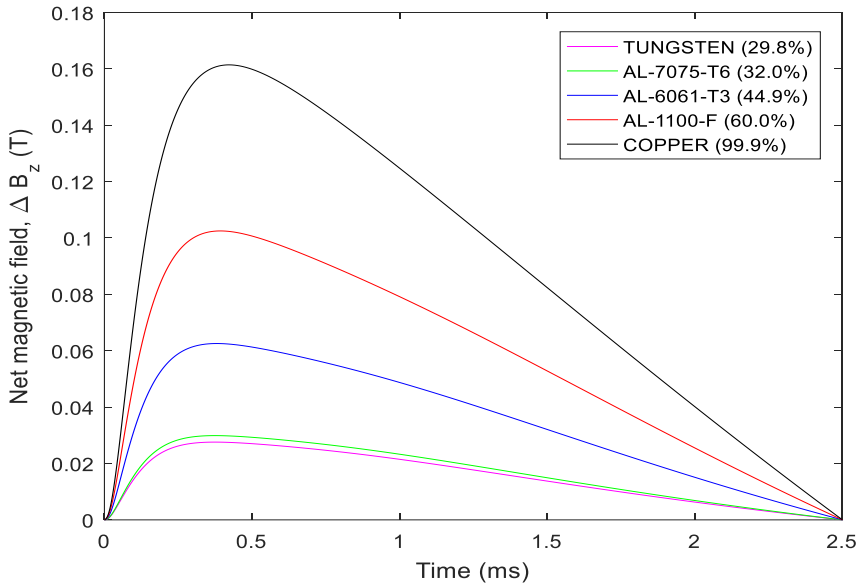

Figure 6: Net magnetic field, ΔBz acquired from FEM simulation works for specimens with different conductivities.

The cross-view of the induced current density for each specimen is as shown in Figure 7. These signals were acquired at a steady state of the transient signal at 2.5 ms. Based on the visualisation obtained from the simulation, the induced current density changes with increasing conductivity values. It can be surmised that the electromagnetic characteristics and the specimen's geometry influence the induced transient eddy currents. The current flow within the specimen increases with increasing conductivity, resulting in increased current density, per Figure 7(a)-(e). This will, in turn, result in increased induced current density and magnetic field density in the specimen.

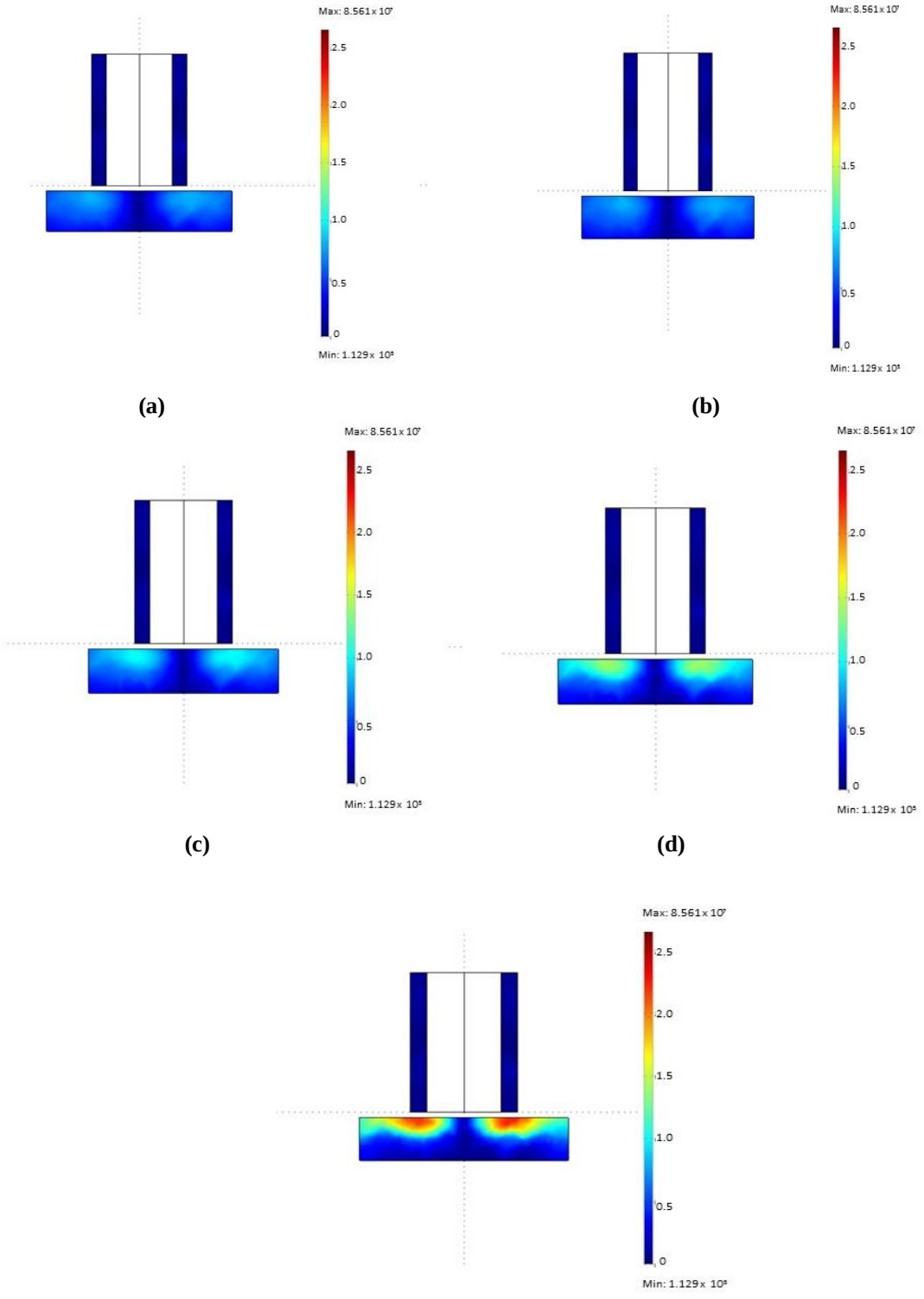

Figure 7: Visualisation of simulated induced current density for the specimens: (a) tungsten, (b) Al- 6061-T6, (c) Al-6061-T3, (d) Al-1100-F, and (e) copper.

Figure 8 shows the amplitude of ΔB_z acquired from both the experimental and simulation works. It can be seen that the magnetic fields obtained from both approaches are in good agreement as they produce the same pattern of amplitude increment. The amplitude of ΔB_z increases with increasing specimen's conductivity. The magnetic field acquired from the experiment is slightly higher than the simulation works due to the presence and influence of the external magnetic field. These noises came from various sources, such as the existing magnetic field in the ambient and electrical components.

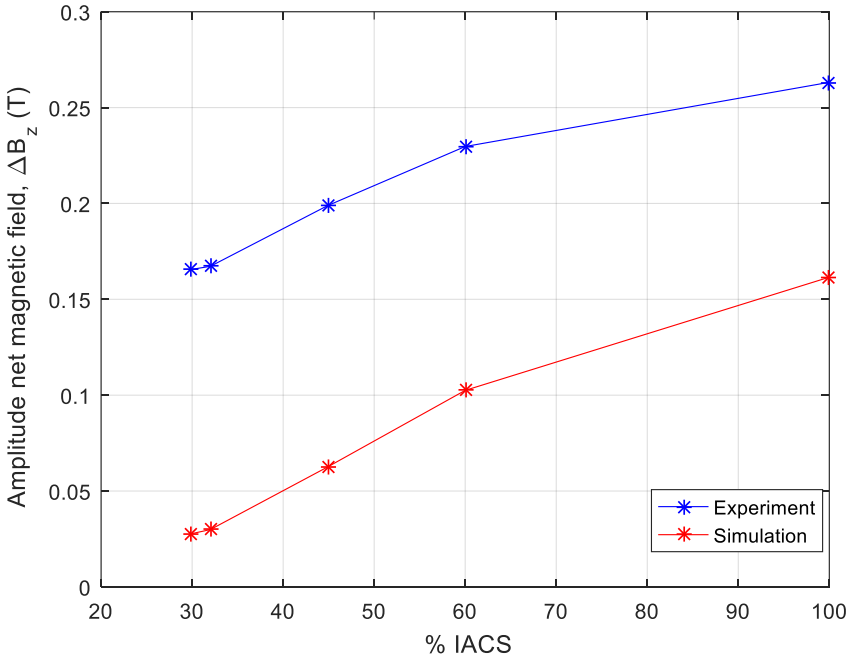

Figure 8: Amplitude of ΔB_z acquired from experimental works and FEM simulation for specimens with different conductivity values

4. CONCLUSION

This paper detailed out the experimental and simulation works for PEC and the correlation between the acquired PEC transient signals with non-ferromagnetic materials having different conductivities. Through FEM simulation, the underlying theory of PEC responses and the correlation between the obtained magnetic field profiles with induced current density were found to be influenced by the conductivity value of the specimen. The secondary magnetic field's strength depends on the induced eddy current inside the specimen. Therefore, with increasing conductivities, the induced current density also increases, thus increasing the magnetic field density in the specimen. The good agreement between the results acquired from the FEM simulation and experimental works conducted using the developed PEC system could benefit future works on PEC for real-time quantitative defect evaluation.

ACKNOWLEDGEMENT

The authors would like to express gratitude to the Ministry of Science, Technology and Innovation (MOSTI) and the Malaysian Nuclear Agency for funding this work under the ScienceFund grant 03-03-01-SF0220 and the support given for this work.

REFERENCES

Abdalla, A. N., Faraj, M. A., Samsuri, F., Rifai, D. & Ali, K. (2018). Challenges in improving the performance of eddy current testing: Review. *Meas. Control*, **52**: 1-19.

Angani, C. S., Ramos, H. G., Ribeiro, A. L. & Rocha, T. J. (2016). Evaluation of transient eddy current oscillations response for thickness measurement of stainless steel plate. *J. Int. Meas. Confed.*, **90**: 59–63.

Brauer, H. & Ziolkowski, M. (2019). Motion-Induced Eddy Current Testing. *Handbook of Advanced Nondestructive Evaluation*. Springer, Cham.

Chandran, P., Rantatalo, M., Odelius, J., Lind, H. & Famurewa, S. M. (2019). Train-based differential eddy current sensor system for rail fastener detection. *Meas Sci Techno*l., **30**: 125105.

Fan, H., Wang, J., Feng, Q., Hu, Q., Zuo, S., Nabaei, V. & Heidari, H. (2021). Detection techniques of biological and chemical Hall sensors. *RSC Advances*., **11**: 7257–7270.

Han, Y., Tao, Y. C., Shao, C. B., Yan, H. & Peng, Z. Z. (2022). Pulsed eddy currents in ferromagnetic pipes with cladding in nuclear power plants. *Energy Rep*.., **8**: 104–111.

Johnston, D. P., Buck, J. A., Underhill, P. R., Morelli, J. & Krause, T. W. (2018). Pulsed eddy current detection of loose parts in steam generators. *IEEE Sens J*., **18**:2506-2512.

Latif, N. A. A., Abidin, I. M. Z. & Jamaludin, N. (2018). Simulation and experimental investigation of pulsed eddy current technique for defect evaluation. *Indones. J. Electr. Eng. Inform.*, **6**: 317–322.

Li, Y., Ren, S., Yan, B., Abidin, I. M. Z. & Wang, Y. (2017). Imaging of subsurface corrosion using gradient-field pulsed eddy current probes with uniform field excitation. *Sensors*., *17*:1747-1760.

Ma, Q., Gao, B., Tian, G. Y., Yang, C., Xie, L. & Chen, K. (2020). High sensitivity flexible double square winding eddy current array for surface micro-defects. *Sensor Actuat A-Phys*.,**309**: (1-13).

Piao, G., Guo, J., Hu, T., Deng, Y. & Leung, H. (2019). A novel pulsed eddy current method for high-speed pipeline inline inspection. *Sensor Actuat A-Phys*., **295**: 244–258.

Rocha, T. J., Ramos, H. G., Lopes Ribeiro, A., Pasadas, D. J. & Angani, C. S. (2015). Studies to optimize the probe response for velocity induced eddy current testing in aluminium. *J. Int. Meas. Confed*., **67**: 108–115.

Sha, J., Fan, M., Cao, B. & Liu, B. (2021). Noncontact and nondestructive evaluation of heat-treated bearing rings using pulsed eddy current testing. *Sol St Phen*.,**521**: e167516.

Shim, H. S., Choi, M. S., Lee, D. H. & Hur, D. H. (2016). A prediction method for the general corrosion behavior of Alloy 690 steam generator tube using eddy current testing. *Nucl. Eng. Des*., **297**: 26–31.

Sophian, A., Tian, G. & Fan, M. (2017). Pulsed eddy current non-destructive testing and evaluation: A review. *Chin. J. Mech. Eng.*, **30**: 500–514.

Wen, D., Fan, M., Cao, B. & Ye, B. (2019). Adjusting LOI for Enhancement of Pulsed Eddy Current Thickness Measurement. *IEEE Trans. Instrum. Meas*.,**69**: 1–7.

Xie, S., Zhang, L., Zhao, Y., Wang, X., Kong, Y., Ma, Q., Chen, Z., et al. (2020). Features extraction and discussion in a novel frequency-band-selecting pulsed eddy current testing method for the detection of a certain depth range of defects. *NDT E Int*.,**111**: e102211.

Yang, H., Cao, A. & Sun, J. (2017). Lift-off Effect Reduction Based on the Dynamic Trajectories of the Received-Signal Fast Fourier Transform in Pulsed Eddy Current Testing. *NDT E Int*., **1**: 85–92.

Ye, C., Huang, Y., Udpa, L. & Udpa, S. S. (2016). Novel rotating current probe with GMR array sensors for steam generate tube inspection. *IEEE Sens. J*., **16**: 4995–5002.

Yu, Z., Fu, Y., Jiang, L. & Yang, F. 2021. Detection of circumferential cracks in heat exchanger tubes using pulsed eddy current testing. *NDT E Int* .,**121**: e102444

Zhang, K., He, Y. & Dong, Z. (2018). Pulsed eddy current nondestructive testing for defect evaluation and imaging of automotive lightweight alloy materials. *J. Sens*., **2018**:1-11.

DEFECT ECHO ENHANCEMENT FOR PULSE-ECHO GUIDED WAVE INSPECTION IN A STRAIGHT PIPE

Rokhmadi[1,2], Nor Salim Muhammad[1*], Abd Rahman Dullah[1], Ruztamreen Jenal[1], Juhari Ab Razak[3] & Zulfahmy Awaldin[4]

[1]Faculty of Mechanical Engineering, Universiti Teknikal Malaysia Melaka (UTeM), Malaysia
[2]Research Center for Nuclear Reactor Technology, National Research and Innovation Agency (BRIN), Indonesia
[3]Faculty of Mechanical and Manufacturing Engineering Technology, Universiti Teknikal Malaysia Melaka (UTeM), Malaysia
[4] ZL Technologies Sdn. Bhd., Malaysia

[*]Email: norsalim@utem.edu.my

ABSTRACT

Nowadays, guided wave technology is increasingly accepted in the industries due to its capability for detection of discontinuities in pipelines that are long, under insulation or in buried condition. Guided wave propagation in structures is very complex, where there are multimodal wave propagations, reflections, mode conversions and wave interference, as well as the presence of electrical noise from inspection sites. This study aimed at enhancing the amplitude of reflected waves from defects and reduce the level of noise without increasing the number of transducers. This is achieved by combining several pulse-echo signals that are obtained from the excitation of the L(0,2) mode at different locations of transducers. The results show that post signal processing can improve the ability of acoustic waves for defect screening in large structures.

Keywords: *Non-destructive testing; guided wave; pipeline; pipe inspection; discontinuity.*

1. INTRODUCTION

Structural health monitoring is widely used in petrochemical industries, power plants, transportation and defence equipment (Davidson, 2014). Pipe and tube structures are the most important components in fuel distribution and hydraulic actuators for public or military use. Pipelines in petrochemical industries are used for transmission of supplies such as crude oil as well as distribution of chemicals (Cawley *et al.*, 2003; Ho *et al.*, 2020; Lu *et al.*, 2020). Generally, petrochemical industries produce products including liquefied petroleum gas (LPG), gasoline, kerosene and diesel oil as well as waste materials that can harm our health and contribute to the environmental pollution. Concerns on pipe failures have increased the awareness on the monitoring and maintenance of pipe structures to prevent failures or accidents that may result in production loss and fatality. Concurrently, military operations whether involving the army, navy or air force have their own fuel logistic systems and maintenance that are used to ensure real-time accountability for fuels logistics and supply operations (Davidson, 2014).

The ultrasonic guided wave technique is one of the advanced techniques for structure health monitoring in pipe structures (Rose, 2021). It has capability for defect inspections for insulated pipes and also along pipelines found beneath the ground. The use of pulse-echo mode in guided wave technique allows for defect screening from pipe at a certain distance from a ring transducer that is placed on the surface of the pipe (Mariani *et al.*, 2019). The inspection over long distance from the fixed point reduces the work to access the surface of insulated pipelines and underground pipes, which also reduces labour costs and allows for the job to be completed earlier than the previous techniques (Cawley *et al.*, 2003).

Guided waves can propagate in long distances and provide defect information in large or long structures. At the same time, the propagating waveform probably undergoes reflections and superposition of the multiple wave modes along the pipes and becomes complicated (Malo *et al.*, 2017). In some cases, the propagating waveform may completely obscure the information of defects due to their complex interactions in pipes. Thus, advanced signal processing is required to obtain the information through analysis of the recorded wave signals (Hesse & Cawley, 2007).

This study is conducted to observe the effects of group velocities on the enhancement of the defect echo in a pipe when the L(0,2) mode is excited from a set of piezoelectric transducers. The results of the signal enhancements at different velocities are compared to the actual defect location in the pipe for discussion on the enhanced defect echo in pipes.

2. MEASUREMENT AND SIGNAL PROCESSING

2.1 Location of Transducer and Defect

Piezoelectric (PZT) elements were used to form two guided wave transducers for inspection to locate a groove defect in an aluminium pipe that is 6 m long and 6 mm thick with internal and external diameters of approximately 98 and 110 mm respectively. The defect was placed at distance of 5 m from the location of the transducer as illustrated in Figure 1. At the inspection points, the two transducers were placed on their shoes to form angle beam transducers for L(0,2) (Muhammad *et al.*, 2017) in configurations of two piezoelectric transducers as shown in Figure 2. In addition, the defect on the pipe surface was made by fabricating a 3 mm depth groove about 100 mm length in circumferential direction with opening of 10 mm in width as shown in Figure 3.

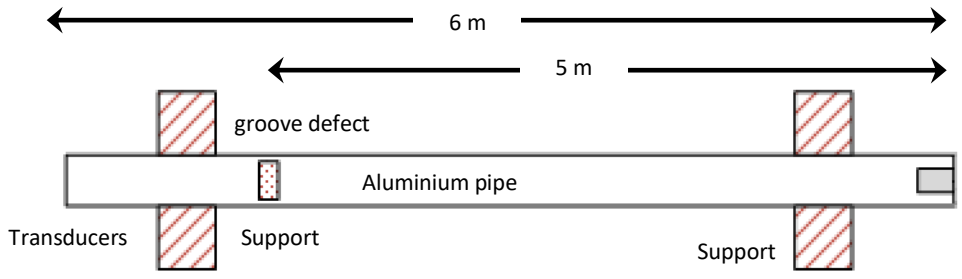

Figure 1: Defect location in the pipe.

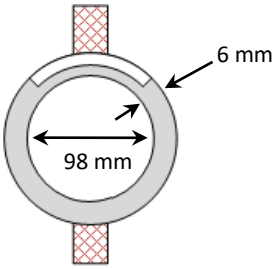

Figure 2: Arrangements of two transducers for defect detection in pipe.

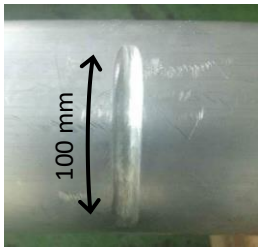

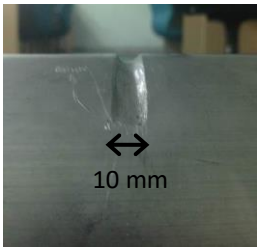

(a) **(b)**

Figure 3: Circumferential defect of 3 mm depth in the pipe: (a) Top view (b) Side view.

2.2 Guided Wave Inspection in Pipe

The guided wave inspection system is shown in Figures 4 and 5, which consists of signal generator, power amplifier, diplexer, transducer, preamplifier, logger data and host computer to synchronise the measurement. A signal generator (AFG3022C Electronics) was controlled using a LabVIEW program to synthesise five cycles of toneburst signal from 100 to 150 kHz, while a power amplifier (NF HAS4052) was used to amplify the synthesised signals with gain of 40 dB. The amplified signal was passed to a diplexer that controls the excitation and measurement of signals. The interaction waves received from the diplexer were amplified using a preamplifier (Ritec PAS-0.1-20) with gain of 20 dB. Simultaneously with signal excitation from the function generator, a data logger (NI USB 5133) was triggered by the LabVIEW program to acquire the guided wave signal and transfer the data to the host computer.

Figure 4: Equipment for the guided wave inspection.

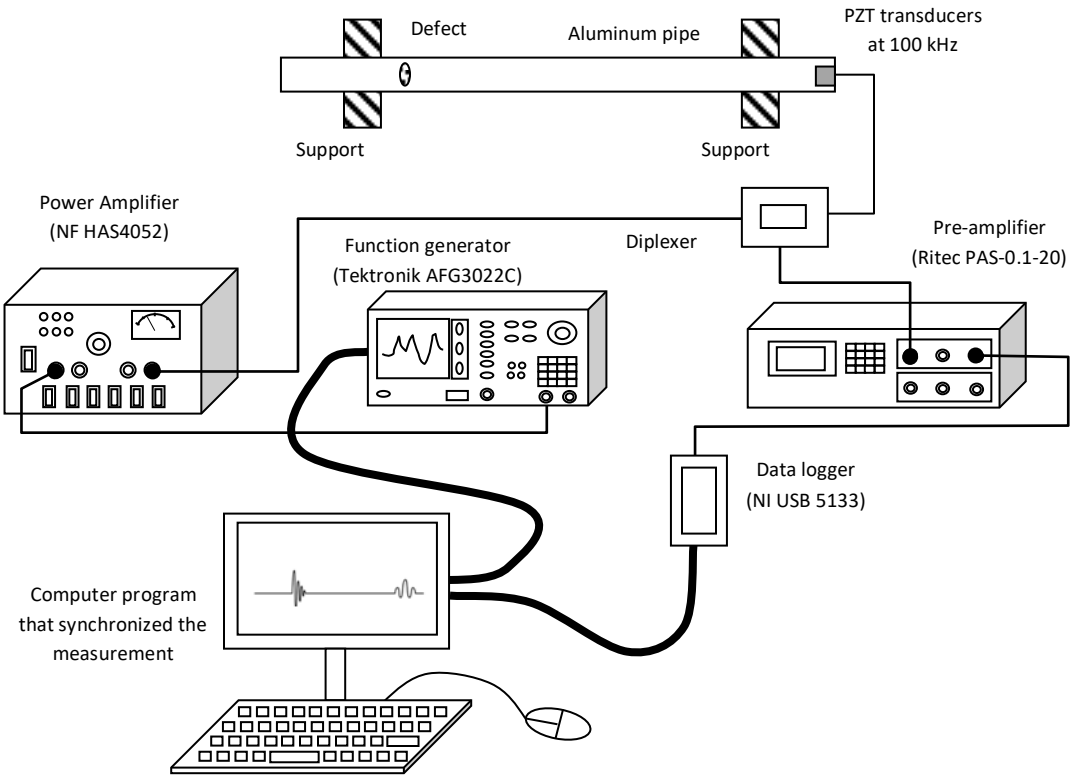

Figure 5: Signal connections for the pulse-echo inspection.

2.3 Selection of Frequency Range

Dispersion curves for the longitudinal and flexural modes in the aluminium pipe shown in Figure 6 form the CIVA guided wave module which was developed by Extend Inc. (at thickness of 6 mm with longitudinal and transverse wave velocities of 6,260 and 3,080 m/s respectively). The figure shows the fastest L(0,2) which propagates close to the velocity of the flexural mode F(1,3) (Cawley *et al.*, 2003; Mariani *et al.*, 2019; Ho *et al.*, 2020). At frequency higher than 100 kHz, the other flexural modes, such F(2,3), F(3,3) and F(*n*,3) modes are also expected to be propagating as well as the L(0,2) and F(1,3) modes. Although, the velocity of L(0,2) changes with respect to the frequency increase, frequency range of 100 to 150 kHz still has small dispersion of the L(0,2) mode, which propagates together with the third flexural modes F(*n*,3). This study used the frequency range that has little dispersion on L(0,2) with considerable difference in wave velocities of flexural modes on pipe.

2.4 Signal Enhancement

The use of two transducers in this study is likely to produce flexural modes together with the desired L(0,2). Therefore, five waveforms of guided wave pulse-echo were collected from different positions for each measurement frequency as depicted in Figure 7 to enhance the defect echo of L(0, 2) mode. The data collection was conducted from two transducers placed in opposite directions at fixed interval of Δx = 14 mm, which produced total spatial interval of $2\Delta x$ in a round trip wave propagation in pulse-echo mode as illustrated in the figure. Figures 7 and 8 show the measurements from the longest propagation distance, $x_{i-2}(t)$ to the shortest propagation distance, $x_{i+2}(t)$ and their related waveforms. The predicted waveforms

from the five positions in pulse-echo measurement are depicted in Figure 8(a) with the positions at $x_{i-2}(t)$ and $x_{i-1}(t)$ having longer propagation distances than the centre of about $4\Delta x$ and $2\Delta x$ respectively. At the same time, the positions at $x_{i+1}(t)$ and $x_{i+2}(t)$ were placed at shorter propagation distance than the centre at differences of $2\Delta x$ and $4\Delta x$ respectively. The actual signal enhancement involved the shift of time signal as illustrated in Figure 8(b), whereas the time signals obtained from longer propagation distance than the centre of the measurement were shifted forward, while the time signals obtained from the shorter distance were shifted backwards as shown in Figure 8(b). The shifted time intervals of $-4\Delta t$, $-2\Delta t$, $2\Delta t$ and $4\Delta t$ on the time signals were computed from the wave velocity of L(0, 2) and difference of propagation distance between the transducer positions and the centre point of the pulse-echo. At the end of the signal processing, the enhanced time signal, $x_i'(t)$ with significant defect echo was obtained from the average of the shifted time signals as shown in Figure 8(c).

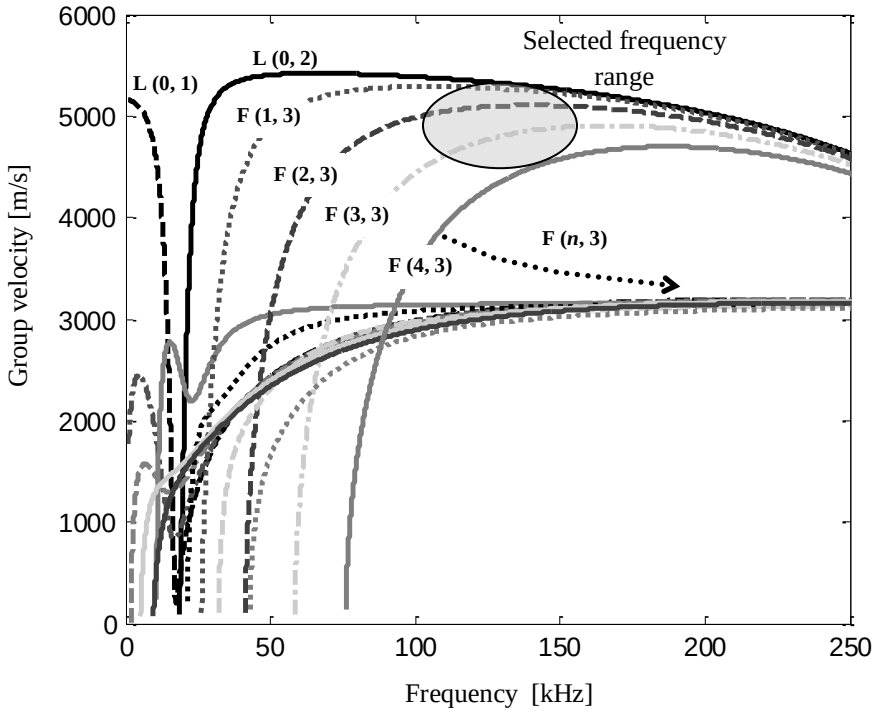

Figure 6: Dispersion curves for longitudinal and flexural modes.

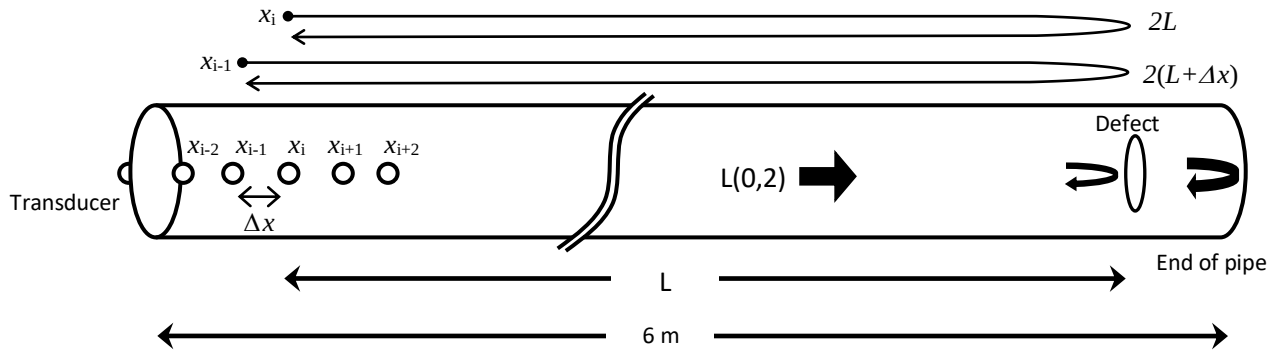

(a) Possible non-mechanical signal **(b) Weak signal**

Figure 7: Pulse-echo measurement at five locations on pipe.

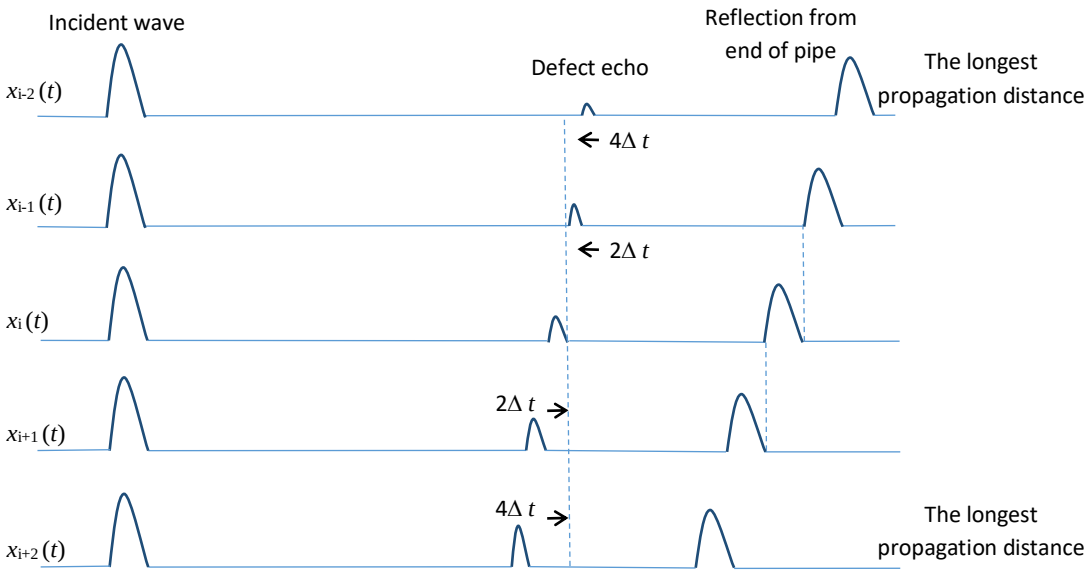

(a) Predicted wave propagation in the pipe.

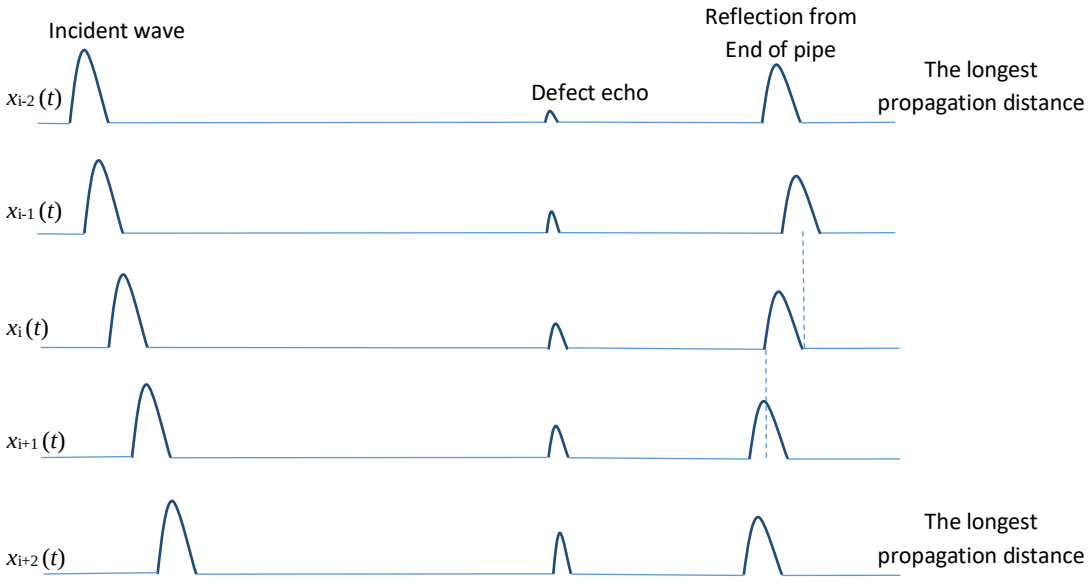

(b) Shifted waveforms in signal processing.

(c) Average of the shifted waveforms.

Figure 8: Signal enhancement on defect echo.

3. RESULTS AND DISCUSSION

3.1 Reflection Waves in Pipe

The excited waves in the pipe are shown in Figures 9 to 11 for measurements at frequencies of 100, 130, and 150 kHz respectively. The results indicate the arrival of reflected wave from the end of pipe at about 2.27 ms and reflection waves from the defect at approximately 1.8 to 2.0 ms in most of the recorded waveforms. From the computed velocity of L(0, 2) at 100 kHz in Figure 6 was calculated at about 5,390 m/s with the end of pipe at about 6.1 m, and the defect was predicted at approximately 4.9 to 5.4 m from the location of the transducers respectively. The signatures indicated the reflected waves from the defect and end of pipe for the 6 m length of the aluminium pipe with defect at location of 5 m as depicted in Figure 1. However, the measured signals show some noise especially from the pulse-echo results at 100 kHz as shown in Figure 9. The noise found in the time waveform made it difficult to determine the time of arrival for the reflected waves. Therefore, signal processing was applied to enhanced the defect echo from the five signals of the pulse-echo inspection, shown as $x_{i-2}(t)$, $x_{i-1}(t)$, $x_i(t)$, $x_{i+1}(t)$, and $x_{i+2}(t)$. The recorded signals were measured from the transducers at different inspection points that begun from the longest distance, x_{i-2} and moved to the next positions until to the shortest distance, x_{i+2} as shown in Figure 7. The enhanced signal is indicated as $x'(t)$, which averaged the shifted five waveforms as explained in the signal enhancement.

3.2 Signal Improvement

The averages of the shifted waveforms $x'(t)$ are shown in Figures 9(f), 10(f) and 11(f). The enhancements at 130 and 150 kHz were performed at velocities of 5,320 and 5,260 m/s respectively. Overall, the enhanced signals exhibited noise reduction at frequencies from 100 to 150 kHz, which were compared to the recorded waveforms from transducers. At the same time, enhancement was significantly observed at 100 kHz, where the noise was obvious. Although the conducted test probably had inconsistent contact conditions between the transducers and pipe, which reflected the different amplitudes from the defect, the enhanced signals contained the average of the defect echoes based on the shifted time intervals computed from velocity of L(0,2) and locations of the pulse-echo on pipe.

3.3 Effect of Frequency on the Reflected Wave from Defect

Varying the frequency from 100 to 150 kHz in the pulse-echo tests resulted in defect echoes at approximately 1.9 ms with different sizes of wave packets as shown in Figures 9(f), 10(f) and 11(f). Calculations from the velocities indicated that defect locations at 5.12, 5.05 and 5.00 m from the transducers for inspection at frequencies of 100, 130 and 150 kHz respectively. The enhanced signal at 100 kHz also indicated a defect echo at the widest wave packet at approximately 0.22 ms as in Figure 9(f) and the echo became narrower at 150 kHz as in Figure 11(f) that indicated about 0.12 ms. This shows the effect of frequency shifts on the pulse-echo tests using two transducers even after the signal enhancement.

The enhanced signals exhibited lower grass noise as compared to the raw data due to the average of the shifted signals. This also indicated that the noise occurred randomly during the measurements used for the enhancement (Dobson & Cawley, 2015; Pedram *et al.*, 2018; Bombarda *et al.*, 2021). The selection of the frequency for the test that used two transducers could also possibly affect the results of the enhanced signals. Good results were obtained at 130 kHz and 150 kHz probably due to the smaller difference in velocities between the longitudinal L(0,2) and flexural F(n,3) modes as compared to the difference at 100 kHz as shown in Figure 6. The small difference in the group velocity allows for the arrivals of wave packets at 150 kHz almost at the same time while large differences at 100 kHz will cause arrivals at several time intervals. Thus, the defect echo appeared at narrower time interval at 150 kHz of about 0.12

ms and at the same time became wider at 100 kHz at approximately 0.22 ms. Similar results were also obtained in previous inspections that explained the effect of group velocity dispersion on wave propagation (Leinov *et al.*, 2015; Leinov *et al.*, 2016). At the same time, there is also the possibility for the flexural modes to be dominant at lower frequencies compared to higher frequencies. Although there are many elements to be considered in order to improve the results, the study successfully reduced the grass noise using the average of the shifted signals and indicated the requirement to consider the effect of flexural mode in guided wave pipe inspection using the L(0,2) mode. The results can be further improved using many transducers around the pipe rather using two transducers, which would be more expensive. The use of PZT ring transducer is very expensive but it has been proven for reducing the element of flexural mode in guided wave pipe inspections (Leinov *et al.*, 2015; Leinov *et al.*, 2016).

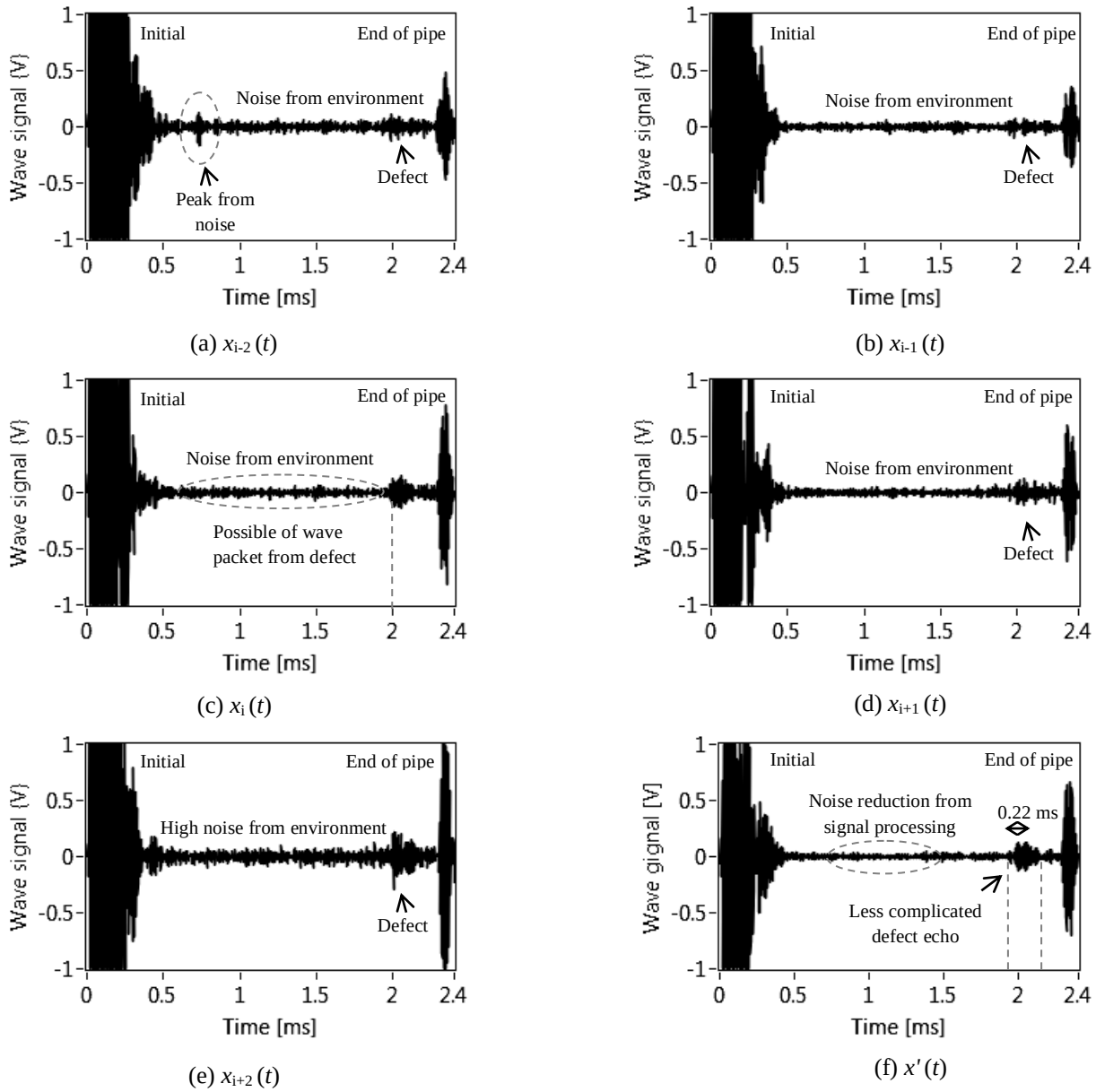

Figure 9: Defect inspection at 100 kHz.

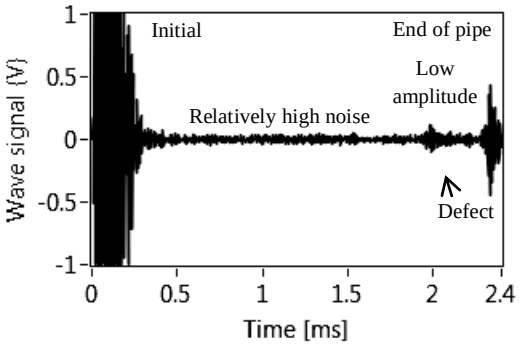

(a) $x_{i-2}(t)$

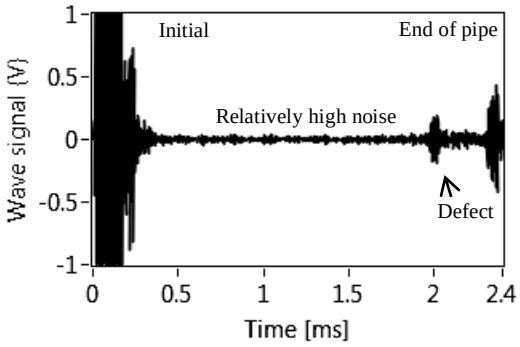

(b) $x_{i-1}(t)$

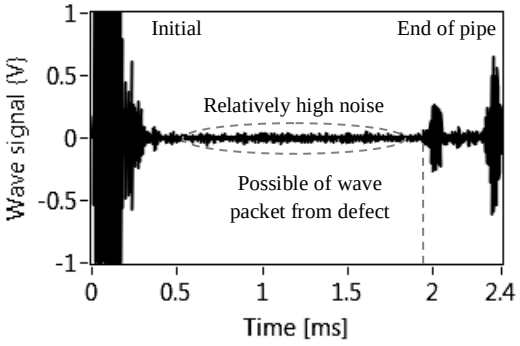

(c) $x_i(t)$

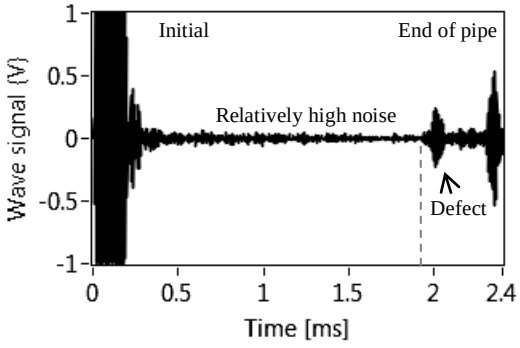

(d) $x_{i+1}(t)$

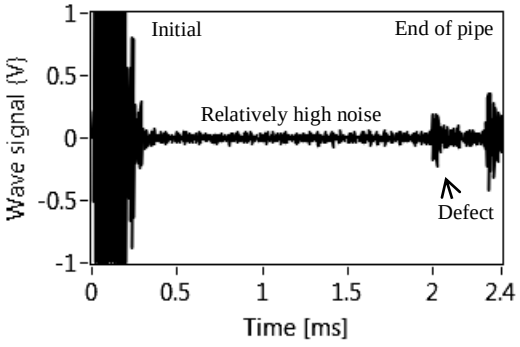

(e) $x_{i+2}(t)$

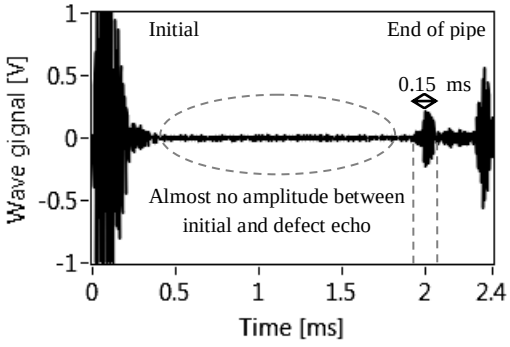

(f) $x'(t)$

Figure 10: Defect inspection at 130 kHz.

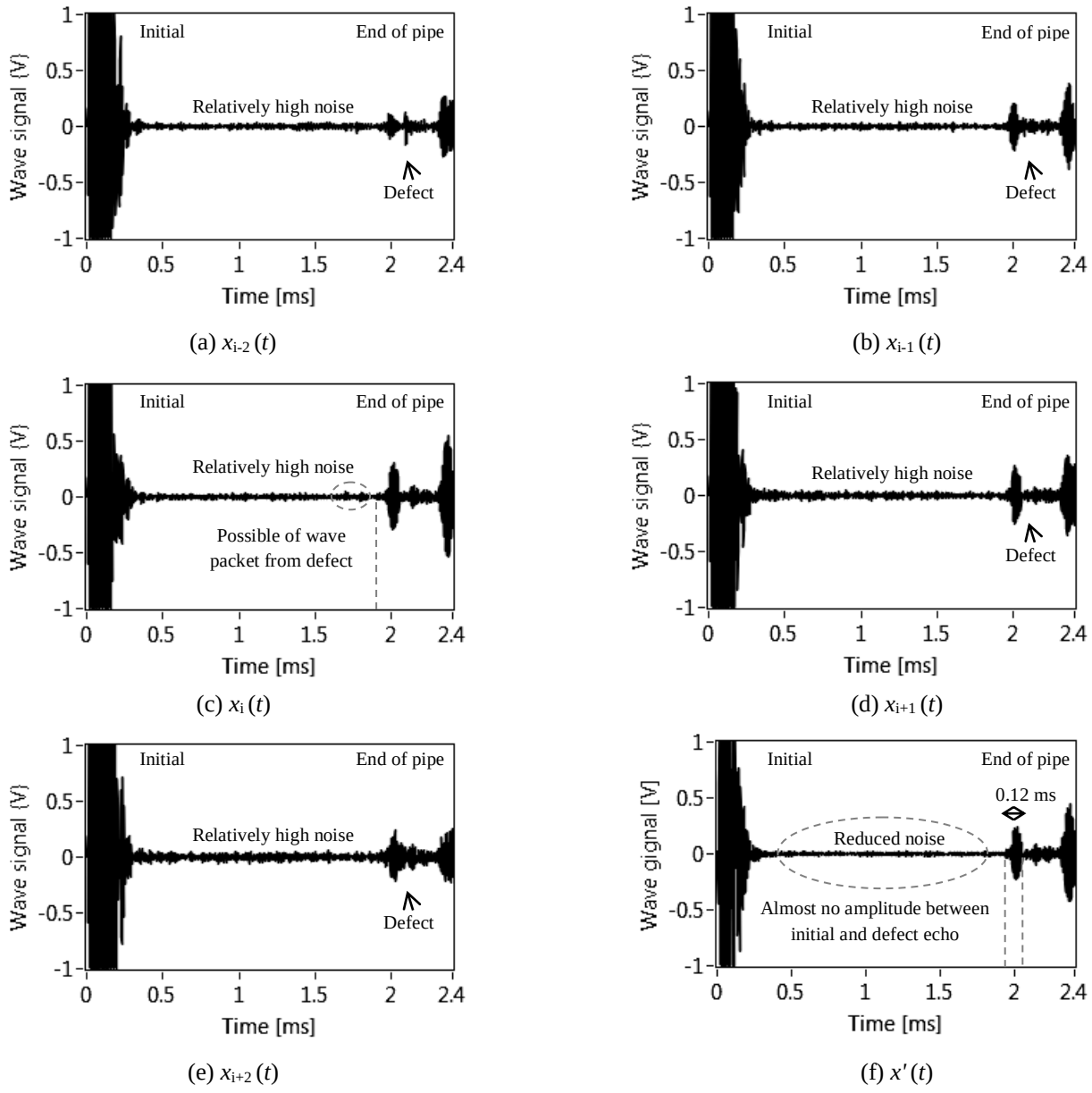

Figure 11: Defect inspection at 150 kHz.

4. CONCLUSION

Excitation of predominant L(0,2) mode from the two transducers was used to locate a perpendicular defect at high resolution to its exact location in pipe. The use of five shifted signals in signal processing was conducted to reduce the component of noise and other wave modes including the flexural mode of F(*n*,3). The enhanced signal reduced the noise level of the measured waveforms and averaged the reflected waves from the defect and end of the pipe. The enhanced signal showed almost no amplitude between the initial wave and defect echo at the frequencies of 130 and 150 kHz, with less complicated wave at 100 kHz. Improvement on the pulse-echo signals is very helpful in determining the time of arrival

of the defect echoes that is used to locate defects in pipes. The study also indicates the requirements for considering the effect of flexural modes in order to increase the spatial resolution using PZT transducers for inspection of pipes.

ACKNOWLEDGMENT

The authors would like to express their deepest gratitude to ZL Technologies Sdn. Bhd. for their assistance. This work was supported by Universiti Teknikal Malaysia Melaka (UteM) and Malaysian Ministry of Higher Education (MOHE) under research grants FRGS/1/2014/TK01/FKM/02/1/F0211, FRGS/2/2013/TK01/UTEM/02/F0171 and ERGS/1/2013/FKM/ TK01/UTEM/02/01/E00014.

REFERENCES

Bombarda, D., Vitetta, G.M. & Ferrante, G. (2021). Rail diagnostics based on ultrasonic guided waves: an overview, *Appl. Sci*., **11 :** 1071-1112.

Cawley, P., Lowe, M. J. S., Alleyne, D. N., Pavlakovic, B., & Wilcox, P. (2003). Practical long range guided wave inspection-applications to pipes and rail, *Mater. Eval.,* **61**: 66-74.

Davidson, C., Newes, E., Schwab, A. & Vimmerstedt, L. (2014), An Overview of Aviation Fuel Markets for Biofuels Stakeholders, *National Renewable Energy Laboratory*.

Dobson, J. & Cawley, P. (2015). Independent Component analysis for improved defect detection in guided wave monitoring, *Proc. IEEE*, **104**: 1620 - 1631.

Hesse, D. & Cawley, P. (2007). A single probe spatial averaging technique for guided waves and its application to surface wave rail inspection, *IEEE Trans. Ultrason. Ferroelectr. Freq. Control*, **54**: 2344 - 2356.

Ho, M., El-Borgi, S., Patil, D. & Song, G. (2020). Inspection and monitoring systems subsea pipelines: A review paper, *Struct. Health Monit.*, **19**: 606–645

Leinov, E., Lowe, M J.S. & Cawley, P. (2015). Investigation of guided wave propagation and attenuation in pipe buried in sand, *J. Sound Vib*., **347**: 96-114.

Leinov, E., Lowe, M. J. S. & Cawley, P. (2016). Investigation of guided wave propagation in pipes fully and partially embedded in concrete, *J. Acoust. Soc. Am.*, **140**: 4528–4539.

Lu, H., Iseley, T., Behbahani, S., & Fu, L. (2020). Leakage detection techniques for oil and gas pipelines: State-of-the-art. Tunn. Undergr. Space Technol., **98** : https://doi.org/10.1016/j.tust.2019.103249

Malo, S., Fateri, S., Livadas, M., Mares, C. & Gan, T.H. (2017). Wave mode discrimination of coded ultrasonic guided waves using two-dimensional compressed pulse analysis, *IEEE Trans. Ultrason. Ferroelectr. Freq. Control*, **64**: 1092 - 1101.

Mariani, S., Heinlein, S. & Cawley, P. (2019). Location specific temperature compensation of guided wave signals in structural health monitoring, *IEEE Trans Ultrason Ferroelectr Freq Control*, **67**: 146 - 157.

Muhammad, N.S., Nyet, J.N., Dullah, A.R., Ghani, A.F.A. & Jenal, R. (2017). Piezoelectric transducers in guided wave inspection for defect detection in a straight pipe, *Defence S&T Tech. Bull.*, **10**: 40-49.

Pedram, S. K., Fateri, S., Gan, L., Haig, A. & Thornicrof, K. (2018). Split-spectrum processing technique for SNR enhancement of ultrasonic guided wave, *Ultrasonics*, **83** : 48-59.

Rose, J.L. (2021). Guided wave studies for enhanced acoustic emission inspection, *Res. Nondestruct. Eval*., **32**: 192-209.

STUDY ON HUMAN COMFORT OF MILITARY VEHICLES IN MALAYSIAN TROPICAL ENVIRONMENT

Fadzli Ibrahim* & Shamsul Akmar Ab Aziz

Mechanical & Aerospace Technology Division, Science and Technology Research Institute for Defence (STRIDE), Ministry of Defence, Malaysia

*E-mail: fadzli.ibrahim@stride.gov.my

ABSTRACT

Human comfort testing for military vehicles in Malaysia should be conducted in diverse terrains and actual weather conditions in the field. This is to ensure that the comfort level of the driver and crew in the cabin is at the optimum level according to the relevant standards. In order to measure the level of human comfort, a series of noise exposure, whole-body vibration (WBV) and heat stress tests were carried out on military vehicles according to the test protocols that have been developed. The evaluated vehicles were taken from the categories of logistics, utility and armoured vehicles. The test results found that all three types of vehicles comply with the human comfort standards. However, a more comprehensive study should be conducted in the future to obtain more data from various types of vehicles to obtain a more accurate human comfort trend for military vehicles operating in the Malaysian environment.

Keywords: *Human comfort; noise exposure; whole-body vibration (WBV); heat stress; tropical environment.*

1. INTRODUCTION

Human comfort testing for military vehicles is a common practice that should be conducted before a vehicle enters the service of the Malaysian Armed Forces (MAF). In Malaysia, human comfort testing of military vehicles is carried out by an evaluation team in the actual field to ensure that the evaluated vehicle is exposed to rough terrains and real tropical environments. Malaysia, as a tropical country with a variety of landforms, provides challenges to military vehicle manufacturers in ensuring that the comfort level of the driver and crew is at the optimum level (King *et al.* 1998, 2006; Aziz & Ibrahim 2022).

In order to ensure that the evaluated military vehicles comply with the relevant standards, three types of human comfort tests are usually carried out, which are noise exposure, whole-body vibration (WBV) and heat stress. These three tests are carried out based on ISO 5128: 1980 for noise exposure in the cabin (ISO, 1980), ISO 2631-1: 1997 for WBV (ISO, 1997), and ISO 7243: 2017 for heat stress (ISO, 2017).

Aziz *et al*. (2009, 2014, 2017) conducted noise exposure studies on MAF vehicles, while Aziz *et al*. (2008, 2017) and Khan *et al.* (2010) conducted WBV studies. It was found that difference in road surfaces had significant impact on noise and WBV readings in the vehicle cabin. It was demonstrated that rough road conditions exhibit higher noise and WBV readings as compared to smoother tarmacs. Wang (2010) in his study also explained that different types of vehicles and engines configurations will produce different noise and vibration exposure to the driver. From the aspect of heat stress, Gani & Aziz (2008) conducted studies on various types of MAF vehicles in tropical environments. According to the studies, the evaluated military vehicles' cabin temperatures reached almost 30 °C. As a result, it

is important to ensure that the ventilation and air conditioning system is functioning effectively to lower cabin temperatures, especially when operating in tropical climates.

This study was conducted as an initiative to create a database of MAF vehicles, especially for the aspect of human comfort in the tropical environment of Malaysia. This study was conducted by the Science & Technology Research Institute for Defence (STRIDE) on several MAF vehicles involving a series of tests during the evaluation and acceptance tests of the vehicles as part of the procurement procedure. The evaluated vehicles were divided into three categories based on the type of vehicle usage, namely logistics, utility and armoured vehicles, as shown in Table 1. In order to ensure that the results obtained are valid for current military vehicle technologies, the data collected was for the year 2020 and later.

Table 1: Vehicles evaluated in this study.

Category	List of tested vehicles
Logistics	a) 3-tonne GS Cargo trucks b) 5-tonne GS Cargo trucks
Utility	a) 1-tonne 4x4 multipurpose vehicles b) Weapon carrier vehicles c) Fitted for Radio vehicles
Wheeled Armoured	a) 4x4 vehicles b) 6x6 vehicles

The scope of this study is on human comfort tests, which include noise exposure, WBV and heat stress in the vehicle's cabin. The objective of the study is to analyse the pattern of noise, vibration and heat stress in the cabins of military vehicles during cruising and then to determine the level of human comfort compliance with the international standards based on the weather and topography of Malaysia.

2. RESEARCH METHODOLOGY

This study was conducted using the test protocol that was developed by Gani *et al*. (2009). In their study, the test protocol was made to assess the level of health hazards and performance of MAF vehicles. The protocol includes all three human comfort tests, and each test complies with the standards that have been set.

This study was conducted on a Malaysian highway with only tarmac road surface. This is due to the fact that the present standard testing procedure only applies to tarmac road surfaces, while there is no specific test method for rough road surfaces. All the tests were conducted while the vehicle was cruising at steady speed of 80-100 km/h. The speed selection was made based on the engine capacity of Malaysian Army (MA) trucks and maximum speed limit allowed by the Road Transport Act 1987 for heavy vehicles on Malaysian highways (Aziz *et al*., 2016).

2.1 Noise Exposure

The measurement of noise in the vehicle cabin was based on ISO (1980) and noise exposure compliance with DOSH (2019). The measurements were made using a B&K Type 2250 sound level meter (SLM), with calibration conducted before and after the measurement using a B&K Type 4231 sound calibrator. The calibration frequency was 1 kHz, and the same frequency value was obtained for all weighting networks, with the calibration pressure of 94 dB ± 0.2 dB at reference conditions (Hottinger Brüel & Kjær, 2022).

Frequency A-weighting was used with the noise measuring equipment to give approximately the same response to different frequencies as the human ear (Aziz *et al.*, 2009). The noise reading was taken when the vehicle was cruising at a steady speed of 80-100 km/h. The SLM was placed at the same height as the ear position of the crew as in Figure 1.

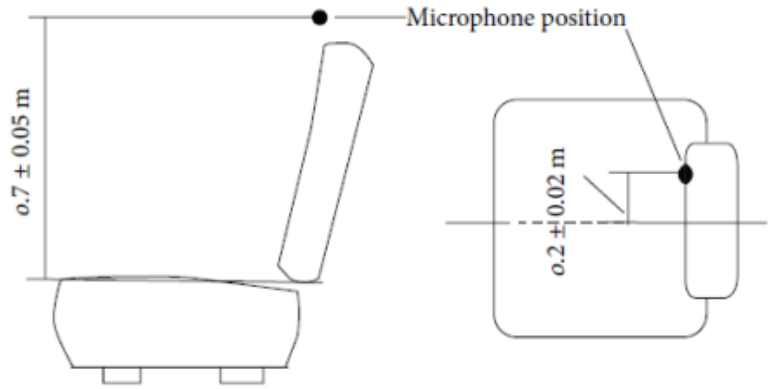

Figure 1: Microphone position with respect to the seat
Source: ISO (1980)

The measurement for each vehicle was repeated for at least three times to ensure that the data is accurate and reliable for further analysis. All the measured raw data was converted to sound pressure level (SPL) in dB(A) using the following equation:

$$SPL = 20\ log_{10} \frac{P}{P_{ref}} \quad (1)$$

where P_{ref} is the reference sound pressure value of 20 x10^{-6} Pa. The arithmetic mean value for each trial was determined. The measurements were considered valid if the range of the measurements at each speed made immediately one after the other was not greater than 2 dB(A) (ISO, 1980).

2.2 Whole-Body Vibration (WBV)

The measurement of WBV in the cabin was performed using a seat pad containing a tri-axial piezoelectric accelerometer that was connected to a B&K Type 4447 vibration analyser, which logged the total vibration levels in each axis. Accelerometer calibrations were conducted prior to all data collection sessions using a calibration exciter with oscillation frequency of 159.2 Hz and acceleration level of 10 m/s^2 (Aziz *et al.*, 2016).

The guidelines for the measurement and evaluation of human exposure to WBV are defined by ISO (1997), while compliance with the daily exposure limits is based on EU-OSHA (2002). Exposure to individual sources of constant WBV was calculated from the magnitude of vibration expressed as acceleration in m/s^2 and the duration of exposure. The daily vibration exposure ($A(8)$) is the amount of vibration to which a driver or crew is exposed during a working day, normalised to an 8 h reference period. $A(8)$ can be calculated using the following equation:

$$A(8) = a_w \sqrt{\frac{T}{T_0}} \quad (2)$$

where a_w is the vibration magnitude (in m/s^2) on the axis that measured highest, including the weighting factor, k =1.4, for the x and y axes; T is the actual duration in hours of exposure to the vibration magnitude a_w; and T_o is the reference duration of 8 h.

2.3 Heat Stress

The measurement of heat stress in the cabin was conducted by measuring the wet bulb globe temperature (WBGT) index, which considers environmental factors in the vehicle cabin such as air temperature, humidity, air movement and radiant heat. The measurements were carried out by placing a portable WBGT meter in the interior of the vehicle cabin for a period of 4 to 5 h, considering the peak hours of environmental heat (11.00 am to 3.00 pm). This is based on the heat stress management guideline issued by DOSH (2016), with the assumption that the peak hours provide the highest heat value in the climatic environment of Malaysia.

By considering the heat radiation factor directly from sunlight, the WBGT index can be calculated using the following equation:

$$WBGT = 0.7T_{wb} + 0.2T_g + 0.1T_a \quad (3)$$

where T_{wb} is the wet bulb temperature, T_g is the globe temperature and T_a is the air temperature (Epstein & Moran 2006; ISO 2017). In this study, being in the vehicle cabin is categorised as an activity that has low metabolic rate. The WBGT reference value was set for the level of acclimatisation to heat of 30 °C (ISO 2017; ACGIH 2022).

3. RESULTS AND DISCUSSION

3.1 Noise Exposure

Analysis of noise in the cabin for all three types of evaluated vehicles as in Figure 2 shows that the average SPL values for logistics and utility vehicles are low, under 80 dB(A). The average SPL value for the armoured vehicles is quite high and almost exceeds the daily noise exposure level of 85 dB(A) (DOSH, 2019). This is due to larger engine capacity used by armoured vehicles causing higher noise levels. However, the SPL values for the three types of vehicles are still below the permitted level and will not cause any consequences to the driver and crew in the cabin during 8 h of operation.

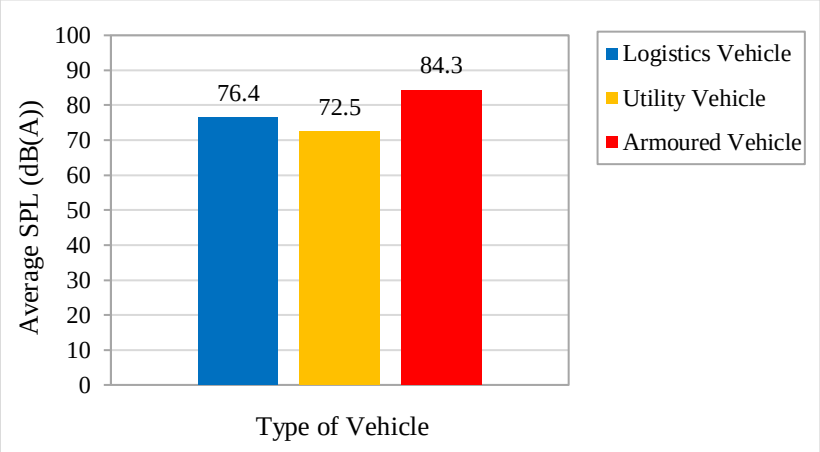

Figure 2: Cabin noise for different types of evaluated vehicles.

3.2 WBV

WBV analysis on the driver and crew in the cabin as in Figure 3 shows that the logistics vehicles gave the highest value of average *A*(8) as compared to the other two types of vehicles. This is due to stiffer suspension and seating configuration used by logistics vehicle causing higher WBV levels. However, the *A*(8) values for the three types of vehicles are still below the permitted daily exposure limit value of 1.15 m/s^2 (EU-OSHA, 2002) and would not cause serious effects on the crew in the cabin during 8 h of operation.

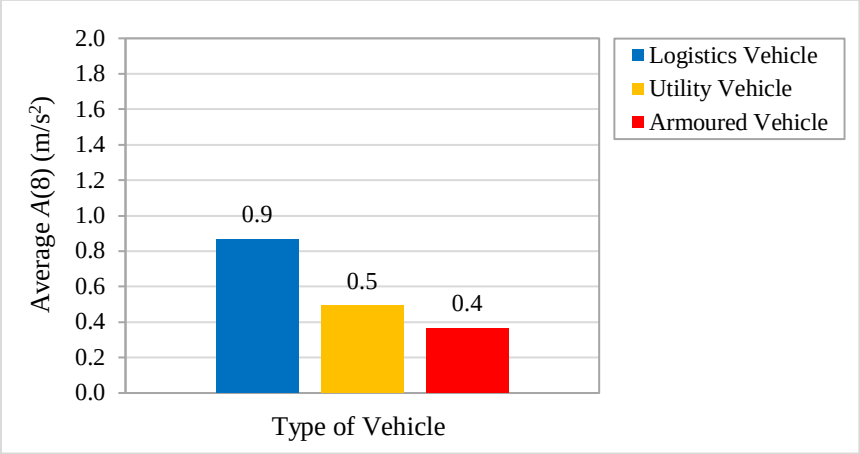

Figure 3: WBV for different types of evaluated vehicles.

3.3 Heat Stress

Analysis of the heat stress index value in the cabin as in Figure 4 shows that the logistics vehicles gave the highest average value as compared to the other two types of vehicles. This is due to larger cabin coverage area of logistics vehicles resulting in higher heat stress index values. Although the heat stress value is close to the action limit value of 30 °C (ISO 2017; ACGIH 2022), the value is still below the permitted level. Therefore, the heat stress index values for these three types of vehicles should not harm the crew in the cabin during operations.

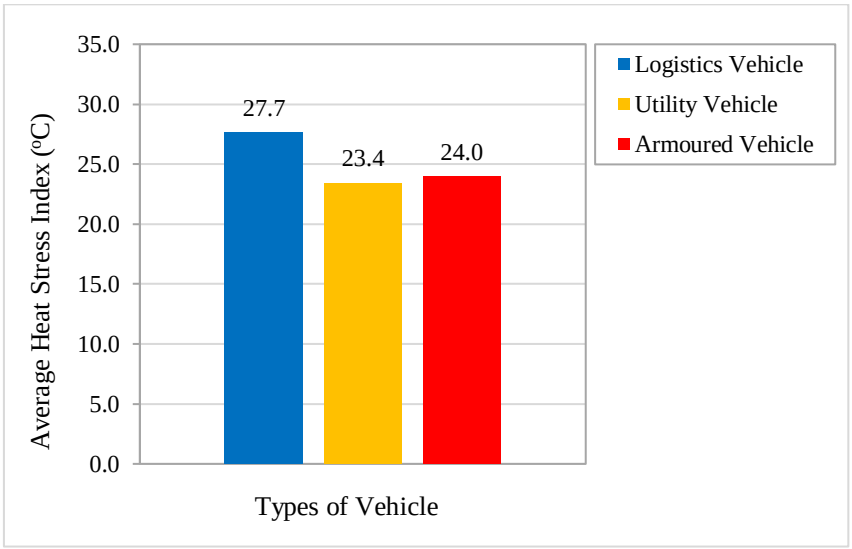

Figure 4: Heat stress index for different types of evaluated vehicles.

4. CONCLUSION

Logistics vehicles were found to have low noise exposure level, but relatively high WBV and heat stress values. Meanwhile, wheeled armoured vehicles have the highest noise exposure level, but low WBV and heat stress values. Among the three types of vehicles tested, utility vehicles showed the highest level of human comfort. However, the overall the human comfort study for the three types of military vehicles showed that the level of noise exposure, WBV and heat stress index are within the permissible range.

A primary limitation of this study is that it was only conducted for tarmac road surfaces. For rough road surfaces, it is expected that values of noise and WBV would have been higher. Furthermore, additional data from more types of military vehicles will need to be collected and analysed.

REFERENCES

ACGIH (American Conference of Governmental Industrial Hygienists) (2022). *Heat Stress and Strain*. Available online at: https://www.acgih.org/heat-stress-and-strain-2/ (Last access date: 8 August 2022).

Aziz, S.A.A. & Ibrahim. F. (2022). Study on Braking Efficiency of Military Armoured Vehicles in Malaysian Tropical Environment. *Defence S&T Tech. Bull.*, **15**, 28–33

Aziz, S.A.A, Gani, A., Suhaimi, A.F., Kalil, S.., Yusuf, A.Y & Nuawi, M.Z., (2017). Noise exposure inside a passenger car cabin in tropical environmental condition. *Defence S&T Tech.*, **10**: 290-296.

Aziz, S.A.A., Nuawi, M.Z. & Nor, M.J.M. (2017). Monitoring of hand-arm vibration. *Int. J. Acoust. Vib.*, **22**: 34-43.

Aziz, S.A.A., Nuawi, M.Z. & Nor, M.J.M. (2016). Predicting whole-body vibration (WBV) exposure of Malaysian Army three-tonne truck drivers using integrated kurtosis-based algorithm for Z-notch. filter technique 3D (I-Kaz 3D). *Int. J. Ind. Ergon.*, **52**: 59–68.

Aziz, S.A.A., Nuawi, M.Z, Nor, M.J.M. & Daruis, D.D.I. (2014). Study of noise exposure inside a Malaysian Army three-tonne truck driver's compartment using I-Kaz^{TM}. *Defence S&T Tech. Bull.*, **7**:107–111.

Aziz, S.A.A., Gani. A. & Hassan, A.H. (2009). Pass-by noise of Malaysian Armed Forces (MAF) vehicles. *Defence S&T Tech. Bull.*, **2**, 10–19.

Aziz, S.A.A., Gani. A. & Hassan, A.H. (2008). Whole body vibration (WBV) on Malaysian Armed Forces (MAF) vehicles. *Defence S&T Tech. Bull.*, **1**: 7–15.

DOSH (Department of Occupational Safety and Health Malaysia) (2016). *Garis Panduan Pengurusan Tegasan Haba di Tempat Kerja*. Department of Occupational Safety and Health Malaysia (DOSH), Ministry of Human Resources, Malaysia.

DOSH (Department of Occupational Safety and Health Malaysia) (2019). *Occupational Safety and Health (Noise Exposure) Regulations 2019*. Department of Occupational Safety and Health Malaysia (DOSH), Ministry of Human Resources, Malaysia.

Epstein, Y. & Moran, D.S. (2006). Thermal Comfort and Heat Stress Indices. *Industrial Health*, **44**: 388-398.

EU-OSHA (European Agency for Safety and Health at Work) (2002). *Directive 2002/44/EC: On the Minimum Health and Safety Requirements Regarding the Exposure of Workers to the Risks Arising from Physical Agents (Vibration)*. European Agency for Safety and Health at Work (EU-OSHA), Bilbao, Spain.

Gani, A., Aziz, S.A.A. & Hassan, A.H. (2009). Test protocol for Malaysian Armed Forces (MAF) vehicles - Health hazard assessment (HHA) and vehicle performance. *Defence S&T Tech.*, **2**: 1-9.

Gani. A. & Aziz, S.A.A., (2008) Heat stress on various types of military vehicles in Malaysian climate. *Defence S&T Tech.*, **1**: 16-29.

Hottinger Brüel & Kjær (2022). *Sound Calibrator Type 4231 - Product Data BP 1311–19*. Denmark.

ISO (International Organization for Standardization) (2017). *ISO 7243:2017: Ergonomics of the thermal environment — Assessment of heat stress using the WBGT (wet bulb globe temperature) index*. International Organization for Standardization (ISO), Geneva, Switzerland.

ISO (International Organization for Standardization) (1997). *ISO 2631-1:1997: Mechanical vibration and shock — Evaluation of human exposure to whole-body vibration — Part 1: General requirements*. International Organization for Standardization (ISO), Geneva, Switzerland.

ISO (International Organization for Standardization) (1980). *ISO 5128:1980: Acoustics - Measurement of noise inside motor vehicles*. International Organization for Standardization (ISO), Geneva, Switzerland.

King, W.C., Harmon, R., Juvik, J., Hendrickx, J.M.H. & Palka, E.J. (2006). *A Technical Analysis of Suriname for Tropical Testing of Army Materiel and Systems*. United States Army Research Office, North Carolina, US.

King,W.C., Harmon, R., Bullard,T., Dement,W., Doe, W., Evans, J., Larsen, M.C., Lawrence, W., McDonald, K. & Morrill, V. (1998). *A Technical Analysis to Identify Ideal Geographic Locations for Tropical Testing of Army Materiel and Systems*. United States Army Research Office, North Carolina, US.

Khan, M.K.J., Gani. A., Aziz, S.A.A. & Hassan, A.H., (2010). Determination of whole body vibration (WBV) of main battle tank (MBT) PT-91M. *Defence S&T Tech.*, **3**: 29–35.

Wang, X. (2010). *Vehicle noise and vibration refinement*. Woodhead Publishing Limited, UK.

INDOOR AIR QUALITY (IAQ) ONBOARD A NAVAL SHIP: A COMPARATIVE STUDY BETWEEN COMPARTMENTS

Nur Alyaa Tasnim Mohammad Zin[1], Amirul Faiz Kamaruddin[2,3], Nur Sarah Fatihah Tamsi[1], Muhammad Firdaus Zamri[1], Noor Artika Hassan[4], Arman Ariffin[5] & Maryam Zahaba[*1]

[1]Department of Chemistry, Kulliyyah of Science, International Islamic University Malaysia (IIUM), Malaysia
[2]Department of Biotechnology Engineering, Kulliyyah of Engineering, International Islamic University Malaysia (IIUM), Malaysia
[3]KD Laksamana Muhammad Amin, Royal Malaysian Navy (RMN) Lumut Naval Base, Malaysia
[4]Department of Community Medicine, Kulliyyah of Medicine, International Islamic University Malaysia (IIUM), Malaysia
[5]Eastern Maintenance Overseer Unit Royal Malaysian Navy (RMN), RMN Naval Base, Malaysia

[*]Email: maryamzahaba@iium.edu.my

ABSTRACT

Naval ships are made up of confined and enclosed spaces where air circulation is limited. For the Royal Malaysian Navy's (RMN) ageing assets that are still in service, inefficient ventilation is one of the concerns. This can lead to the elevation of indoor air pollutants (IAP) and worsen indoor air quality (IAQ) onboard, which can indirectly cause Sick Boat Syndrome (SBoS). In order to prevent SBoS, this study aims to assess the IAQ conditions of compartments inside a naval ship and to determine the parameters of compliance with the relevant standards, namely the Industry Code of Practice on Indoor Air Quality 2010 (ICOP IAQ 2010), United States Environmental Protection Agency (US EPA 2006) and Malaysian Ambient Air Quality Standards (MAAQS 2013). In addition, the differences in the IAQ parameters between the ship's compartments were determined. IAQ assessment was performed at four different compartments, namely the wardroom, cabin, machinery control room (MCR) and bridge, using calibrated handheld IAQ devices. A total of nine parameters were assessed, which were temperature, relative humidity (RH), carbon dioxide (CO_2), carbon monoxide (CO), total volatile organic compound (TVOC) particulate matter ($PM_{2.5}$ and PM_{10}), formaldehyde (CH_2O), and nitrogen dioxide (NO_2). The differences in IAQ parameters were analysed with IBM SPSS version 26, using the Kruskal-Wallis and Dunn's Post Hoc tests. The results found that compliance with the standards can be observed for almost all of the IAQ parameters, except for PM_{10}, $PM_{2.5}$, TVOC, CH_2O, and NO_2, in several compartments. The Kruskal-Wallis test concluded that there were significant differences in the IAQ parameters in the compartments with p-values < 0.05. The results of Dunn's Post Hoc test indicated that all sampling points pairwise had significant differences with p-values < 0.05. The incompliance with the standards and variations of the IAQ parameters were attributed to several factors, namely crews' activities, furnishings and fuel combustion from machinery onboard the ship. In conclusion, continuous monitoring of IAQ is required to ensure good IAQ for the ship's crew to keep them healthy and improve their productivity. In the bigger picture, good IAQ is needed to ensure the readiness of the naval fleet, to preserve the sovereignty of the country.

Keywords: *Indoor air quality (IAQ); naval ships; indoor air pollutants (IAP); Sick Boat Syndrome (SBoS); ship crew.*

1. INTRODUCTION

Poor indoor air quality (IAQ) onboard has been reported to cause unhealthy and uncomfortable indoor environment and even lead to equipment breakdown (Ariffin *et al*., 2021). Equipment can be corroded due to dust accumulation combined with a small amount of moisture exposing the material to the

oxidation process (Xue & Ji, 2004). Studies have also discovered that among the factors causing poor IAQ within a ship include the effectiveness of the ventilation system, the crew's routine, the ship's furnishings and materials, and ship operation (Zahaba *et al.*, 2022). In addition, ageing Royal Malaysian Navy (RMN)'s assets are also one of the contributing factors to poor IAQ, as it can be challenging to maintain the equipment including the mechanical ventilation and air conditioning (MVAC) system due to outdated technology (Halizahari & Melan, 2016). Since naval ships are considered as enclosed and confined spaces consisting of vertically and horizontally adjacent compartments, it is very difficult to maintain good IAQ. The ventilation system onboard has to serve its purposes effectively as the ship must be resilient to airborne chemical and biological agents and at the same time provide safe spaces for the crew. Thus, the MVAC system should work efficiently during war, especially in chemical, biological, radiological, and nuclear (CBRN) war.

The design of the MVAC system of naval ships has to protect the crew from hazardous airborne agents, but this will limit the introduction of fresh air into the ships However, it is important to highlight that the MVAC system is supposed to provide comfort for the crew and dilute indoor air pollutants as well. However, studies have reported on the accumulation of indoor air pollutants (IAPs) that affect IAQ onboard (Tamsi *et al.*, 2021). It is vital to emphasise the IAQ issues on naval ships since there is a large number of crew working and living onboard. In addition, the crew stays onboard for a longer duration according to the task assigned during the operation. Exposure to IAPs such as formaldehyde (CH_2O), carbon monoxide (CO), nitrogen dioxide (NO_2), total volatile organic compounds (TVOC) and particulate matter can adversely affect the health of the crew through either acute or chronic effects (Cretescu *et al.*, 2019; Carro *et al.*, 2020). Among the symptoms of exposure to IAP are dizziness, nausea, cough, stuffy nose, eye irritation, and dry skin. According to Dąbrowiecki *et al.* (2015), symptoms that occur in ships or vessels are termed as Sick Boat Syndrome (SBoS). Crew members who experience SBoS usually feel relieved after they leave the ship.

In order to protect the crew's health and work productivity, as well as machinery life span, it is important to investigate the IAQ condition onboard in order to implement appropriate mitigation measures to reduce the concentration of IAP onboard and maintain good IAQ for the crew. Hence, this study aims to assess the IAQ conditions of compartments inside a naval ship and to determine the parameters of compliance with the relevant standards, namely the Industry Code of Practice on Indoor Air Quality 2010 (ICOP IAQ 2010) by Department of Safety and Health Malaysia (DOSH, 2010), United States Environmental Protection Agency (US EPA 2006) by US EPA (2006) and Malaysian Ambient Air Quality Standards (MAAQS 2013) by Department of Environment Malaysia (DOE, 2013).

In addition, the differences in IAQ parameters between those compartments are also determined to investigate and compare the IAQ trends between the compartments. A naval ship consists of accommodation and workspace compartments that are important for the ship's crew and mission accomplishment. According to the American Bureau of Shipping (2016), the accommodation areas in a ship, known as the rest and recreation area, includes cabins where the crew sleeps and wardroom where the officers dine. On the other hand, the workspaces areas are the areas allocated for crew to work, including, but not limited to, navigation and service spaces such as galley, machinery spaces, and control stations. These compartments serve different purposes and have different nature of surroundings, such as number of crew, size of compartment, furnishing, equipment, as well as different routines based on their roles and tasks. These factors would contribute to different IAQ conditions between the compartments on the ship due to distinct IAP sources in the compartments.

2. METHODOLOGY

This study was conducted on one of the RMN's assets from Handalan class of ships, named as Ship Alpha. The IAQ assessment was conducted in April 2022, while the ship was alongside a jetty located in Pahang, Malaysia. Table 1 describes the general characteristics of Ship Alpha and the year it was commissioned.

Table 1: General characteristics of Ship Alpha.

Class	Fast Attack Craft (Missile)
Dimensions	142.6 m x 23.3 m x 7.4 m
Year of commissioning	1979
Complement	40 crew members, including 6 officers
Number of engines	3
Numbers of gensets	3
MVAC system	Centralised air conditioning system

The sampling was carried out in four compartments: wardroom, cabin, machinery control room (MCR), and bridge. The sampling points were chosen to represent the accommodation areas and workspaces of the crew, as shown in Figure 1.

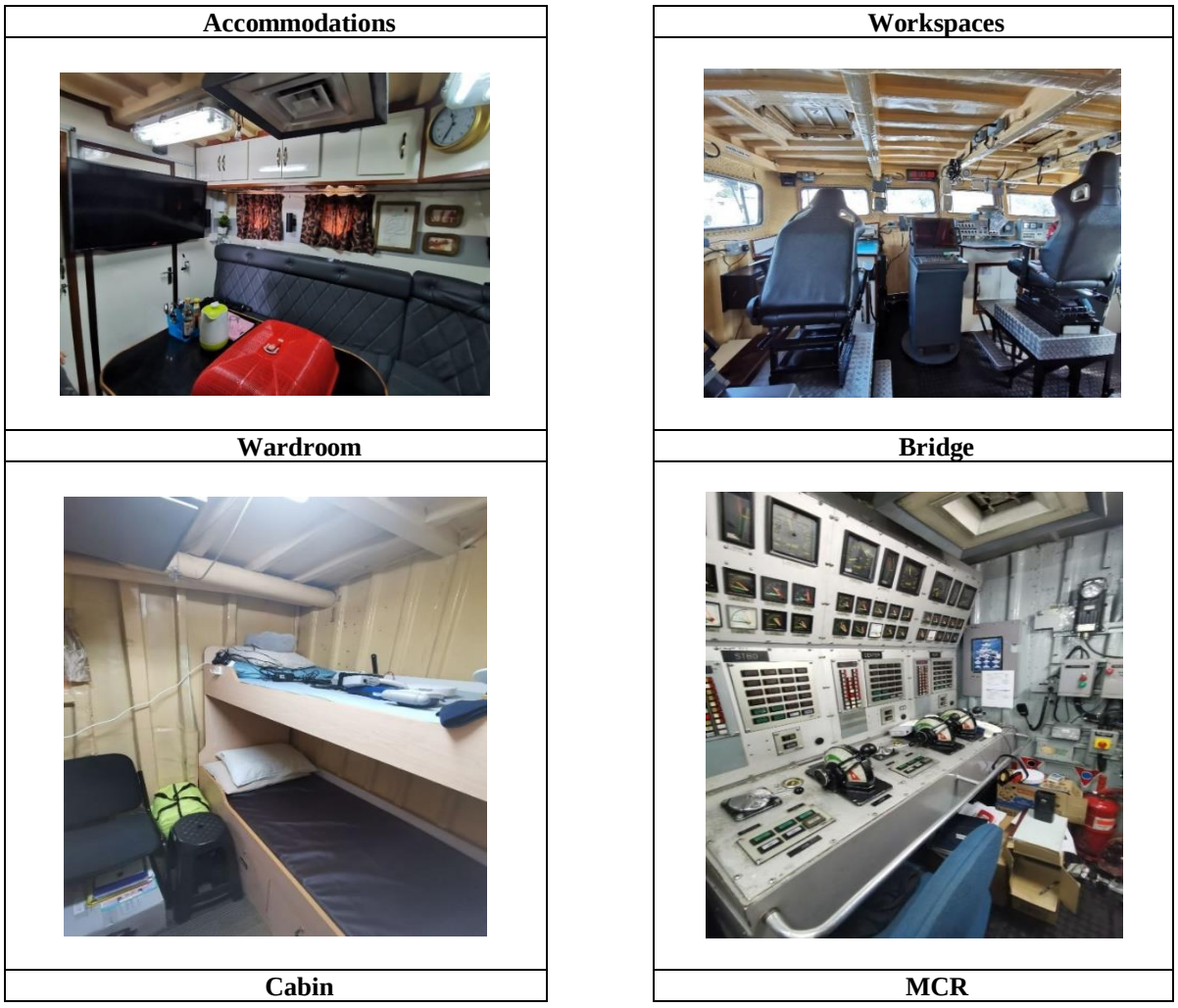

Figure 1: Selected sampling points onboard Ship Alpha.

A total of nine IAQ parameters were assessed, which are temperature, relative humidity (RH), carbon dioxide (CO_2), CO, TVOC, particulate matters ($PM_{2.5}$ and PM_{10}), CH_2O, and NO_2. The sampling was conducted using calibrated handheld IAQ devices, including TSI VelociCalc 9565 ventilation meter (temperature, RH and CO_2), SR Concept indoor air quality monitor (TVOC, CH_2O, and NO_2), and Aeroqual S500 portable air quality monitor sensor ($PM_{2.5}$, PM_{10} and CO). Each sampling point was sampled for 24 h on three consecutive days using real-time continuous monitoring. Readings were taken at 5 min intervals. The average reading then was compared to the standards selected namely, ICOP IAQ 2010 (temperature, RH, CO_2, CO, TVOC, PM_{10} and CH_2O), US EPA 2006 ($PM_{2.5}$) and MAAQS 2013 (NO_2) to observe the compliance of the IAQ parameter readings to the available standards.

Furthermore, the differences in the IAQ parameters readings between the compartments were analysed statically with IBM SPSS version 26, using the Kruskal-Wallis and Dunn's Post Hoc tests. From the analysis, the distribution of all parameters was not normally distributed and thus the non-parametric Kruskal Wallis test was used to determine the significant differences for the nine parameters using the mean rank of all sampling locations. The conservative Dunn's post hoc test was performed for the pairwise differences between all sampling locations according to the indoor air parameters. A *p*-value of < 0.05 was used as the cut-off point for significant factors.

3. RESULTS AND DISCUSSION

3.1 IAQ Parameters Compliance with the Standards

IAQ standard such as ICOP IAQ 2010 that was developed by DOSH aims to protect building occupants from poor IAQ (DOSH, 2010). This standard has helped to educate building occupants on the significance of IAQ and encourage them to recognise the need to ensure good IAQ. Thus, it is important to comply with the standard even though the standards used in this study, as shown in Table 2 are for the building occupant's exposure, not for the crews onboard.

Table 2: Distribution of IAQ parameters at the four sampling points on Ship Alpha.

Parameters	Normal Range	Wardroom	Cabin	Machinery Control Room (MCR)	Bridge
Temperature (°C)	23.0 - 26.0	23.9 ± 1.0	22.2 ± 1.6	25.4 ± 0.9	26.3 ± 3.4
RH (%)	40.0 - 70.0	53.7 ± 5.0	65.9 ± 2.7	57.5 ± 2.0	48.2 ± 2.9
CO_2 (ppm)	C1,000	470 ± 35	478 ± 45	510 ± 30	473 ± 32
CO (ppm)	10	0.13 ± 0.35	0.35 ± 0.83	0.14 ± 0.15	0.10 ± 0.14
PM_{10} (mg/m^3)	0.150	0.097 ± 0.012	0.015 ± 0.039	0.173 ± 0.016	0.153 ± 0.033
$PM_{2.5}$ (mg/mg^3)	0.015	0.063 ± 0.007	0.104 ± 0.027	0.124 ± 0.010	0.009 ± 0.018
TVOC (ppm)	3.000	5.306 ± 4.445	1.780 ± 2.406	0.432 ± 0.416	0.814 ± 0.482
CH_2O (ppm)	0.10	0.060 ± 0.004	0.060 ± 0.005	0.070 ± 0.004	0.130 ± 0.008
NO_2 (ppm)	0.16	0.40 ± 0.20	0.05 ± 0.08	0.30 ± 0.21	0.60 ± 0.65

Notes:

- The values highlighted in red indicate the parameters that are out of the recommended values specified in the standards, namely ICOP IAQ 2010 (temperature, RH, CO_2, CO, TVOC, PM_{10} and CH_2O), US EPA 2006 ($PM_{2.5}$) and MAAQS 2013 (NO_2).
- For chemical contaminants (CO, PM_{10}, $PM_{2.5}$ TVOC, CH_2O and NO_2), the limits are 8 h time-weighted average airborne concentrations.
- mg/m^3 is milligrams per cubic meter of air at 25 °C and one-atmosphere pressure.
- ppm is parts of vapour or gas per million parts of contaminated air by volume.
- C is the ceiling limit that shall not be exceeded at any time. Readings above 1,000 ppm are an indication of inadequate ventilation.
- CO_2 is also known as the ventilation performance indicator (VPI)

Table 2 shows the distribution of the IAQ parameters at the four sampling points on the ship. From all the IAQ parameters assessed, only four IAQ parameters complied with the standards for all the compartments. Temperature and RH complied with the standard ranges between 23 - 26 °C and 40 - 70% respectively. From the observation of the air handling unit (AHU) compartment on Ship Alpha, the cooling coil and fin were clean, not corroded and not clogged with dust. In addition, this ship had just undergone ducting cleaning. The good condition of the AHU helped to get the desired temperature and RH. An efficient cooling system or AHU is crucial onboard to maintain the equipment and weaponry as they need a specific temperature and RH to work efficiently and for longer lifespan.

Furthermore, CO_2, which acts as a ventilation performance indicator (VPI), and CO complied with the standards for all four compartments. Even though Ship Alpha is complemented with a large number of crew onboard, the CO_2 concentration complied with ICOP IAQ 2010. This indicates the ship is well-ventilated and the accumulation of IAP onboard can be prevented. This is due to the design of the MVAC system onboard that allows for introduction of fresh air into the ship. In comparison, higher CO_2 concentrations were recorded in other ships even after forced ventilation was conducted (Zahaba *et al.*, 2022).

Some chemical contaminants were observed to be above the standard range. For example, PM_{10} and $PM_{2.5}$ at the MCR and bridge were incompliant with ICOP IAQ 2010 and US EPA 2006 respectively. This could be due to the large number of crew at the sampling points during the assessments. Increase in the number of occupants can increase the PM concentration, as observed by Algarni *et al.* (2021). Other than that, the possible sources of PM onboard are cooking activities, fuel combustion and smoking. Meanwhile, the $PM_{2.5}$ concentrations in the wardroom, cabin and MCR exceeded the acceptable range of 0.015 mg/mg^3 as stated in US EPA 2006. According to the study by Sankhyan *et al.* (2022), $PM_{2.5}$ is mainly attributed to indoor sources and infiltration from outdoors. This study observed and found that $PM_{2.5}$ originates from indoor sources such as cooking, even though the concentrations vary between compartments. This could be explained by the differences in activities and number of occupants in the said areas. Furthermore, infiltration was observed allowing the IAP from outdoors introduced to indoors. Good and correct practice of closing and opening the door and hatches is one of the strategies to maintain acceptable IAQ.

The highest concentration of TVOC was recorded in the wardroom, which exceeded the acceptable range. It was found that air fresheners and other types of fragrances were used in this compartment, which can contribute to increased concentration of TVOC. Therefore, very minimal use of aerosol fragrance spray is advised onboard. According to the study conducted by Bacaloni *et al.* (2011), common volatile organic compounds released into the air are CH_2O, benzene, ethylene glycol, and carbolic acid. Indoor exposure to TVOCs has been linked to a variety of detrimental health effects, such as mucous membrane irritation, weariness, poor concentration and potential cancer (Kraus & Šenitková, 2020). Therefore, awareness of good IAQ practices and ensuring proper ventilation in the ship is vital to maintain low concentration of TVOC onboard.

In addition, CH_2O concentration in the bridge as well as NO_2 concentrations in all the compartments except for the cabin were not within the permissible ranges. From this study, the incompliance with standards showed the possibility of infiltration of outdoor air into the compartments. Higher CH_2O and NO_2 were observed when an adjacent ship on the outer berth started its engine. IAP infiltrates ships through openings such as fresh air intake and door / hatch openings. Crew members are advised to observe the practice of opening and closing the door according to the standard.

3.2 Comparison of IAQ Parameters between Compartments

Comparison of the IAQ parameters between the compartments are as shown in Table 3. All the parameters in each compartment were significantly different, with *p*-values of <0.001. The levels of pollutants present in the compartments were at different levels. For temperature, RH, CO_2, and CO, although there were differences in the mean rank, all the readings were still within normal range. The mean rank for PM_{10} and $PM_{2.5}$ were the highest at the MCR and cabin, while the mean rank for TVOC and NO_2 were highest at the wardroom, followed by other areas. For CH_2O, the mean rank was highest at the bridge and MCR. Some of these readings surpassed the normal range as presented in Table 3.

Table 3: The association of sampling points and IAQ parameters.

IAQ Parameters / Sampling Points	Mean Rank	*p*-value
Temperature (°C)		< 0.001
Wardroom	505.29	
Cabin	264.96	
MCR	805.54	
Bridge	730.21	
RH (%)		< 0.001
Wardroom	461.41	
Cabin	1008.5	
MCR	634.07	
Bridge	202.02	
CO (ppm)		< 0.001
Wardroom	488.53	
Cabin	697.8	
MCR	602.3	
Bridge	517.38	
PM_{10} (mg/m^3)		< 0.001
Wardroom	445.15	
Cabin	555.09	
MCR	853.22	
Bridge	452.54	
$PM_{2.5}$ (mg/mg^3)		< 0.001
Wardroom	435.9	
Cabin	574.74	
MCR	871.51	
Bridge	423.84	
TVOC (ppm)		< 0.001
Wardroom	959.49	
Cabin	630.01	
MCR	238.66	
Bridge	477.85	
CH_2O (ppm)		< 0.001
Wardroom	328	
Cabin	255.3	
MCR	714.22	
Bridge	1008.48	
NO_2 (ppm)		< 0.001
Wardroom	720.17	
Cabin	243.5	
MCR	683.1	
Bridge	659.24	
CO_2 (ppm)		< 0.001
Wardroom	474.05	
Cabin	507.3	
MCR	821.51	
Bridge	503.14	

Note:
*Kruskal Wallis Test; Sig at *p*-value < 0.05

As shown in Table 4, further analysis with the Dunn's Post Hoc test indicated that most pairwise sampling points had significant differences in the IAQ parameters with *p*-values of <0.05, such as for temperature, RH, TVOC, and CH_2O.

Table 4: Pairwise comparison for all IAQ parameters at all sampling points.

IAQ Parameter	Sampling Points Pairwise	Test Statistic (*z*-score)	*p*-value
Temperature (°C)	Cabin-Wardroom	240.332	<0.001
	Cabin-Bridge	-465.250	<0.001
	Cabin-MCR	-540.578	<0.001
	Wardroom-Bridge	-224.918	<0.001
	Wardroom-MCR	-300.247	<0.001
	Bridge-MCR	75.328	0.007
RH (%)	Bridge-Wardroom	259.387	<0.001
	Bridge-MCR	432.045	<0.001
	Bridge-Cabin	806.477	<0.001
	Wardroom-MCR	-172.658	<0.001
	Wardroom-Cabin	-547.090	<0.001
	MCR-Cabin	374.432	<0.001
CO (ppm)	Wardroom-Bridge	-28.852	0.294
	Wardroom-MCR	-113.767	<0.001
	Wardroom-Cabin	-209.269	<0.001
	Bridge-MCR	84.915	0.002
	Bridge-Cabin	180.417	<0.001
	MCR-Cabin	95.502	0.001
PM_{10} (mg/m^3)	Wardroom-Bridge	-7.384	0.790
	Wardroom-Cabin	-109.934	<0.001
	Wardroom-MCR	-408.064	<0.001
	Bridge-Cabin	102.550	<0.001
	Bridge-MCR	400.681	<0.001
	Cabin-MCR	-298.130	<0.001
$PM_{2.5}$ (mg/mg^3)	Wardroom-Bridge	-29.095	0.294
	Wardroom-Cabin	-33.255	0.230
	Wardroom-MCR	-347.455	<0.001
	Bridge-Cabin	4.160	0.881
	Bridge-MCR	318.359	<0.001
	Cabin-MCR	-314.200	<0.001
TVOC (ppm)	MCR-Bridge	-239.191	<0.001
	MCR-Cabin	391.349	<0.001
	MCR-Wardroom	720.828	<0.001
	Bridge-Cabin	152.158	<0.001
	Bridge-Wardroom	481.637	<0.001
	Cabin-Wardroom	329.479	<0.001
CH_2O (ppm)	Cabin-Wardroom	72.700	0.008
	Cabin-MCR	-458.917	<0.001
	Cabin-Bridge	-753.182	<0.001
	Wardroom-MCR	-386.217	<0.001
	Wardroom-Bridge	-680.483	<0.001
	MCR-Bridge	-294.266	<0.001

NO_2 (ppm)	Cabin-Bridge	-415.741	<0.001
	Cabin-MCR	-439.602	<0.001
	Cabin-Wardroom	476.670	<0.001
	Bridge-MCR	23.861	0.386
	Bridge-Wardroom	60.929	0.027
	MCR-Wardroom	37.068	0.178
CO_2 (ppm)	Wardroom-Bridge	-29.095	0.294
	Wardroom-Cabin	-33.255	0.230
	Wardroom-MCR	-347.455	<0.001
	Bridge-Cabin	4.160	0.881
	Bridge-MCR	318.359	<0.001
	Cabin-MCR	-314.200	<0.001

Note:
Dunn's Post Hoc Test; ; Sig at *p*-value < 0.05

For CO and $PM_{10,}$ no significant differences were found for the pairwise comparison of wardroom and bridge, while for CO_2 and $PM_{2.5,}$ no significant differences were found for the pairwise of wardroom and cabin, wardroom and bridge, as well as bridge and cabin. For $NO_{2,}$ no significant differences were found between the pairwise of bridge and MCR, as well as MCR and wardroom. The variations in the results showed that the IAQ parameters in the compartments of the ships might have been influenced by the machinery, engine and generators of the ships, location and condition of the compartments, as well as crew's activities.

4. CONCLUSION

The IAQ assessment conducted in this study for Ship Alpha found that the temperature, RH, CO_2 and CO were within the acceptable limits of ICOP IAQ 2010. The assessment also revealed the incompliance with the standards for PM_{10} at MCR and bridge; $PM_{2.5}$ at the wardroom, cabin and MCR; TVOC at the wardroom; CH_2O at the bridge; and NO_2 at the wardroom, MCR and bridge. It was also found that all the IAQ parameters varied significantly at the different sampling points. The variations were contributed by fuel combustion from machinery, crew's activities such as cooking, and usage of aerosol sprays, as well as material of furnishings in the ship. Without proper IAQ management onboard, these factors will lead to accumulation of IAP.

Therefore, it is proposed to have continuous monitoring and assessment of the IAQ parameters in order to maintain good IAQ onboard. This study also highlighted the absence of sophisticated systems for continuous monitoring of IAQ onboard naval ships and the lack of awareness of IAQ related issues among crew members. If these factors are neglected, poor IAQ will negatively affect their health and productivity, and can cause the deterioration of the machinery onboard. It is important to emphasise that good IAQ is needed to maintain the state of readiness of the naval fleet in order to ensure the sovereignty of the country.

REFERENCES

American Bureau of Shipping. (2016). *Guide For Crew Habitability on Ships.* American Bureau of Shipping, Texas.

Algarni, S., Khan, R.A., Khan, N.A. & Mubarak, N.M. (2021). Particulate matter concentration and health risk assessment for a residential building during COVID-19 pandemic in Abha, Saudi Arabia. *Environ Sci. Pollut. Res.*, **28**: 65822–65831.

Ariffin, A., Kamaruddin, A.F. & Zahaba, M. (2021). Preliminary study on indoor climate in a naval

Bacaloni, A., Insogna, S. & Zoccolillo, L. (2011). Indoor air quality. volatile organic compounds: sources, sampling and analysis. *In* Mazzeo, N. (Ed.), *Chemistry, Emission Control, Radioactive Pollution and Indoor Air Quality*. InTechOpen, London, UK, pp. 261-276.

Carro, G., Jacobs, W., Storme, P., Cabal, A., Demeyer, S. & Schalm, O. (2020). A new approach to make indoor air quality in the accommodation of ships understandable and actionable for seafaring staff. *Proc. 8th Int. Conf. Maritime Transport: Tech., Innov. Research (Maritime Transport 2020)*, Universitat Politècnica de Catalunya. Departament de Ciència i Enginyeria Nàutiques, pp. 418-435.

Cretescu, I., Isopescu, D.N., Lutic, D. & Soreanu, G. (2019). Indoor air pollutants and the future perspectives for living space design. *In* Korhan, O (Ed.), *Indoor Environment and Health*. InTechOpen, London, UK pp. 85-100.

Dąbrowiecki, Z., Dąbrowiecka, M., Olszański, R., Siermontowski, P. & Jóźwiak, D. (2015). Sick boat syndrome. *PolHypRes*, ***53*:** 81-92.

DOE. (2013). *Malaysian Ambient Air Quality Standard.* Available online at: https://enviro2.doe.gov.my/ekmc/wp-content/uploads/2018/07/PIL-Existing-AQM-SNA-Amended-5-August-2016.pdf (Last access date: 8 February 2023).

DOSH. (2010). *Industry Code of Practice on Indoor Air Quality*. Available online at: https://www.dosh.gov.my/index.php/legislation/codes-of-practice/chemical-management/594-02-industry-code-of-practice-on-indoor-air-quality-2010/file (Last access date: 8 February 2023).

Halizahari, M. & Melan, M. (2016). Initiatives to prolong aging assets life cycle: A case study in Royal Malaysian Navy. *Int. J. Supply Chain Manag.*, **5:** 122-126.

Kraus, M. & Šenitková, I.J. (2020). Level of total volatile organic compounds (TVOC) in the context of indoor air quality (IAQ) in office buildings. *IOP Conf. Ser. Mater. Sci. Eng.*, **728**: 012012.

Sankhyan, S., Witteman, J.K., Coyan, S., Patel, S. & Vance, M.E. (2022). Assessment of $PM_{2.5}$ concentrations, transport, and mitigation in indoor environments using low-cost air quality monitors and a portable air cleaner. *Environ. Sci. Atmos*., **2:** 647-658.

Tamsi, N.S.F., Zahaba, M., Kamaruddin, A.F., Mohammad Shariff, M.N., Abdul, N. & Ariffin, A. (2021). A case study on a naval ship: indoor air quality (IAQ) chemical parameters on different ship conditions and engine sequences. *YSN-ASM Int. Sci. Virt. Conf (ISVC 2021))*, 29 Mar - 1 Apr 2021, Kuala Lumpur, Malaysia.

US EPA. (2006). *What are the Air Quality Standards for PM?* Available online at: https://www3.epa.gov/region1/airquality/pm-aq-standards.html#:~:text=Since 1997%2C (Last access date: 8 February 2023).

Xue, Y.L. & Ji, G.Z. (2004). Dust corrosion. *Proc. IEEE Holm Conf. Electric Contacts*., pp. 255-262.

Zahaba, M., Tamsi, N.S.F., Engliman, S., Kamaruddin, A.F., Hassan, N.A. & Ariffin, A. (2022). Indoor air quality (IAQ) in a naval ship after refit program: a time variation analysis. *IOP Conf. Ser.: Earth Environ. Sci.*, **1013**: 012004.

LITERATURE REVIEW ON THE EFFECT OF ORAL REHYDRATION DRINKS ON THE MARKERS OF CARDIAC MUSCLE DAMAGE FOLLOWING STRENUOUS EXERCISE UNTIL EXHAUSTION

Audrey Lim Jia Yee[1], Brinnell Caszo[2] & Justin Gnanou[2*]

[1]School of Pharmacy
[2]School of Medicine
International Medical University, Malaysia

[*]Email: justingnanou@gmail.com

ABSTRACT

Moderate-intensity exercise has positive health benefits, whereas extreme exercise enhances oxidant production, which contributes to elevated cardiac output in the blood and consequently causes transient damage to cardiac muscles. Functional sports drinks are a palatable and convenient way to hydrate and recover carbohydrates, electrolytes, protein and other nutrients that have been lost throughout physical activity. This paper provides a review of the effect on cardiac biomarkers following endurance exercise as well as the effectiveness of oral rehydration drinks in reducing cardiac muscle injury. Based on the review conducted, we conclude that cardiac biomarkers levels are elevated following high-intensity exercise. Besides that, oral rehydration drinks appear to have an enhancing effect on endurance performance with the lowering of cardiac biomarkers concentration.

Keywords: *Cardiac muscle damage; sports drinks; supplementation; isotonic drinks.*

1. INTRODUCTION

Military training involves strenuous physical activities that can precipitate acute myocardial infarction. In an observational study conducted by Singh *et al.* (2021), they studied soldiers who were admitted with ST elevation myocardial infarction after strenuous military training activity. They found that 88% of respondents had symptoms within the first hour of strenuous activity. This effect of strenuous unaccustomed physical activity on cardiac muscle was related to the body's response to stress. In a study on elite airmen, it was shown the blood markers of stress were elevated after a preparator training course (Jenz *et al*., 2021).

A variety of cardiac biomarkers have been used to examine the impact of strenuous exercises on cardiomyocytes. Historically, the preferred biochemical marker has been creatine kinase-MB (CK-MB) whereas cardiac troponin (cTn) is currently the biomarker that is used as the gold standard indicator of cardiac muscle injury (Kavsak *et al*., 2018). Troponin has three distinct subunits namely troponin C, troponin I (cTnI) and troponin T (cTnT), in which cTnI and cTnT occur as the specific forms in cardiac myocytes (Perrone *et al*., 2021). Besides that, lactate dehydrogenase (LDH) and myoglobin have also gained acceptance as markers of myocardial injury (Bodor, 2016).

A growing body of evidence has shown that endurance exercises contribute to the elevation of cardiac biomarkers (Tian *et al*., 2012; Lippi *et al*., 2012; Eijsvogels *et al*., 2015; Klinkenberg *et al*., 2016; Ranjbar *et al*., 2017; Li *et al*., 2017; Keselman *et al*., 2017; Richardson *et al*., 2018; Tesema *et al*., 2019). Bates & Miller (2008) showed that dehydration and electrolytes lost through excessive sweating during strenuous exercise caused the increase in cardiac biomarkers.

Supplementation of electrolytes before, during and / or after strenuous exercise has thus become an effective strategy to avoid and minimise damage to the heart muscle (Harty *et al*., 2019). Functional sports drinks play a significant role in hydrating and thus in enhancing physical performance (Stachenfeld, 2014). Indeed, dehydration greatly reduces sports performance and can become a health risk (Orrù *et al*., 2018). The key role of these drinks is to hydrate athletes and recover the electrolytes, carbohydrates (CHO), protein (PRO) and other nutrients that are depleted throughout exercise (Evans *et al*., 2017).

The use of functional sports drinks and their benefits have been studied in in many different sports (Wojcik *et al*., 2001; Romano-Ely *et al*., 2006; Greer *et al*., 2007; Luden *et al*., 2007; Baty *et al*., 2007; Valentine *et al*., 2008; Rahnama *et al*., 2011; Howatson *et al*., 2012; Areces *et al*., 2014; Oosthuyse *et al*., 2019). According to Shirreffs *et al*. (2007), isotonic drinks such as Gatorade during exercises significantly lowered the electrolytes deficit and the subjects were essentially euhydrated. However, there is uncertainty in the data regarding oral rehydration drinks and reduction in cardiac muscle injury. An investigation by Rahnama *et al*. (2011) stated that carbohydrate supplementation had no major impact on level of cTn.

Therefore, this review addresses the impact of exercise on markers of myocardial injury, with an emphasis on the effect of oral rehydration drinks on cardiac muscle. The objective is to review the efficacy of rehydration with functional sports drinks in attenuating cardiac muscle damage following extreme exercise.

2. METHODOLOGY

2.1 Search Strategy

The study began with a search on seven databases (PubMed, Science Direct, Ovid, ProQuest, Google Scholar, Cochrane Library and Springer Link). Search terms included a mix of Medical Subject Headings (MeSH) and text words related to cardiac muscle damage, sports drink, isotonic drink, carbohydrate, supplementation, water and exercise as follows: ((cardiac muscle damage [MeSH Terms]) AND (sports drink[MeSH Terms]) OR (isotonic drink [MeSH Terms]) OR (carbohydrate [MeSH Terms]) OR (supplementation [MeSH Terms]) OR (water [MeSH Terms]) AND (exercise[MeSH Terms])). Reference lists of relevant studies were also screened to identify additional studies.

2.2 Experimental Protocol

The search was limited to publications using the English language. No articles were omitted based on the publication date. Duplicates retrieved from the search were removed manually. Titles and abstracts were first screened before retrieval of the full articles according to the eligibility criteria in Table 1.

Table 1: Inclusion and exclusion criteria.

Inclusion criteria	Exclusion criteria
- Human studies - Randomised or non-randomised trial - Prospective case-control or cohort study - Articles in English language - Articles in full text - Subjects aged 18 and above - Any sex or race	- Mechanistic and animal studies - Articles not available as full text - Articles not written in English language - Persons under 18 years - Review articles, case reports, editorials, letters and comments

2.3 Data Extraction and Measurements

All the papers that met the criteria were read in detail and important data was extracted. The following characteristics were extracted: authors, publication year, country, experimental design such as the population and age of the subjects, exercise protocol, oral rehydration drink or supplementation, as well as level of cardiac biomarkers. The measurements included determination of the level of cardiac markers such as cTnI, cTnT, CK-MB, CK, LDH and myoglobin.

3. RESULTS

3.1 Main Search

The literature search provided a total of 286 articles, but only 20 articles met all the criteria as reported in Figure 1. From 286 articles, 70 articles were removed due to duplication; 130 articles were removed because of unrelated title and abstract; four articles were removed because of unsuitable age; two articles were removed due to irrelevant exercise; while 60 articles were removed as there was no measurement of cardiac biomarkers or no oral rehydration drink.

Hence, the final review included 20 studies; six from PubMed; four from Science Direct, two from Ovid, 3 from ProQuest, three from Google Scholar, one from Cochrane Library, and one from Springer Link. Of these 20 articles, nine articles were chosen to study the effect of cardiac muscle damage on strenuous exercise, and 11 publications were chosen to study the impact of oral rehydration drink on cardiac muscle damage markers after strenuous exercise.

Thus, the articles were categorised into two categories:

1) To study the effect of strenuous exercise on markers of cardiac muscle damage
2) To study the effect of oral rehydration drinks on markers of cardiac muscle damage following strenuous exercise.

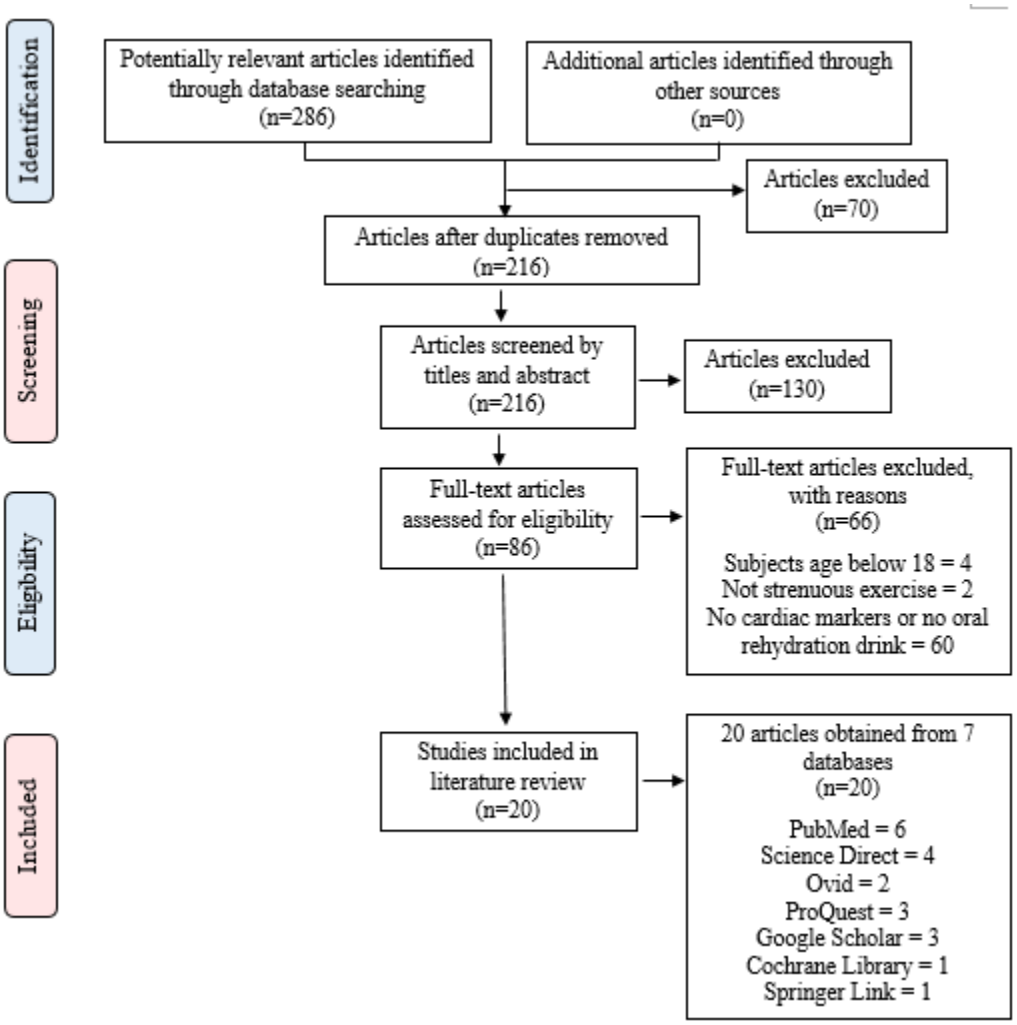

Figure 1: Flowchart showing the literature search method. (n=number of articles)

3.2 Effect of Strenuous Exercise on Markers of Cardiac Muscle Damage

Table 2 shows the overview of the selected studies (n=9) on effect of strenuous exercise on markers of cardiac muscle damage. Overall, we noticed that the level of cardiac markers (cTnI, cTnT, CK-MB and LDH) increased post-strenuous exercise.

Table 2: Effect on markers of cardiac muscle damage following strenuous exercises (n=9).

No.	Study (years)	Country	Participants and mean age (years)	Exercise protocol	Cardiac markers	Outcomes (level of cardiac markers)
1	Tian *et al*. (2012)	China	13 male runners (24.0±3.6 years)	90 min treadmill run	cTnT	Increased
2	Lippi *et al*. (2012)	Italy	17 trained males (47.0 years)	21 km marathon	cTnI	Increased
3	Eijsvogels *et al*. (2015)	Netherlands	92 trained runners (45.0±8.0 years)	Self-selected speed marathon	cTnI	Increased
4	Klinkenberg *et al*. (2016)	Netherlands	25 runners (40.0±13.0 years)	30 km run	cTnT cTnI	Increased
5	Ranjbar *et al*. (2017)	Ireland, United Kingdom and Denmark	11 sedentary men (22.3±1.9 years)	40 minutes aerobic exercise on a treadmill (Intermittent (IE) or continuous (CE) exercise)	cTnT CK-MB	Increased - cTnT level in CE higher than IE - CK-MB level only in CE
6	Li *et al*. (2017)	China	21 marathon runners (22.9±4.5 years)	90 min treadmill run	cTnT	Increased
7	Keselman *et al*. (2017)	Sweden	17 runners (25.7±5.2 years)	5 km race	cTnT	Increased
8	Richardson *et al*. (2018)	United Kingdom	52 marathon runners (39.0±11.0 years)	42.2 km marathon	cTnT	Increased
9	Tesema *et al*. (2019)	Ethiopia	32 male athletes (19.4±1.3 years)	Continuous endurance run	cTnI LDH CK-MB	Increased

3.3 Effect of Oral Rehydration Drinks on Markers of Cardiac Muscle Damage following Strenuous Exercise

As reported in Table 3 (n=11), the studies showed varied results; nine studies observed that oral rehydration drinks decreased cardiac biomarkers level, whereas two studies suggested that oral rehydration drinks were not effective due to increased level of cardiac biomarkers.

Table 3: Effect of oral rehydration drinks on the markers of cardiac muscle damage following strenuous exercises (n=11).

No	Study (year)	Country	Population and mean age (years)	Exercise Protocol	Mode of rehydration	Cardiac markers	Outcomes (level of cardiac markers)
1	Wojcik *et al*. (2001)	United States of America	26 untrained males (≥18 years)	Incremental activity on cycle ergometry	i) Milk-based carbohydrate-protein (CHO-PRO) drink (Nestle Corp., San Francisco, CA)	CK	Decreased - In CHO-PRO and CHO drink - Lowest level in CHO-PRO followed by CHO
					ii) Carbohydrate (CHO) drink (Gatorade, Chicago, IL)		
					iii) Aspartame-flavoured placebo (P) (Crystal Light, Kraft Foods Inc., White Plains, NY)		
2	Romano-Ely *et al*. (2006)	United States of America	14 males (24.0±4.1 years)	Two sets of rides to exhaustion on a cycle ergometer	i) Carbohydrate-protein-antioxidant (CHOPA) drink (Accelerade and Endurox, Pacific Health Laboratories, Inc)	LDH CK	Decreased - In both drink - Lowest level in CHOPA
					ii) Carbohydrate (CHO) drink (Gatorade, Inc)		
3	Greer *et al*. (2007)	United States of America	Nine untrained males (21.6±3.2 years)	Three 90 min cycling bouts	i) Branched-chain amino acid (BCAA) supplementation (Musashi, Notting Hill, Australia)	LDH CK	Decreased (LDH) - BCAA drink attenuates LDH level
					ii) Carbohydrate (CHO) drink (Gatorade, Inc., Chicago, IL)		Decreased (CK) - CHO drink attenuates CK level
					iii) Placebo (water, lemon flavour, salts, artificial sweetener)		

4	Luden *et al*. (2007)	United States of America	11 men (19.4±1.0 years) 12 women (19.4±1.0 years)	8 km race (men) 5 km race (women)	i) Carbohydrate-protein-antioxidant (CHOPA) drink ii) Carbohydrate (CHO) drink	CK	Decreased - In both drink - Lowest level in CHOPA
5	Baty *et al*. (2007)	United States of America	34 male subjects (21.5±1.7 years)	Three sets resistance exercise with eight repetitions (high pull, leg curl, standing overhead press, leg extension, leg press, bench press)	i) Carbohydrate-protein (CHO-PRO) drink (Pacific Health Laboratories Inc., Woodbridge, NJ) ii) Placebo (electrolyte and artificial sweetener drink, Pacific Health Laboratories Inc., Woodbridge, NJ)	CK Myoglobin	Decreased - Only in CHO-PRO drink
6	Valentine *et al*. (2008)	United States of America	11 male cyclists (20.8±2.4 years)	Four rides to exhaustion on cycle ergometer	i) Carbohydrate-protein (CHO+PRO) drink ii) Placebo (P) iii) Carbohydrate (CHO) drink	CK Myoglobin	Decreased - In CHO+PRO and CHO drink - Lowest level in CHO+PRO drink
7	Cockburn *et al*. (2010)	United Kingdom	32 males (20.0±2.0 years)	Cycling on a cycle ergometer, knee flexion repetitions, three separate drop jumps	i) Milk-based carbohydrate-protein (CHO-PRO) (For Goodness Shakes, My Goodness Ltd, London, UK) ii) Water	CK	Decreased - Only in CHO-PRO drink
8	Rahnama *et al*.(2011)	United States of America	i) Four soccer players (CHO) (22.0±2.6 years) ii) Four soccer players (P) (24.2±2.6 years)	90 min intermittent exercise bouts specific to soccer	i) Carbohydrate (CHO) drink (lemon flavoured glucose solution 6%) ii) Placebo (P) (lemon flavoured drink)	cTnI CK-MB	No effect - In 3 drinks

			iii) Four soccer players (C) (25.2±0.5 years)		iii) Control (C)		
9	Howatson *et al*. (2012)	United Kingdom	12 trained males (23.0±2.0 years)	Resistance exercise (100 drops-jump from a height of 0.6 m)	i) Branched-chain amino acid (BCAA) supplementation (Myprotein, Cheshire, UK) mixed with water ii) Placebo (aspartame based artificial sweetener)	CK	Decreased - Only in BCAA drink
10	Areces *et al*. (2014)	Spain	i) 50 runners (41.4 years)	42.2 km marathon foot race	i) Branched-chain amino acid (BCAA) supplementation (leucine, isoleucine, valine) mixed with water ii) Placebo (cellulose: dextrose)	Myoglobin	No effect - In both drinks - Both drinks showed similar myoglobin level
11	Oosthuyse *et al*. (2019)	South Africa	i) Seven male cyclists (35.9±5.4 years) ii) Seven male cyclists (40.1±4.8 years)	Mountain bike race	i) Casein protein hydrolysate-carbohydrate (CHO-PRO) drink (PeptoPro Litely Fruity; DSM Nutritional Products, Johannesburg, South Africa) mixed with water ii) Carbohydrate (CHO) drink (CarboFuel, Optimum Cadence, Cape Town, South Africa) mixed with water	cTnI CK-MB	Decreased - In both drinks - Lowest level in CHO-PRO drink

4. DISCUSSION

4.1 Effect of Strenuous Exercise on Markers of Cardiac Muscle Damage

A total of nine studies examined the effect of heart muscle injury following strenuous exercise (Table 2). During strenuous exercise, myofibrillar damage is a significant physiological process that correlates with the intensity of strenuous exercise (Thorpe & Sunderland, 2012). Rise in serum levels of cardiac markers reflects myofibrillar damage. Tian *et al*. (2012) and Li *et al*. (2017) carried out studies on 13 males (24.0±3.6 years) and 21 marathon runners (22.9±4.5 years) respectively to perform a 90 min treadmill race. The authors concluded that cTnT levels increased with increase in intensity of exercise and peaked at 3 to 4 h post-exercise.

These findings were substantiated by Lippi *et al*. (2012), where they reported elevation of cTnI in 17 trained males (47.0 years) following a 21 km half marathon with cTnI levels peaking at about 6 h. In another study by Eijsvogels *et al*. (2015), for 92 trained runners (45.0±8.0 years) ran a marathon with self-selected speed, it was found that cTnI concentration increased significantly from 14±12 ng/L at baseline to 94±102 ng/L. The study on 52 marathon runners (39.0±11.0 years) by Richardson *et al*. (2018) suggested that cTnT concentration increased significantly after a full (42.2km) marathon. Similar results were obtained by Klinkenberg *et al*. (2016) following a 30 km race and Keselman *et al*. (2017) following a 5 km race.

Along these lines, Ranjbar *et al*. (2017) reported that intermittent (IE) and continuous (CE) aerobic exercise on treadmills for 11 sedentary men (22.3±1.9 years) can elevate cTnT concentration with CE, resulting in higher cTnT level as compared to IE. Moreover, Tesema *et al*. (2019) found that the concentration of cTnI, CK-MB and LDH significantly elevated at the end of the exercise with 13 males (19.4±1.3 years) who participated in a continuous endurance run.

It is also important to point out that cardiac biomarkers increased and returned to baseline within 2 to 3 days post-exercise, suggesting that endurance exercise induces normal physiological cardiac adaptations that promote acceptable increases in cardiac output rather than pathological process and do not indicate irreversible cell death (Nystoriak & Bhatnagar, 2018).

The mechanism that might explain the elevated cardiac markers may be related to enhanced membrane permeability or bleb formation (Gresslien & Agewall, 2016; Nystorial & Bhatnagar, 2018), thereby enabling passive diffusion of cardiac markers from intracellular to extracellular compartments (Shave *et al*., 2010). Such an increase in the membrane permeability might be due to increased production of oxidative radicals, increased mechanical stress on cardiomyocytes, and / or altered acid base balance. Mechanical stimuli might then produce transient disruptions of the myocardial plasma membrane, termed as ‘cell wounds’, making it possible for the release of exercise-induced cTn (Shave *et al*., 2010; Gresslien & Agewall, 2016; Nystoriak & Bhatnagar, 2018).

4.2 Effect of Oral Rehydration Drinks on Markers of Cardiac Muscle Damage following Strenuous Exercise

A total of 11 investigations studied the impact of oral rehydration drinks on cardiac muscle injury. Overall, these studies showed that functional sports drinks were useful with only two exceptions (Table 3).

Nine studies observed that functional sports drinks are beneficial in reducing myocardial injury. The study by Greer *et al*. (2007) and Howatson *et al*. (2012) determined the effect of BCAA supplementation. Greer *et al*. (2007) demonstrated that ingestion of BCAA drink resulted in decreased LDH and CK levels, whereas

Gatorade drink was found to be effective in reducing CK concentration in a cycling activity with nine males (21.6±3.2 years). Howatson *et al*. (2012) showed that BCAA supplementation namely Myoprotein shared similar outcome with the previous study following a resistance exercise with 100 drops-jump from a height of 0.6 m for 12 trained males (23.0±2.0 years).

In addition, another three studies investigated the impact of CHO-PRO drink. Baty *et al*. (2007) chose 34 male subjects (21.5±1.7 years) to determine the impact of CHO-PRO drink and a placebo by conducting three sets of resistance exercises with eight repetitions which included high pull, leg curl, standing overhead press, leg extension, leg press and bench press. The investigation showed that CHO-PRO supplement provided lower CK,and myoglobin levels as compared to the placebo. The outcomes of this study were similar with a study by Valentine *et al*. (2008) that involved 11 males in a cycling activity (20.8±2.4 years). Furthermore, Oosthuyse *et al*. (2019) investigated the effect of CHO-PRO drink namely PeptoPro Litely Fruity and CHO drink in seven male cyclists by conducting a 3-day mountain bike race and found that this drink augmented cardiac tissue injury and displayed smaller effect for increases in cTnI and CK-MB level.

In addition, Wojcik *et al*. (2001) and Cockburn *et al*. (2010) examined the impact of milk-based CHO-PRO drink. The studies by Wojcik *et al*. (2001) with 26 untrained subjects and Cockburn *et al*. (2010) with 32 runners (20.0±2.0 years) in a cycling activity examined the level of cardiac muscle damage with the ingestion of milk-based CHO-PRO drink. The authors concluded that the milk-based rehydration drink was beneficial in blunting increase in CK level followed by CHO drink and a control as demonstrated by Elliot *et al*. (2006), which suggested that milk ingestion after resistance exercise will result in a positive net muscle protein.

Additionally, another two studies investigated the impact of CHOPA drinks following endurance exercise. Romano-Ely *et al*. (2006) found that CHOPA drinks, namely Accelerade and Endurox, with one serving of recovery drink tended to decrease LDH and CK concentration as compared to CHO drink following two prolonged bouts of cycle ergometry to fatigue for 14 males (24.0±4.1 years). Moreover, Luden *et al*. (2007) performed 8 and 5 km races with 11 men (19.4±1.0 years) and 12 women (19.4±1.0 years) respectively. The authors observed improvements in performance and suggested that CK level was significantly attenuated with CHOPA drinks ingestion when compared to CHO drink.

The above studies concluded that oral rehydration drinks are beneficial in reducing cardiac muscle damage, particularly with the ingestion of mixed CHO-PRO functional drink (Wojcik *et al*., 2001; Baty *et al*., 2007; Valentine *et al*., 2008; Cockburn *et al*., 2010; Oosthuyse *et al*., 2019), CHO-electrolyte drink (Wojcik *et al*., 2001; Romano-Ely *et al*., 2006; Greer *et al*., 2007; Luden *et al*., 2007; Valentine *et al*., 2008; Oosthuyse *et al*., 2019), CHOPA drinks (Romano-Ely *et al*., 2006; Luden *et al*., 2007) and BCAA supplementation (Greer *et al*., 2007; Howatson *et al*., 2012) due to their absorptive properties. These were in agreement with studies by Miller *et al*. (2003) and Koopman *et al*. (2004), which suggested that protein catabolism might be reduced due to increase in tricarboxylic-acid-cycle intermediates, which replenishes the amino acid pool. Besides that, Williams *et al*. (2003) and Areta *et al*. (2013) also proposed that ingestion of CHO and PRO promoted glucose uptake and increased insulin activities, which further promoted amino acid uptake into muscle cells, increased glycogen and protein synthesis, as well as increased anabolism of muscle protein, thereby facilitating muscle recovery (Baty *et al*., 2007; Valentine *et al*., 2008).

In addition, protein ingestion increases the availability of amino acids and stimulates protein synthesis through the activation of mammalian target of rapamycin (mTOR) signalling pathway by elevating the expression of mRNA (Baty *et al*., 2007; Howatson *et al*., 2012). This would reduce protein degradation and preserve the integrity of the cell membrane, thus promoting muscle growth and recovery (Greer *et al*., 2007; Howatson *et al*., 2012).

In contrary, Rahnama *et al*. (2011), with 12 soccer players, observed that consumption of lemon-flavoured glucose solution was not effective in reducing cardiac muscle injury as CHO supplementation did not show any significant effect on cTnI and CK-MB indices. Another study by Areces *et al*. (2014) observed a similar outcome for 50 runners (41.4 years) after completing a 42.2 km marathon by suggesting that BCAA supplementation mixed with water was not effective in reducing cardiac muscle injury compared to a placebo as both drinks showed similar myoglobin concentration after race.

4.3 Endurance Sports and Oral Rehydration Drinks

The above findings can be of benefit while planning oral rehydration rations and standard operating procedures for military training programmes. In a study conducted on the U.S. Armed Forces, in one year, 365 cases of heat stroke were detected, whereby immediate intervention with oral rehydration prevented further complications. They also found that rice based oral rehydration was superior to water alone in maintaining body weight during prolonged strenuous training (Gerold *et al*., 2013). Hence, based on the observations from the studies above, oral rehydration drinks with water, CHO, PRO, electrolytes and vitamins becomes an important strategy to rehydrate after strenuous activities such as military training.

Water would help maintain hydration during exercise, thus enabling muscles and joints to work better. It provides adequate nutrients inside and outside the cells of contracting muscles effectively removes waste when an individual is well hydrated. Additionally, CHO would provide energy intake and enable physical exertion to proceed. CHO intake before or during exercise can also help to slow down the pace at which the body runs out of its own CHO stores. Moreover, PRO would slow down tiredness and improve muscle function as protein-based drink provides the body with fuel for tissue repair and building whereas electrolytes would restore salts lost in sweat, and promote water and CHO assimilation. Blood electrolytes such as potassium, sodium, chloride and bicarbonate also help in regulating nerve and muscle function, as well as maintain acid-base balance and water (Orrù *et al*., 2018; Shirreffs, 2009). This strategy would allow for enhancing performance as well as reducing heat stroke related complications for soldiers

5. CONCLUSION

In summary, this review found that oral rehydration drinks ingested before, during and / or after exercise reduces cardiac biomarkers concentration as sufficient hydration is not only a physiological necessity but also reduces the possibility of medical problems from fluid losses. Nonetheless, further research is required to evaluate the impact on cardiac-specific biomarkers such as cTnI and cTnT because the general markers, CK, LDH and myoglobin are not specifically cardiac-sensitive although they were regularly assessed in previous studies. Therefore, future studies including cardiac-specific indicators would be informative and more research is warranted to investigate: i) Whether nutritional interventions such as oral rehydration drinks are clinically beneficial for the runners as the published articles were limited with only nine studies, which may lead to poor standard of evidence; and ii) Further explanation on how oral rehydration drinks limit cardiac muscle damage, as the mechanisms are currently speculative.

It should be noted that there were limitations to our review. Firstly, several experiments enrolled only limited number of subjects, which means they had small sample sizes. Secondly, not all the participants were experienced runners, with some of them being previously untrained, which can skew the outcome. Besides that, different types of muscle-damaging exercises were carried out and the amount of drink ingested was also varied. Other limitations include different blood measurement time points and lack of control in diet. Moreover, there was no study on changes in the heart activity after endurance exercises. Thus, the occurrence of abnormalities cannot be ruled out.

REFERENCES

Areces, F., Salinero, J.J., Abian-Vicen, J., González-Millán, C., Gallo-Salazar, C., Ruiz-Vicente, D., Lara, B. & Del Coso, J. (2014). A 7-day oral supplementation with branched-chain amino acids was ineffective to prevent muscle damage during a marathon. *Amino Acids.*, **46**: 1169–1176.

Areta, J. L., Burke, L.M., Ross, M.L., Camera, D.M., West, D.W., Broad, E.M., Jeacocke, N.A., Moore, D.R., Stellingwerff, T., Phillips, S.M., Hawley, J.A. & Coffey, V.G. (2013). Timing and distribution of protein ingestion during prolonged recovery from resistance exercise alters myofibrillar protein synthesis. *J. Physiol.*, **591**: 2319–2331.

Bates, G.P. & Miller, V.S. (2008). Sweat rate and sodium loss during work in the heat. *J. Occup. Med. Toxicol.*, **3**: 4.

Baty, J.J., Hwang, H., Ding, Z., Bernard, J.R., Wang, B., Kwon, B. & Ivy, J.L. (2007). The effect of a carbohydrate and protein supplement on resistance exercise performance, hormonal response, and muscle damage. *J. Strength Cond. Res.*, **21**:321–329.

Bodor G.S. (2016). Biochemical markers of myocardial damage. *J. Int. Fed. Clin. Chem. Lab. Med.*, **27**: 95–111.

Cockburn, E., Stevenson, E., Hayes, P. R., Robson-Ansley, P., & Howatson, G. (2010). Effect of milk-based carbohydrate-protein supplement timing on the attenuation of exercise-induced muscle damage. *Appl. Physiol. Nutr. Metab.*, **35**:270–277.

Eijsvogels, T.M., Hoogerwerf, M.D., Maessen, M.F., Seeger, J.P., George, K.P., Hopman, M.T., & Thijssen, D. H. (2015). Predictors of cardiac troponin release after a marathon. *J. Sci. Med. Sport.*, **18**:88–92.

Elliot, T.A., Cree, M.G., Sanford, A.P., Wolfe, R.R., & Tipton, K.D. (2006). Milk ingestion stimulates net muscle protein synthesis following resistance exercise. *Med. Sci. Sports. Exerc.*, **38**: 667–674.

Evans, G.H., James, L.J., Shirreffs, S.M., & Maughan, R.J. (2017). Optimizing the restoration and maintenance of fluid balance after exercise-induced dehydration. *J. Appl. Physiol.*, **122**:945–951.

Gerold, K. B., Greenough, W. B., & Yasar, S. (2013). Rice-based electrolyte drinks more effective than water in replacing sweat losses during hot weather training and operations. *J. Spec. Oper. Med.*, **13**:12–14.

Greer, B.K., Woodard, J.L., White, J.P., Arguello, E.M., & Haymes, E.M. (2007). Branched-chain amino acid supplementation and indicators of muscle damage after endurance exercise. *Int. J. Sport Nutr. Exerc. Metab.*, **17**:595–607.

Gresslien, T., & Agewall, S. (2016). Troponin and exercise. *Int. J. Cardiol.*, **221**: 609–621.

Harty, P.S., Cottet, M.L., Malloy, J.K., & Kerksick, C.M. (2019). Nutritional and Supplementation Strategies to Prevent and Attenuate Exercise-Induced Muscle Damage: a Brief Review. *Sports Med.*, **5**:1.

Howatson, G., Hoad, M., Goodall, S., Tallent, J., Bell, P.G., & French, D.N. (2012). Exercise-induced muscle damage is reduced in resistance-trained males by branched chain amino acids: a randomized, double-blind, placebo controlled study. *J.Int. Soc. Sports Nutr.*, **9**: 20.

Jenz, S.T., Goodyear, C.D., Graves, P.R., Goldstein, S., Shia, M.R., Redei, E.E. (2021). Blood and affective markers of stress in Elite Airmen during a preparatory training course: A pilot study. *Neurobiol. Stress.*, **9**:100323.

Kavsak, P. A., Andruchow, J. E., McRae, A. D., & Worster, A. (2018). Profile of Roche's Elecsys Troponin T Gen 5 STAT blood test (a high-sensitivity cardiac troponin assay) for diagnosing myocardial infarction in the emergency department. *Expert. Rev. Mol. Diagn.*, **18**:481–489.

Keselman, B., Vergara, M., Nyberg, S., & Nystrom, F.H. (2017). A randomized cross-over study of the acute effects of running 5 km on glucose, insulin, metabolic rate, cortisol and Troponin T. *PloS One*, **12**: e0179401.

Klinkenberg, L.J., Luyten, P., van der Linden, N., Urgel, K., Snijders, D.P., Knackstedt, C., Dennert, R., Kietselaer, B.L., Mingels, A.M., Cardinaels, E.P., Peeters, F.E., van Suijlen, J.D., Ten Kate, J., Marsch, E., Theelen, T.L., Sluimer, J.C., Wouters, K., Bekers, O., Bekkers, S.C., van Loon, L.J.,

Meex, S.J. (2016). Cardiac Troponin T and I Release After a 30-km Run. *Am. J. Card.*, **118**:281–287.

Koopman, R., Pannemans, D.L., Jeukendrup, A.E., Gijsen, A.P., Senden, J.M., Halliday, D., Saris, W. H., van Loon, L.J., & Wagenmakers, A.J. (2004). Combined ingestion of protein and carbohydrate improves protein balance during ultra-endurance exercise. *Am. J. Physiol. Endocrinol. Metab*., **287**:E712–E720.

Li, F., Yi, L., Yan, H., Wang, X., Nie, J., Zhang, H., Fu, F., Zang, Y., Yang, S., & Lu, Y. (2017). High-sensitivity cardiac troponin T release after a single bout of high-intensity interval exercise in experienced marathon runners. *J. Exerc. Sci. Fit.*, **15**:49–54.

Lippi, G., Schena, F., Salvagno, G.L., Tarperi, C., Aloe, R., & Guidi, G.C. (2012). Comparison of conventional and highly-sensitive troponin I measurement in ultra-marathon runners. *J. Thromb. Thrombolysis.*, **33**:338–342.

Luden, N.D., Saunders, M.J., & Todd, M.K. (2007). Postexercise carbohydrate-protein- antioxidant ingestion decreases plasma creatine kinase and muscle soreness. *Int. J. Sport Nutr. Exerc. Metab*., **17**:109–123.

Miller, S.L., Tipton, K.D., Chinkes, D.L., Wolf, S.E., & Wolfe, R.R. (2003). Independent and combined effects of amino acids and glucose after resistance exercise. *Med. Sci. Sports Exerc.*, **35**:449–455.

Nystoriak, M.A., & Bhatnagar, A. (2018). Cardiovascular Effects and Benefits of Exercise. *Front. Cardiovasc. Med.*, 5:135.

Oosthuyse, T., Bosch, A.N., & Millen, A. (2019). Effect of ingesting carbohydrate only or carbohydrate plus casein protein hydrolysate during a multiday cycling race on left ventricular function, plasma volume expansion and cardiac biomarkers. *Eur. J. Appl. Physiol.*, **119**:697–711.

Orrù, S., Imperlini, E., Nigro, E., Alfieri, A., Cevenini, A., Polito, R., Daniele, A., Buono, P., & Mancini, A. (2018). Role of Functional Beverages on Sport Performance and Recovery. *Nutrients.*, **10**:1470.

Perrone, M. A., Storti, S., Salvadori, S., Pecori, A., Bernardini, S., Romeo, F., Guccione, P., & Clerico, A. (2021). Cardiac troponins: are there any differences between T and I?. *J. Cardiovasc. Med.*, **22**:797–805.

Rahnama, N., Faramarzi, M., & Gaeini, A.A. (2011). Effects of Intermittent Exercise on Cardiac Troponin I and Creatine Kinase-MB. *Int. J. Prev. Med.*, **2**:20–23.

Ranjbar, R., Ahmadi, M.A., Zar,A., & Krustrup, P. (2017). Acute effect of intermittent and continuous aerobic exercise on release of cardiac troponin T in sedentary men. *Int. J. Card.*, **236**:493–497.

Richardson, A.J., Leckie,T., Watkins, E.R., Fitzpatrick, D., Galloway, R., Grimaldi, R., & Baker, P. (2018). Post marathon cardiac troponin T is associated with relative exercise intensity. *J. Sci. Med Sport.*, **21**:880–884.

Romano-Ely, B.C., Todd, M.K., Saunders, M.J., & Laurent, T.S. (2006). Effect of an isocaloric carbohydrate-protein-antioxidant drink on cycling performance. *Med. Sci. Sports Exerc.*, **38**:1608–1616.

Shave, R., Baggish, A., George, K., Wood, M., Scharhag, J., Whyte, G., Gaze, D., & Thompson, P.D. (2010). Exercise-induced cardiac troponin elevation: evidence, mechanisms, and implications. *J. Am. Coll. Cardiol.*, **56**:169–176.

Shirreffs, S.M. (2009). Hydration in sport and exercise: water, sports drinks and other drinks. *Nutr. Bull.*, **34**:374-379.

Shirreffs, S.M., Aragon-Vargas, L.F., Keil, M., Love, T.D., & Phillips, S. (2007). Rehydration after exercise in the heat: a comparison of 4 commonly used drinks. *Int. J. Sport. Nutr. Exerc. Metab.*, **17**:244–258.

Singh, N., Kumar, A., Datta, R., Bhardwaj, P., Aggarwal, N., Chadha, D. S., Singh, S. P., Sharma, P., Barwad, P., & Gupta, H. (2021). Analysis of ST-elevation myocardial infarction occurring in soldiers during strenuous military training. *Med. J. Armed Forces India*, **77**:413–418.

Stachenfeld N. S. (2014). The interrelationship of research in the laboratory and the field to assess hydration status and determine mechanisms involved in water regulation during physical activity. *Sports Med.*, **44**:S97–S104.

Tesema, G., George, M., Mondal, S., & Mathivana, D. (2019). Effects of one week different intensity endurance exercise on cardiorespiratory and cardiometabolic markers in junior young athletes. *BMJ Open SEM.*, **5**:e000644.

Thorpe, R., & Sunderland, C. (2012). Muscle damage, endocrine, and immune marker response to a soccer match. *J. Strength Cond. Res.*, **26**:2783–2790.

Tian, Y., Nie, J., Huang, C., & George, K.P. (2012). The kinetics of highly sensitive cardiac troponin T release after prolonged treadmill exercise in adolescent and adult athletes. *J. Appl. Physiol.*, **113**:418–425.

Valentine, R.J., Saunders, M.J., Todd, M.K., & St Laurent, T.G. (2008). Influence of carbohydrate-protein beverage on cycling endurance and indices of muscle disruption. *Int. J. Sport Nutr. Exerc. Metab.*, **18**:363–378.

Williams, M., Raven, P.B., Fogt, D.L., & Ivy, J.L. (2003). Effects of recovery beverages on glycogen restoration and endurance exercise performance. *J. Strength Cond. Res.*, **17**:12–19.

Wojcik, J.R., Walber-Rankin, J., Smith, L.L., & Gwazdauskas, F.C. (2001). Comparison of carbohydrate and milk-based beverages on muscle damage and glycogen following exercise. *Int J. Sport Nutr. Exerc. Metab.*, **11**:406–419.

ECONOMIC DEVELOPMENT AND DEFENCE OFFSETS: THE CASE OF REINDUSTRALIZING COUNTRIES

Hugo B. Santos[1], Pedro B. Água[1] & Armindo Frias[1,2,*]

[1]CINAV, Escola Naval, Instituto Universitário Militar, Portugal
[2]Advance/CSG, ISEG-Universidade de Lisboa, Portugal

[*]Corresponding Author: armindo.frias@gmail.com

ABSTRACT

Offsets are agreements or contracts in which the buying country tries to compel the exporting company to reinvest part of the contract value back into the importing country. As defense equipment and systems acquisitions involve large costs for a country, offsets can be a way to balance such costs, improve national technological and industrial development, as well as meet economic and industrial development strategies. However, some countries cannot do this type of contracts, following the European Union Directives, while others continue to use military or defense offsets in a successful way. Lack of effectiveness, efficiency and trust is common in such agreements, dictating a country's loss of wealth and reputation. Therefore, increasing accountability around offset transactions is critical. The objective of this paper is to contribute to the understanding of different offset policies by analyzing a sample of failure and success cases.

Keywords: *Acquisition; offsets; technological and industrial development; accountability; defense equipment.*

1. INTRODUCTION

Defense offsets, or compensatory measures, is a mechanism that has been used by several countries to foster technology transfer and development, with varying results. This subject is relevant in the context of the European Union (EU) and World Trade Organization (WTO). The use of offsets has been increasingly difficult to apply to new contracts, preventing buying countries from using it as a strategy to develop their economies and technological domains. Since defense contracts are costly, the government wants part of that cost to either benefit the industry or allow the country to gain in terms of technology. Furthermore, some countries hinder the use of offsets to protect their technologies and economies (Kaushik, 2020). Portugal, as an importing country, is put into perspective against several other countries. This analysis brings clarity over performance by illustrating success cases, while pointing to some negative collateral effects (Weidenbaum, 1993).

Increasingly, countries institute implicit or flexible approaches to driving defense industry growth through their defense acquisitions, although these strategies remain difficult to quantify. Although the demand for offset defense procurement contracts may have declined, it remains a very common requirement in many countries (Jovovic *et al*., 2021).

Besides the introduction, this text contains a background section regarding relevant legislations together with the focus on an EU country, Portugal, taken as an example, and provides relevant information from several countries around the globe on what offsets concerns. An analysis and discussion regarding the main subject is made, followed by some conclusions.

2. THEORETICAL BACKGROUND

2.1 WTO & EU Policies

WTO deals with the rules of trade between countries in order to expand trade for the benefit of overall societies, as well as to assist governments to establish trade agreements and resolve trade disputes. According to the WTO's Agreement on Government Procurement (GPA), accepted and implemented by 48 countries, the use of offsets is prohibited, with the following exceptions (WTO, 2021):

- In GPA countries, offsets may be negotiated provided that they are not considered as award criteria.
- If the purchase process falls outside the scope of the GPA, they may include compensatory measures.

The last exception is the one most used by most countries to demand offsets in defense procurements. The financing of many military programs is not subject to WTO rules (Maennig & Wittig, 2010).

EU countries may use the exception provided by Article 346 of the *Treaty on the Functioning of the EU* (TFEU) (EU, 2012), which allows countries to make defense-related purchases, where some compensation procedures may be allowed, provided that it does not affect EU market competition. EU Directive 2009/81/EC (EU, 2009) for public procurement in the fields of defense and security lays down the rules for public procurement, following the principles of transparency and fair competition. Prior to the implementation of the directive, several Member States required offsets from non-national suppliers when purchasing defense equipment and systems, but such public procurement procedure was at odds with the TFEU.

2.2 The Failure of Offsets - The Case of Portugal

For some countries, the acquisition of defense technologies is a way to improve their defense capacity and capability, develop R&D activities, as well as improve their economy (Mazzucato, 2015; Harutyunyan, 2017). The application of technologies obtained for military use in the civilian field can help improve the efficiency of industries and catapult economies. Another way is the inclusion of offsets that introduce cutting-edge technology directly into the national industry (Maennig & Wittig, 2010). When importing weapons and defense equipment, countries often require suppliers to reinvest part of the amount spent in the buyer's country.

In some countries that use offsets, the market is highly competitive, where sales are not made only on the basis of the price-quality ratio, but also considering the overall sales attractiveness and potential reciprocal investment. However, this kind of environment could encourage ineffectiveness and lack of transparency. *Transparency International* reports suggest that corruption is very common in contracts including offsets (Magahy *et al*., 2010). Beyond such failures or underperforming cases, there are countries that successfully enjoy the benefits of offsets, giving legitimacy to the following question: *If there are countries that benefit from offsets, why are there others that are unable to take such advantage and improve their technological and economic development?*

With such trade-offs in defense acquisitions, it is reasonable to consider an increase in the importing country's technological and industrial development, if approached systemically. A benefit for an importing country, originating from such contracts, comes from the fact that besides getting the required equipment and capabilities, it gets some indirect "return" by spending such amount of public funds. This is expected to stimulate economic development by encouraging the balance of payments improvement through investments or technology transfer.

In the case of Portugal, offsets apparently have not been having the desired impacts, preventing it from obtaining the maximum benefits. One of the possible reasons is the lack of coordination between distinct State departments involved in the process, attached to different Ministries, leading to the establishment

of contracts with vague terms and without properly specifying the aspired compensatory measures. The fact that there is not a single entity in charge of the entire negotiation process on the Portuguese side, nor an active participation of the Defense Technological and Industrial Base (DTIB), may be among the reasons for such underperformance.

As such negotiations are complex and comprehensive business processes, they require a professional approach, taking the task as a process with several stages, as shown in Figure 1.

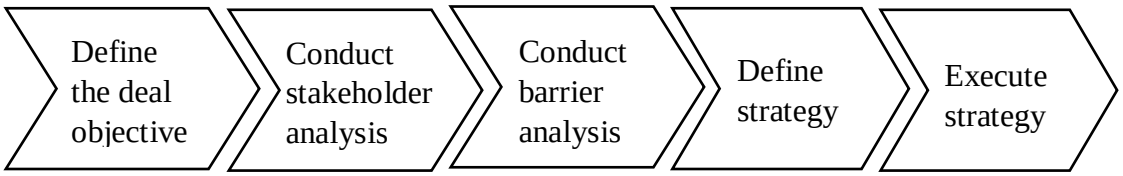

Figure 1: Stages of a negotiation process.
Source: Adapted from Lax & Sebenius (2006).

In 1999, the Portuguese Government set up the Standing Committee on Offsets (OPC) to centralize offsets contracts negotiation. Its effort fell short of expectation, which may be due to the fact that such committee met sporadically; did not include industry representatives; participated poorly and still did not have a permanent operational entity caring for the ongoing negotiations. In an attempt to reorganize its action, a new classification of offsets was presented: (1) Direct offsets; (2) Defense industry indirect offsets; and (3) Non-defense related indirect offsets (EuroDefense, 2007).

Direct offsets are those that incorporate goods and services directly related to those goods being acquired and that may be produced locally. For example, the Australian purchase of 22 helicopters from the French company Eurocopter included an offset contract that required local (Australian) production of components, local assembly of 18 of the 22 helicopters and local production of the Eurocopter EC-120 for the Asian market (Herrera & Matthews, 2014). This type of offset is more suitable for developed countries, as these have a diversified economy and an established DTIB, hence allowing them to effectively absorb the benefits of offset agreements (Erikson et. al, 2007).

Indirect offsets involve goods and services that are not directly related to the acquisition. For example, Russia's transport of a Malaysian astronaut to the international space station in exchange for Malaysia's purchase of the Russian Sukhoi Su 30 fighter jet (Khan, 2010). This type of offset is more suitable for developing countries, since they usually use the benefits that result from indirect offsets as a strategy to boost their economic and social development goals (Erikson et. al, 2007). Non-defense related indirect offsets include a great variability of subjects and it is not the focus of this text.

The need to comply with complex and bureaucratic procedures; hierarchical dependence of two distinct entities (bicephalous leadership); the lack of clarity in the definition of goods and services to be included under offset contracts; as well as the valuation of those transactions jeopardize the action of the OPC. The countries or companies that sell them, realizing that there are gaps in the contracts, tend to take advantage, preferring in some cases to pay fines rather than respect the offsets contracted (Magahy, 2010).

Participation in long and complex negotiation processes requires professionals taking part in them to be skilled in formal negotiating techniques. Therefore, there is a need, not only for professional care in the design and writing of such contracts, but sometimes also for “post-negotiation negotiation”, after the acquisition contract, to detail out those points where more value can be created from the negotiation (Mendenhalt, 1996).

Nowadays, Portugal does not carry out offset contracts anymore due to the existence of legal constraints at the national and EU levels. Past underperformance may have eliminated an effective tool to encourage development and collaboration between industries and countries through the acquisition of defense systems (EU, 2009).

2.3 Towards the Successful Use of Offsets

A reflection and alignment strategy among all the relevant governance sectors should be established in order to involve the DTIB players and national industry. If successful, it may increase exports, stimulate foreign investment, and obtain technology by transfer or by progressive self-development (EuroDefense, 2007).

Lack of an adequate strategy and involvement of relevant stakeholders may have negative consequences for the procurement of defense systems. Countries with less developed economies tend to fail to take advantage of the benefits of offsets, often resulting in the acquisition of defense technology at increased costs in the future (Straubhaar, 1986). The execution of the *Defense Acquisition Plan* oftentimes might have fallen short of expectations and anomalies in its execution are common (Silva, 2005; TdC, 2017). Hence, for the survival and revitalization of the national defense industry, it requires a properly engineered strategy in order to promote the acquisition of technology and knowledge in parallel with the acquisition of defense systems. Besides meeting the DTIB expectations, it would be desirable to establish a closer dialogue with the end users (the Armed Forces), in order to involve the DTIB in a timely manner (Santos, 2021).

2.4 Offsets in Other Countries

Several countries have implemented defense-offset policies for international procurement successfully as a way to enhance their economic and industrial development. If in the 1970s, few countries had rudimentary guidelines regarding offsets, nowadays there are more than seventy countries with formalized policies and comprehensive guidelines (Herrera & Matthews, 2014).

After the Cold War military demobilization and 40% decreasing demand for defense items, the trend seems to have reversed with increasing defense spending (Figure 2). Many countries face the problem of having high production costs and low defense budgets. Despite this problem, imports were capitalized through offsets, hence making offsets almost universally associated with defense procurement. Indonesia, for example, launched its first offsets policy in 2014, as did other countries (e.g., Argentina in 2015), providing opportunities for increasing local defense industrialization (Wezeman *et al*., 2021).

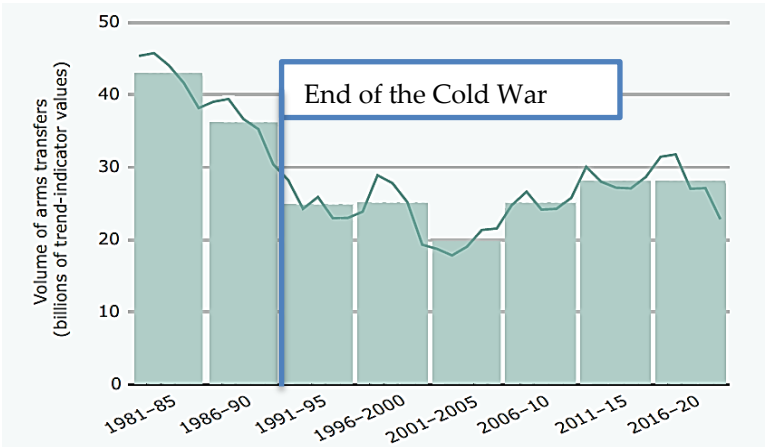

Figure 2: The trend in international transfers of major arms (1981–2020).
Source: Adapted from Wezeman *et al*. (2020)

High oil prices and high economic growth have caused several Middle East and Asian countries to increase their defense budgets, and some countries have shown considerable developments across their defense technological and industrial capabilities, hence the emerging of the offsets market. Figure 3 shows the GDP of several countries, which supports the view of economic growth at the mentioned countries (Gnidchenko *et al*., 2016).

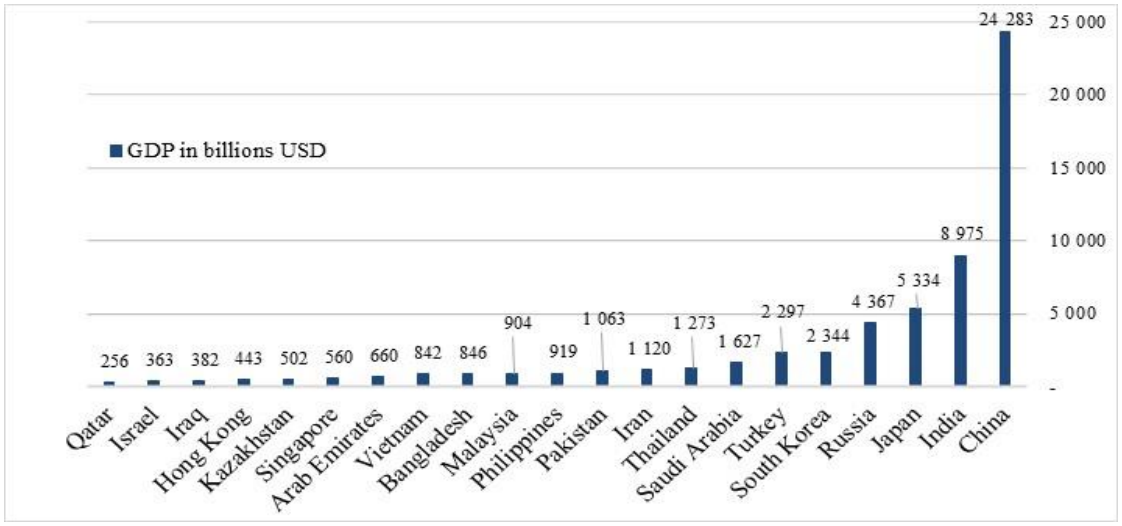

Figure 1: GDP of Asian and Middle East countries in 2020.
Source: Adapted from World Bank (2022)

China is the leader in the high-tech exports market as a whole. In the case of Russia, it holds leading positions in the trade of goods related to nuclear technologies, turbines and engines, where these exports far exceed the country's imports. Russia has practically no import dependency, as it is able to independently satisfy its own defense requirements (Gnidchenko *et al*., 2016).

According to the Stockholm International Peace Research Institute (SIPRI),Trend Indicator Value (TIV) is a unique system that measures the volume of international transfers of large conventional arms using a common unit. Figure 4 shows how arms exports differ by country across the Middle East and Asia, with the highest exporting values in the Middle East belonging to Israel and Turkey, with USD 707 mil. and USD 364 mil. respectively. In Asia, the countries with the highest values are Russia and China, with USD 6,409 mil. and USD 1,040 mil. respectively. These figures cover major conventional weapons, such as aircrafts, armored vehicles, artillery, radars and other sensor systems, missiles, as well as naval ships. Other military equipment, such as most types of small arms, trucks, ammunition, technology transfer and services, are excluded (Wezeman *et al*., 2021).

Due to defense spending, defense companies in the case of countries with competitive DTIBs have shifted their focus from domestic markets to the international market, where exports are seen as a mechanism to achieve sales growth. Therefore, being aware of the ability to offer offsets where they are allowed, defense companies regard such mechanism as a critical factor to close deals, which prompts them to approach such negotiations in a comprehensive way. China, for example, was the fifth largest defense exporter in 2012, and has recognized the need to specialize in the complexity of offsets negotiations in order to increase exports (Herrera & Matthews, 2014).

Several Latin American countries recognize offsets as a tool for the development of the national defense industry and technological transformation, and have begun to attract defense-related companies. Due to their specific economic development (Figure 5), such countries have engaged in large procurement programs and consequently, have developed and created new policies regarding defense offsets (Herrera & Matthews, 2014). Since 2000, most Latin American countries have already adopted offset policies.

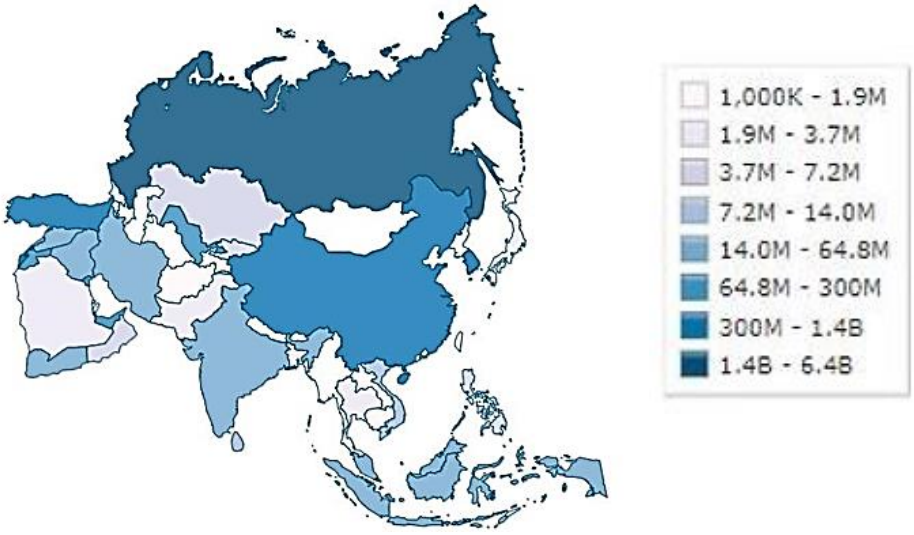

Figure 4: Arms exports in TIV for countries in the Middle East and Asia.
Source: IndexMundi (2019)

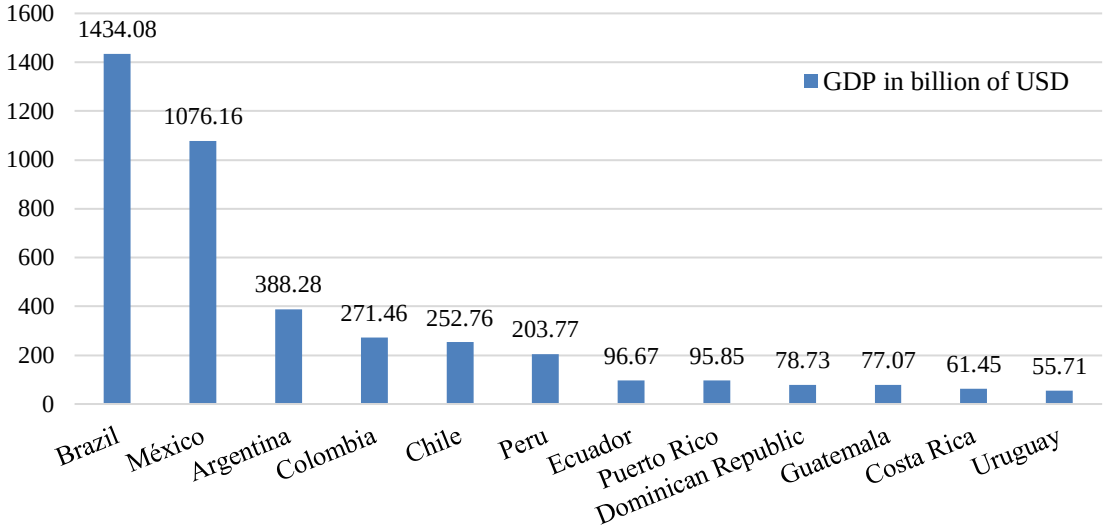

Figure 5: GDP of Latin American and Caribbean countries in 2020.
Source: Adapted from Pasquali (2021)

In order to negotiate attractive contracts involving offsets, vendors tend to offer some competitive advantage during the bidding phase. However, such vendors are careful about “how they offer" it, in order to keep their technological competitiveness and global brand reputation. This is evidenced by the difficulties that some importing countries have to obtain detailed information about the technologies that they intend to procure.

Argentina began using offsets to promote their defense industry through the optimization of supply chains and technological progress, and has been able to progress the development of its defense research and technological capabilities. Meanwhile, this evolutionary process was interrupted by fiscal problems and the country’s inability to finance the necessary increase in defense budgets (Herrera & Matthews, 2014).

Another example, Brazil, was successful in developing its defense industrial base by selecting a strategy focused on technology transfer, with a focus on dual use technologies. Such a focus proved to be a wise move, given that with the end of the Cold War, the demand for defense products and systems slowed down, and the Brazilian defense industry focused on products for civilian use. In particular, Embraer focused on civil aviation in order to survive. In Brazil, for both civil and military applications, offsets have been playing an important role, stimulating local research and development, and increasing production and systems integration capabilities. In fact, the genesis and development of Embraer itself was due to a successful offset process, making it one of the world leaders in aircraft manufacturing within its market. In recent years, Brazil has also been demanding offsets associated with various projects, such as: (1) Acquisition of four submarines; (2) A contract for production of submarines under license; (3) Acquisition of 11 patrol vessels; (4) A surveillance network, including vessels and satellites; (5) Acquisition of unmanned aerial vehicles (UAVs) and fighters; as well as (6) Acquisition of a frigate and a possible aircraft carrier (Herrera & Matthews, 2014).

Regarding the wise use of offsets, one of the most successful and highly competitive examples comes from the experience that Brazil has had with the use of offsets when it acquired 36 JAS-39 Gripen E multirole combat aircrafts from Swedish manufacturer Saab. In order to choose Saab as a supplier, Brazil considered various aspects, such as costs, performance and technology transfer. It proved to be an attractive contract because the associated trade-offs were valued at 175% of the contract value. Saab even 'offered' 100% of the technology from the latest Gripen model, to which a 'deferred contract' clause was included as part of the agreement, with the intention that Sweden would in the future purchase aircrafts manufactured in Brazil. Lastly, Chile’s defense technological and industrial capacity has also improved due to defense acquisition projects including offsets. Acquisitions along the same lines as for Brazil were planned, with the aim of developing the DTIB, and national technological development. The arms supply to Latin American countries comes essentially from countries such as the US, EU countries, Russia and China, with the US accounting for some 78% of sales (Herrera & Matthews, 2014).

3. ANALYSIS AND DISCUSSION

Restricted by laws and directives, the EU Member States have abolished or revised their policies accordingly, where industrial offsets may only be considered on a case-by-case basis and provided that the conditions set out in Article 346 of TFEU are met. According to the data, it can be concluded that Member States still use offset requirements, but their frequency is decreasing and there is a trend towards the elimination of non-military offsets (EU, 2016).

Regarding the use of offsets by Portugal, it is possible to find a few cases of success, such as the modernization of P-3 Orion aircrafts and F-16 fighter jets. After the acquisition from the Dutch Navy of five P3 Orion aircrafts for the Portuguese Air Force in February 2005, it was decided to modernize them. However, it was not until 2007 that the modernization program was resumed with the involvement of Lockheed Martin, and the conditions of the acquisition contract and associated offsets were defined (overall value of offsets of € 99.7 mil., corresponding to 100% of the contract amount) (Ferro, 2014). The identified local beneficiaries were the Portuguese Aerospace Industry Consortium (PAIC), involving the design and development of UAVs, EDISOFT, and the information technology company ETI. Such offset contracts covered technology transfer for maintenance and modification of operational software, involving the Portuguese defense aeronautical industry, which included the modification of three aircrafts. In 2013, it was found that this process had exceeded the agreed value by 1.4%, where Portugal received an offset value of € 101 mil. instead of € 99.7 mil. The same could be said of the modernization of F16 fighter jets, where it was noted that the contract value had been exceeded by 43%, amounting to a value of € 214 mil. instead of € 149 mil. in return (Simões, 2007).

However, there were cases where offset contracts were not so successful, such as the acquisition of two submarines in 2004 from the German Submarine Consortium (GSC). Throughout the acquisition process, there were several contractual changes, finalizing the contract with the delivery of the

submarines by 2010, with its last contractual obligation performed in 2014. The way this process was carried out was not very judicious, and there were reports where seven Portuguese businessmen and three German businessmen from the GSC were accused of document forgery and fraud. Subsequently, it was also found that the GSC had failed to comply with the respective offset commitments (Ferro, 2014).

Similarly, for the purchase of torpedoes from WASS to equip the two submarines, offsets associated with nine projects, amounting to € 46.5 mil., were not executed (Simões, 2007). The acquisition of 12 C-295 aircrafts from Airbus Defence and Space (ADS) in 2006 also seems to have been a less than successful contract, since ADS was supposed to provide an industrial return of € 464 mil., which was not fulfilled. Due to decrease in the value of the penalty percentage from 15 to 10%, it resulted in non-compliance and a loss of € 9.25 mil. (Aguiar, 2020). A final example is the acquisition of 260 Pandur armored vehicles from Styler in 2004, with offsets worth € 700 mil. spread over 13 programs. Throughout this process, changes arose that were not included in the contract, and in 2012 the Ministry of Defense decided to cancel the contract for non-compliance (Ferro, 2014).

Due certain contractual gaps that may exist in offset contracts, exporting countries would have an incentive to default on commitments, preferring to pay the incurred fines. It would be preferable for the acquisition and offset contracts to be negotiated and managed by the same entity. However, in some countries, these two contracts may be under the responsibility of different entities (e.g., acquisition contract under the Ministry of Defense and offset contract under the Ministry of Economy).

Moreover, in some cases, supplier companies hire local companies that negotiate with local clients on behalf of the suppliers. Such local companies may tend to favor the interests of their principals, the suppliers, and not as much the interests of the national industry. Therefore, it would be necessary to establish: (1) An organization familiar with the national DTIB; (2) Potential programs that encourage new projects; (3) Potential areas of interest for the industry where technology transfer is advantageous; (4) The capacity to participate in R&D projects; and (5) The capability to use offsets as an investment approach, stimulating strategic partnerships across borders (Santos, 2021).

International experience shows that countries with focused and well-defined offset policies, such as the case of Brazil, have a greater chance of success. On the other hand, South Africa, as an example, seems to have a very broad and unfocused policy, where it is more difficult to assess the success of such policies, and thus has a lower chance of obtaining the desired benefits. Table 1 presents some examples from Latin America of contracts using offsets (Herrera & Matthews, 2014).

Table 1: Some of the acquisitions using offset contracts in Latin America.

Country	Type of Assets Acquired with the Use of Offsets
Brazil	KC-390, JAS-39, Xavante and UAV aircrafts, Gripen and F-5 fighters, Submarines, frigates, patrol and logistic support vessels, Sensors, Satellites.
Colombia	CN235 aircrafts, Black Hawk helicopters, Missiles, Armored vehicles, Maritime technology systems
Chile	F-16 fighter; Super Tucano Aircrafts, Scorpène Submarines Type 23, Frigates
Peru	C-37J and KT-1 aircrafts, and EC145 Helicopters.

Another successful example worth mentioning is the case of Malaysia, focusing mainly on building technological capabilities and developing human resources. In this case, offsets have been successfully used to diversify commercial industries, mainly aerospace and electronics, leading to increased exports and jobs, as well as technology enhancements across relevant industries (Khan, 2010).

In summary, one of the main criticisms for the poor performance of offsets seems to have been lack of

preparation in defense procurement, which has as its weakest link the inability to conduct complex negotiations (multivariable and involving multiple parties). The elements that integrate negotiation teams, as well as a lack of clarity and coordination, excessive bureaucracy, and lack of reports that would provide the gathering of lessons learned from all the projects to be retained are among the identified issues. Moreover, a further source of complexity may derive from lack of adequate human resources, whereby some national companies do intermediate the negotiation process on behalf of the suppliers (EuroDefense, 2007).

On the other hand, offset programs should be managed by stable and specialized teams, where it would be possible to regulate, monitor and define the acquisition projects of interest to the national DTIB. If defense procurement is defined with a focus on the development of the DTIB, offsets could be an important instrument for its development. This would be made possible through technology transfer and training programs, as well as facilitating access to markets and launching national industrial strategic programs. Only through efforts to analyze the processes behind offsets, professionalizing and specializing the elements involved with such negotiations, and developing mechanisms for technology transfer and accountability would it be possible to justify its use again.

4. CONCLUSION

In an increasingly economically interconnected world, the idea of a reciprocal investment is not new, and in many ways, it can be called generically in the defense sector as offsets. When countries acquire high-value defense equipment, contracted to defense companies in exchange for benefits, they may be expanding their own industrial capabilities related to defense production. It is almost impossible for many defense companies to sell weapon systems to rich or poor countries without attracting demand for offsets. Recognizing the sensitivity of the subject, the EU established rules for the award of such contracts regarding the scopes of defense and security based on the principles of transparency and equal treatment. Therefore, the process of offset contracts negotiation is complex. In order to achieve success, the involved teams must have adequate profiles and negotiations must be approached in a professional manner across various dimensions.

The practice of offsets is universally accepted, but there are countries that use them primarily to expand their participation in the defense industrial market, acquire technology, as well as to promote and develop their local industry, which is especially critical in industrializing and developing countries. This paper draws some lessons from Portugal's experience, which probably resembles the cases of many similar countries.

In order to make it work, transparency and accountability in procurements involving offsets should be improved, as these are susceptible to risks and lack of effectiveness that prevents them from benefiting the importing countries. Offsets are dependent on good professional negotiating skills. It is not fully proven whether an offsets policy is an effective mechanism for defense technological development, but if an adequate set of standardized requirements is considered, which complies with laws, rules and legitimate interests while minimizing possible loopholes in contracts, offset policies that benefit both parties in the contract could be established and implemented.

REFERENCES

Aguiar, C. (2020). *Estado perde 9 milhões nas contrapartidas dos aviões C-295M*. Available online at: https://www.dn.pt/dinheiro/estado-perde-9-milhoes-nas-contrapartidas-dos-avioes-c-295m-12493183.html (Last access date: 2 March 2022).

EU (2009). *Council Directive 2009/81/EC, of the European Parliament and of the Council of 13 July 2009*. European Union (EU), Brussels, Belgium.

EU (2012). *Treaty on European Union and the Treaty on the Functioning of the European Union, Consolidated Version of 26th of October 2012*. European Union (EU), Brussels, Belgium.

EU (2016). *Report from the Commission to the European Parliament and the Council on the Implementation of Directive 2009/81/EC on Public Procurement in the Fields of Defence and Security, to Comply with Article 73(2) of that Directive*. European Union (EU), Brussels, Belgium.

EuroDefense (2007). *As Contrapartidas Como Instrumento da Economia de Defesa*. Centro de Estudos EuroDefense, Portugal.

Erikson, E. (2007). *Study on the Effects of Offsets on the Development of a European Defence Industry and Market*. Final report, University of Birmingham, Birmingham, UK.

Ferro, M. (2014). *Comissão Parlamentar de Inquérito aos Programas Relativos às Aquisições de Equipamento Militares*. Assembleia da República Portuguesa, Portugal.

Gnidchenko, A., Mogilat, A., Mikheeva, O. & Salnikov, V. (2016). Foreign technology transfer: an assessment of Russia's economic dependence on high-tech imports. *Foresight STI Gov.*, **10**: 53-67.

Harutyunyan, G.E. (2017). The impact of military R&D on the innovative development of the civilian sector. *Public Adm. Issues*, **5**: 27–37.

Herrera, M. & Matthews, R. (2014). Latin America in step with global defence offset phenomenon. *RUSI J.*, **159**: 50-57.

IndexMundi (2019). *Arms exports (SIPRI trend indicator values) - Middle East.* Available online at: https://www.indexmundi.com/facts/indicators/MS.MIL.XPRT.KD/map/asia (Last access date: 8 March 2022).

Jovovic, A., Strang, A. & White, R. (2021). *Defense Offsets Expectations are Considerable, but Implementation is Uneven*. Available online at: https://www.avascent.com/news-insights/perspectives/defense-offsets-expectations-are-considerable-but-implementation-is-uneven/ (Last access date: 8 March 2022).

Kaushik K. (2020). *Explained: What are Defence Offset? Here Everything You Need to Know*. Available online at: https://indianexpress.com/article/explained/defence-ministry-acquisition-procedure-offsets-6654837/lite/ (Last access date: 16 September 2022)

Khan, A. (2010). Market trends and analysis of defence offsets. *DISAM J. Int. Secur. Assist. Manage.*, **32**: 138-153.

Lax, D. A. & Sebenius, J. K. (2006). *3-D Negotiation: Powerful Tools to Change the Game in Your Most Important Deals*. Harvard Business School Press, Boston, US.

Maennig, W. & Wittig, S. (2010). WTO dispute settlement proceedings: European support for airbus in the spotlight. *Inter. Econ.*, **45**: 180-187, doi:10.1007/s10272-010-0334-7

Magahy, B., Cunha, F. & Pyman, M. (2010). *Defence offsets: Addressing the risks of corruption & raising transparency*. Transparency International-UK, London, UK.

Mazzucato, M., Cimoli, M., Dosi, G., Stiglitz, J.E., Landesmann, M.A., Pianta, M., Walz, R. & Page, T. (2015). Which industrial policy does Europe need?. *Inter. Econ.*, **50**: 120-155.

Mendenhalt R. W. (1996). Post-settlement settlements: Agreeing to make resolutions efficient. *J. Disp. Resol.*, **1996**: 81-113.

Pasquali, M. (2021). *Latin America & Caribbean: Gross Domestic Product 2020, By Country*. Available online at: https://www.statista.com/statistics/802640/gross-domestic-product-gdp-latin-america-caribbean-country/ (Last access date: 8 March 2022).

Santos, H. (2021). *Um Modelo De Apoio À Negociação Na Aquisição De Produtos De Defesa: Maximização De Transferência De Tecnologi*a. MSc Thesis, Escola Naval, Almada, Portugal.

Silva, J. (2005). *Do Levantamento De Capacidades À Execução Da LPM Numa Óptica De Gestão De Projectos: Modelo De Optimização Da Gestão Da LPM*. Instituto de Altos Estudos Militares, Lisbon, Portugal.

Simões, B. (2017). *Contrapartidas Dos Torpedos Não Foram Cumpridas E As Do C-295 Estão Atrasadas*. Available online at: https://www.jornaldenegocios.pt/economia/defesa/detalhe/contrapartidas-dos-torpedos-nao-foram-cumpridas-e-as-do-c-295-estao-atrasadas (Last access date: 6 March 2022).

Straubhaar, T. (1986). The economics of Third World arms imports. *Inter. Econ.*, **21**: 137-141.

TdC (2017). *Relatório n.º 21/2017, 2.ª Secção, Relatório de Auditoria à Execução da Lei de Programação Militar em 2015 (aprovada pela Lei Orgânica n.º 7/2015, de 18 de maio*). Tribunal

de Contas (TdC), Lisbon, Portugal.
Weidenbaum, M. (1993). How companies overcome barriers to overseas business. *Intereconomics*, **28**: 188-190.
Wezeman, P.D., Kuimova, A. & Wezeman, S.T. (2021). *Trends in International Arms Transfers, 2020,* Stockholm International Peace Research Institute , Stockholm, Sweden.
World Bank (2022). *GDP (Current International $)*. Available online at: https://data.worldbank.org/indicator/NY.GDP.MKTP.PP.CD (Last access date: 6 March 2022).
WTO (2021). *Government Procurement: The Plurilateral Agreement on Government Procurement (GPA)*. Available online at: https://www.wto.org/english/tratop_e/gproc_e/gp_gpa_e.htm (Last access date: 7 March 2022).